2011-01-01

An Integrated Geological And Geophysical Study Of The Fresh And Brackish Water Boundary In The Hueco Bolson, West Texas

Sandy Stephanie Marrufo
University of Texas at El Paso, sandymarrufo@gmail.com

AN INTEGRATED GEOLOGICAL AND GEOPHYSICAL STUDY OF THE FRESH AND BRACKISH WATER BOUNDARY IN THE HUECO BOLSON, WEST TEXAS

SANDY STEPHANIE MARRUFO, B.S.

Department of Geological Science

APPROVED:

Richard P. Langford, Ph.D., Chair

Diane I. Doser, Ph.D.

Eric A. Hagedorn, Ph.D.

Benjamin C. Flores, Ph.D.
Acting Dean of the Graduate School

Dedication

This thesis is dedicated to my family. To my mother, Etta E. Armijo, who was always there to help me in any way she could. To my father, David Marrufo, who always supported my education and did whatever he could to help me achieve my dreams. To my husband, J. Matthew R. Cannon, who supported me academically and emotionally throughout my academic career. Finally, to my stepfather, Ernesto Armijo, for all of his words of wisdom and encouragement he gave over the years.

AN INTEGRATED GEOLOGICAL AND GEOPHYSICAL STUDY OF THE FRESH AND BRACKISH WATER BOUNDARY IN THE HUECO BOLSON, WEST TEXAS

by

SANDY STEPHANIE MARRUFO, B.S.

THESIS

Presented to the Faculty of the Graduate School of

The University of Texas at El Paso

in Partial Fulfillment

of the Requirements

for the Degree of

MASTER OF SCIENCE

Department of Geological Science

THE UNIVERSITY OF TEXAS AT EL PASO

August 2011

Acknowledgements

I would like to acknowledge Sarah Quiñonez who began this research and analyzed wells 601 and 605. I would like to thank Dr.'s Rip Langford and Diane Doser for all of their help and guidance throughout this study. I want to give thanks to El Paso Water Utilities, namely Alfredo Ruiz, who provided the well logs and cuttings necessary for this research. I would also like to thank Fort Bliss, namely Stephen Sanchez, for granting me access in order to conduct my gravity survey. I also want to thank UTEP and Pathways for the funding and support during my undergraduate research years on this study. I want to thank Carlos Montana for all of his assistance with my computer and software problems. Last, but not least, I want to thank everyone who helped during the collection and processing of my gravity data, Galen Kaip, Rip Langford, Niti Mankhemthong, Tai Subia, Anita Thapalia, Pawan Budhathoki, Matt Cannon, and Sarah Cervera.

Abstract

The Hueco Bolson in West Texas is located in the Rio Grande rift basin and provides water to El Paso County, Texas and Juarez, Mexico. El Paso Water Utilities (EPWU) drilled many wells up to 1000 ft (305) m into this aquifer, which provide 40% of El Paso's water supply. Stratigraphy and sedimentation in active extensional basins have received little study because they are usually buried and this research helped document these processes. The study area within the West Texas region of the Hueco Bolson Aquifer (HBA) lies within a transition zone between the fresh and brackish water sections of the aquifer. The boundary between fresh and brackish water in this study area (as indicated by previous studies) is more vertical and abrupt than typical fresh and brackish water boundaries which are usually gradual and have a lenticular shape.

A total of twenty-six wells drilled by EPWU were analyzed (grain-size and well log analysis) for this study; three wells in the MW series were drilled in 2003, seven wells in the 500 series drilled in 2006 and sixteen wells drilled in 2005. An increase in salinity, measured in total dissolved solids (TDS), is observed from northwest to southeast (from 374 to 7410 TDS) across the study area. The 600 series wells were drilled to provide brackish water to a desalination plant to increase the longevity of the aquifer and to create a trough in the ground water to help prevent incursion of brackish water from the east into the fresh water section of the aquifer.

Five wells (601, 605, 610, 615, and 509A) located in the fresh and brackish water sections of the HBA were chosen for grain-size analysis. Grain-size distribution for wells 601, 605, 610, 615, and 509A were analyzed using sieves for particles larger than 1 mm and a Malvern particle analyzer for particles smaller than 1 mm. The wells penetrate numerous clay and silt beds. These beds can be correlated between wells and help to vertically subdivide the reservoir. Four depositional environments were identified after grain-size analysis: playa lake, playa margin, alluvial fan, and fluvial environments.

There are abrupt changes in the energy in the environments from low energy playa lake and play margin deposits to high energy alluvial fan and fluvial deposits.

Well log correlations were created in Kingdom Suites software to correlate from well 601 to 509A. Correlations show the alluvial fan deposits thin heading into the basin, while the playa lake deposits begin to appear at shallower depths out in the basin. There is an increase in the volume of clay (13.9% to 42.9%) from well 601 to 509A (northwest to southeast). Seven faults were identified during well log analysis, two of which have been previously mapped by Collins and Raney (2000).

A gravity survey was conducted to model the basin and identify the faults seen in cross-section. Two of previous faults mapped by Collins and Raney (2000) located in the study area were extended farther south into the urbanized area of the city of El Paso. The five faults identified in this study were constrained and mapped. One of the five faults identified in this study extends about 12.4 miles (21 km) N-S and appears to belong to a series of step-over faults heading into the basin.

There are a series of three faults (one small and two extending about 21 km N-S across the study area) in the transition zone between the fresh water and brackish water sections of the HBA with increasing amounts of clay in the brackish water section. The combination of clay (impeding the flow of water) and barrier faults are creating a natural seal helping to prevent the incursion of brackish water into the fresh water section of the aquifer.

Table of Contents

List of Tables

List of Figures

List of Plates

Introduction

Living in a desert border region puts constraints on available water supplies. Groundwater is the main source of drinking water in an arid environment like El Paso, and using desalination processes lengthens the longevity of the communities' water supply (San Diego County Water Authority, 2005). The Hueco Bolson Aquifer (HBA) in West Texas provides about 40% of El Paso's water, in addition to supplying water to other neighboring cities. The HBA covers approximately 1.6 million acres (El Paso Water Utilities, 2004; Hutchison, 2006) and is located east of the Franklin Mountains, west of the Hueco Mountains, south of the Tularosa Basin, and north of the Sierra Guadalupe (Figure 1).

There are twenty-six wells drilled by El Paso Water Utilities (EPWU) within the study area that were analyzed for this study, which lie within the Fort Bliss and El Paso Airport properties (Figure 2). Seven wells identified as the 500 series, were drilled in 2006, sixteen wells in the 600 series were drilled in 2005, and three wells identified as MW wells were drilled in 2003. The 600 series wells were drilled by EPWU for two purposes: 1) provide brackish water to the Kay Bailey Hutchison Desalinization plant: and 2) to help create a trough to prevent the incursion of brackish water into the fresh water aquifer.

The boundary between the fresh and brackish water sections of the HBA lies within the study area (Figure 2). Water analysis of the 500 and 600 series wells (EPWU, 2009) indicate a northwest to southeast increase in total dissolved solids (TDS) from 374 to 7410 TDS across the study area (Figure 3). The upper limit of potable water is 1000 TDS (El Paso Water Utilities, 2004). The purpose of this research is threefold: 1) to identify the constraints of the boundary between the fresh water and brackish water aquifer, 2) to examine and describe the stratigraphy, 3) to depict the lithology of this active rift basin. Gravity measurements, well logs, and well

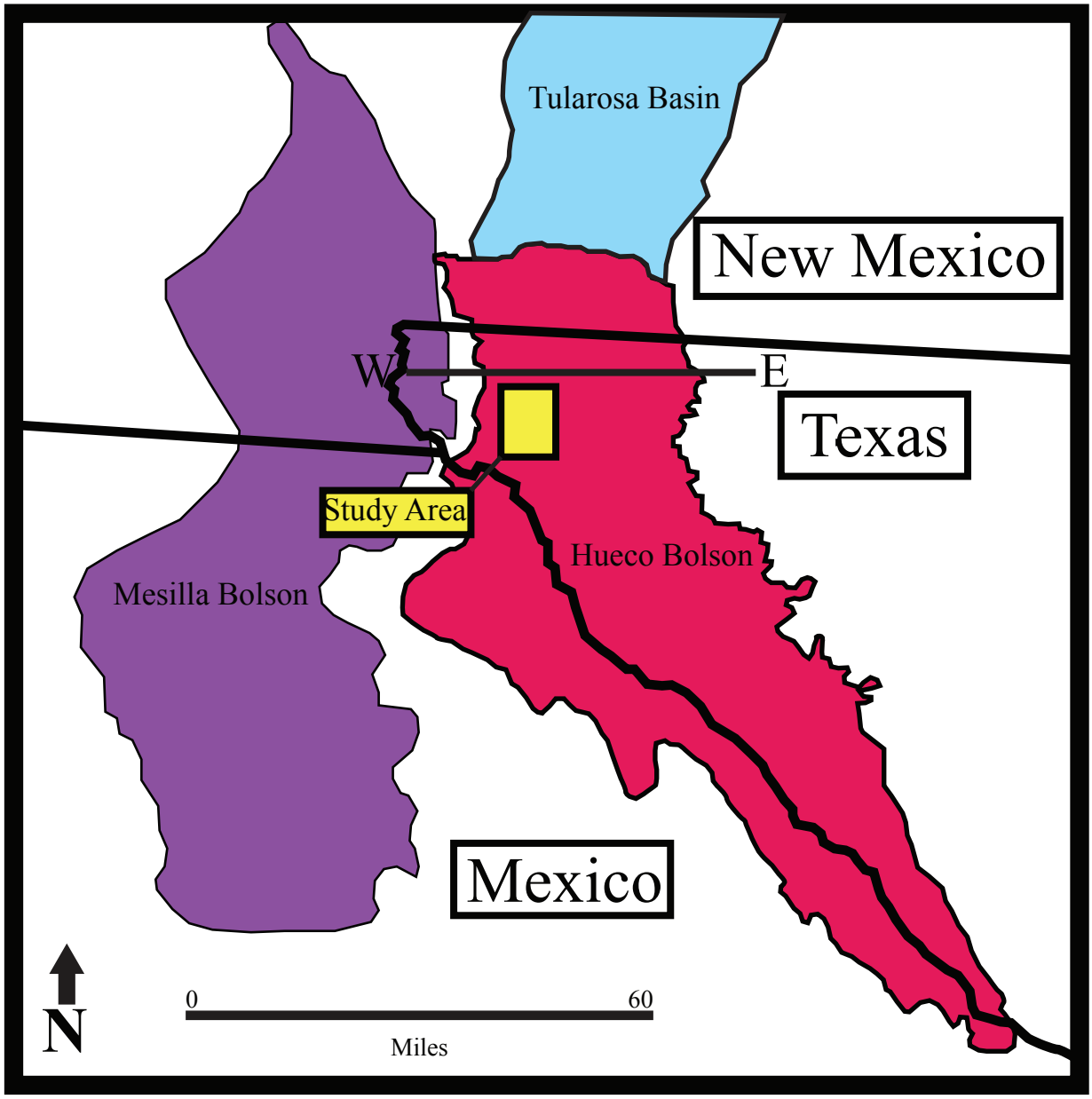

Figure 1. This location map shows the major aquifers in the West Texas region. Modified from Hutchison (2006) and Hawley (2004).

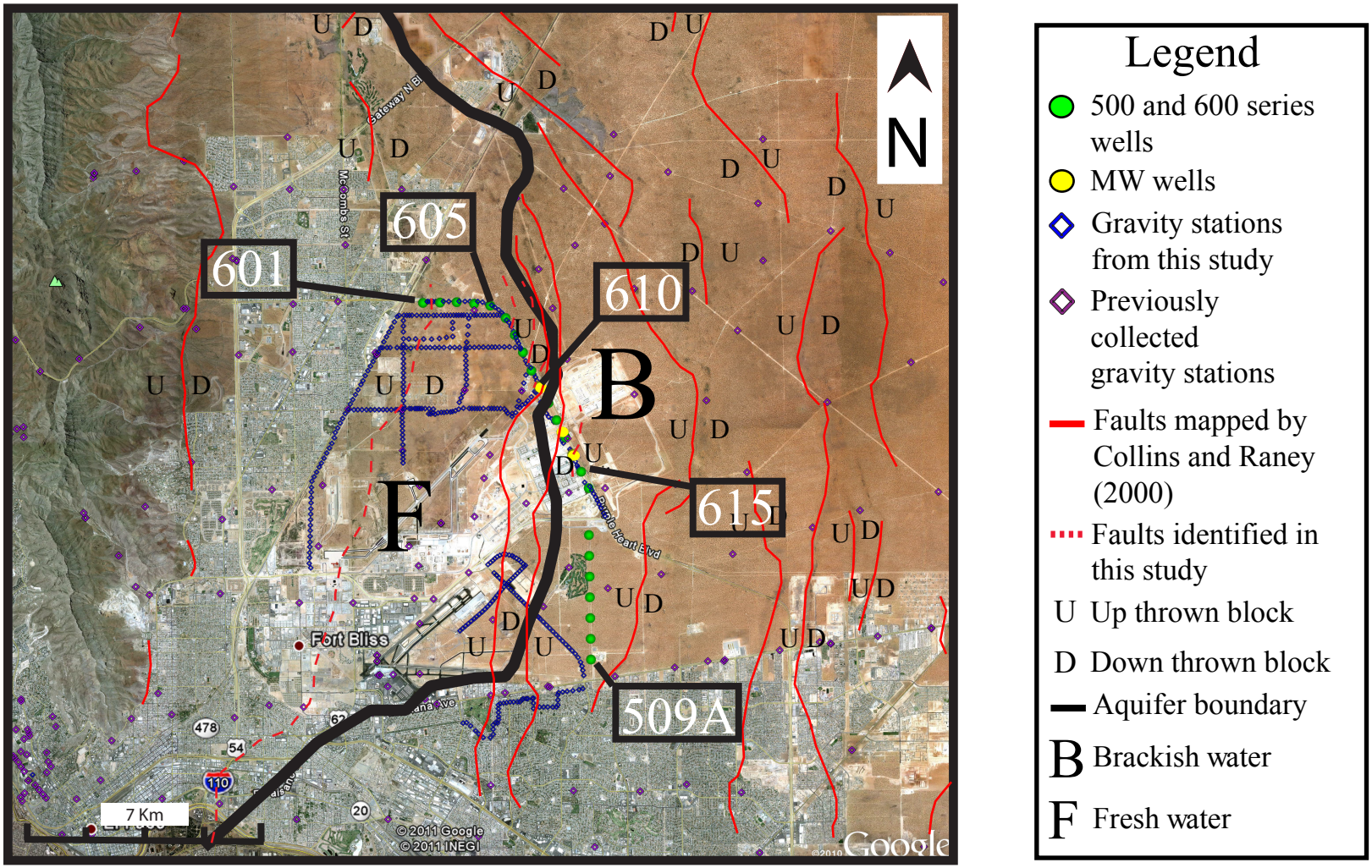

Figure 2. Well map from EPWU superimposed onto a Google Earth image of El Paso, TX. The faults in solid red lines are modified from Collins and Raney (2000) and the dashed red lines are faults interpreted from this study. The fresh and brackish water boundary is modified from Hutchison (2009). The green dots represent the 600 and 500 series wells, while the yellow dots are the MW wells. There are three MW wells, which are located within feet of an already existing 600 series well. Aquifer boundary modified from Hutchison, 2006.

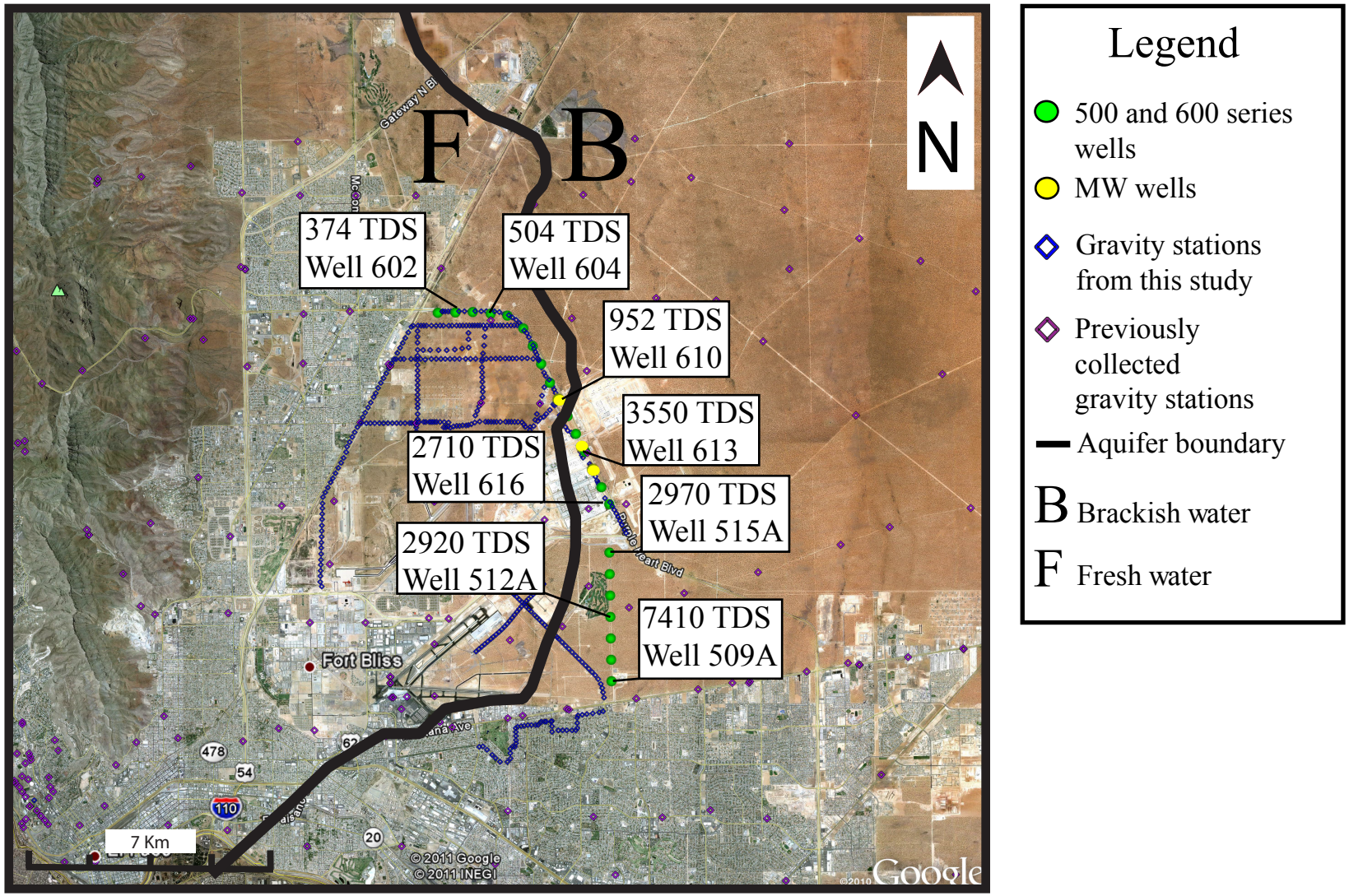

Figure 3. This map shows the change in total dissolved solids (TDS) across the study area from well 601 to 509A. The TDS information was acquired from an analytical report for EPWU, 2009. Aquifer boundary modified from Hutchison, 2009.

cuttings (obtained from EPWU) assist in identifying the parameters of the HBA. The parameters include the free water salinity, permeability, lateral extent, vertical isolation between aquifers, and the relationship of aquifers to faults, fractures, voids, and paleosols (ancient soils) (Doser and Langford, 2007). Faults can influence the flow of water in an aquifer by either acting as conduits or barriers, while paleosols control the lateral and vertical extent of the aquifer.

The HBA is contained within sands of the Santa Fe group (Fort Hancock and Camp Rice formations), sediments of Pliocene and Quaternary age that were deposited in desert basins, playa lakes, and channels of the Rio Grande and its tributaries (Kottlowski, 1958; Cliett, 1969; Gile et. al, 1981; Hawley and Kernodle, 2000; Eastoe et. al, 2008). In El Paso and its surrounding area, two basins formed, separated by the uplifted Franklin Mountains. Each of these basins contains an aquifer that supplies the surrounding cities. The Mesilla Bolson Aquifer lies on the west side of the Franklin Mountains. The HBA extends north and south through the center of the city east of the Franklin Mountains, and west of the Hueco Mountains (Figure 4).

Ground Water

The depth to the water table in the HBA is much lower today than in 1971 because more water is pumped out of the aquifer than is put into the system (Hutchison, 2006). The demand for water is higher now than it was in 1971, so pumping has increased to meet those demands (Hutchison, 2006). Water quality and quantity was affected by over-pumping the aquifer to meet those demands (Muller and Price, 1979 and Boyle Engineering, 1991), so regional water planning began in Texas in 1997 (Hutchison, 2006). Since 1997, pumping has been reduced and the world's largest inland desalination plant was built to filter the brackish water in the aquifer and produce potable water.

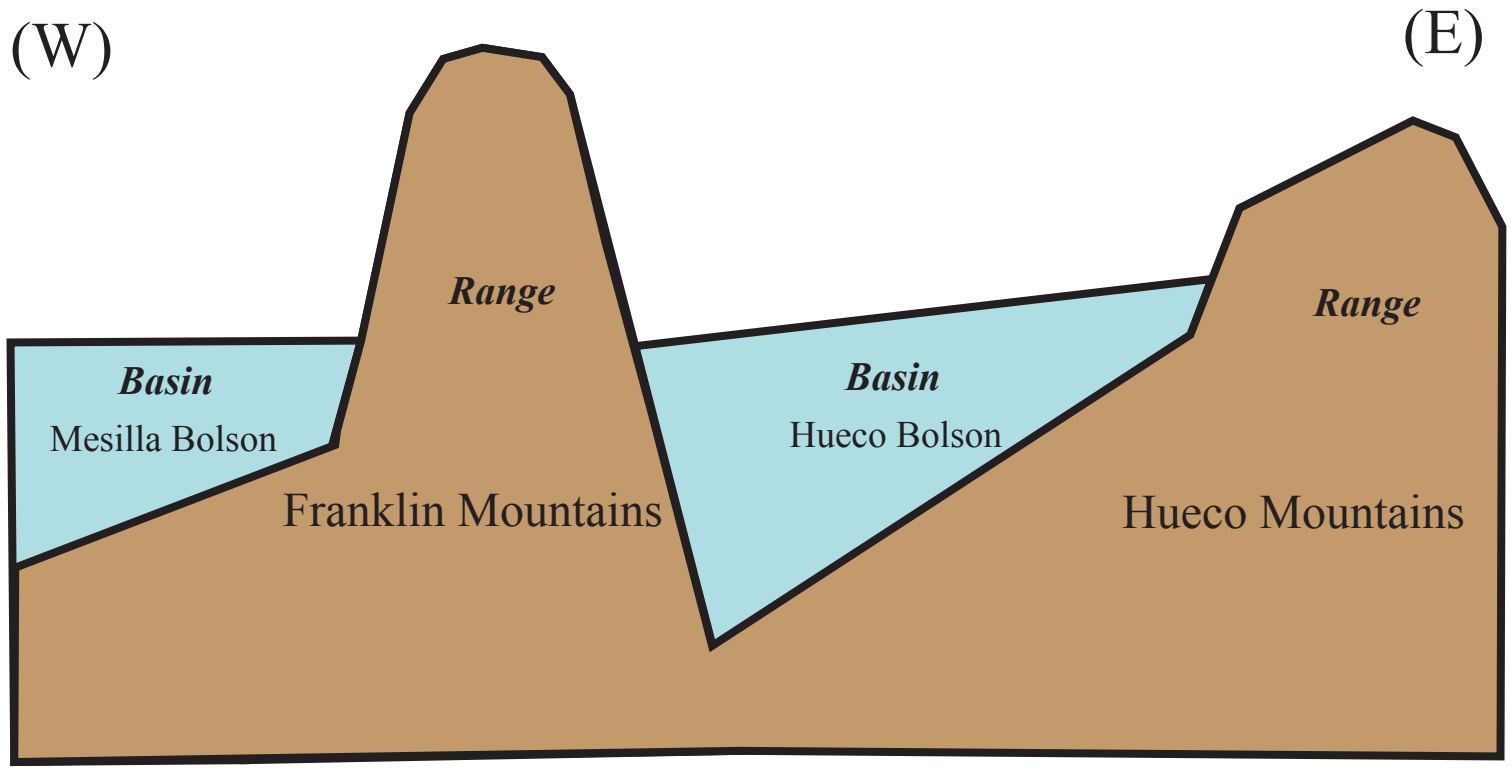

Figure 4. The profile line from Figure 1 showing an extensional basin and range half graben model for the Hueco Bolson. Modified from Hutchinson (2006).

The HBA is divided into two sections, fresh and brackish water sections, in the aquifer along a line trending north-south through the basin (Hutchinson, 2006) (Figure 2 and 3). The fresh water lies on the west side of the boundary and the brackish water is on the east side of the boundary (Figure 3). The fresh water in the HBA corresponds with the course of the ancestral Rio Grande River and the brackish water with the areas with playa lake deposits (Hutchison, 2006). The pumping of fresh water and the proximity of the brackish water causes the incursion of brackish water into the fresh water section of the aquifer (Hutchison, 2006).

Geologic History

Tectonic History

Two major tectonic events in recent geologic history impacted the shaping of the El Paso region's landscape, the Laramide orogeny and the Rio Grande Rift (RGR). The Laramide Orogeny began about 70 Mya during the late Campanian age (Kellogg, 1999), which is marked by the subduction of the Farallon Plate beneath the North American Plate. This compressive event created the Rocky Mountains orogenic belt (Kellogg, 1999), of which the Franklin Mountains are a part. The event also caused major thrust faulting and the subsidence of open, round basins from the Canadian Rockies, through Colorado to the El Paso region, where there was a transition to a more typical fold and thrust belt (Chapin, 1971, 1979; Cordell, 1978; Collins and Raney, 1991).

The transition from compressional to extensional stress began around 30 Mya and was fully developed by about 24 Mya (Henry and Price, 1985, 1986; Stevens and Stevens, 1985). The approximate time frame of fault movement and sediment deposition in the Hueco Bolson is unknown (Collins and Raney, 1991). The HBA lies within the southern end of the north-trending Rio Grande Rift (Collins and Raney, 1991) which extends from central Colorado through New Mexico into northern Mexico (Chapin, 1971, 1979; Cordell, 1978). There are two major events related to rifting that show different motions and types of volcanism. The first began in the late Oligocene to early Miocene (Veatch, 1998), and the second began in the mid-Miocene and continues today (Veatch, 1998). Extensional forces created a series of normal faults including the east Franklin fault within the Hueco Bolson.

Hueco Bolson Aquifer

The HBA is an asymmetrical basin (Eastoe et al., 2008; Hutchison, 2006) that is

Approximately 9,000 feet at its deepest extent along the east side of the Franklin Mountains (Cleitt, 1969; Ashworth and Hopkins, 1995). Within the study area of the HBA there are several identifiable normal faults, which visibly offset the basin surface and underlying strata. Many of these faults have been mapped by Collins and Raney (2000). Seven faults were identified between wells 601 and 509A (Figure 2 and Plate 2) in this study.

Ancestral Rio Grande

The fluvial history of the area is based on studies of ancestral Rio Grande river deposits within the Mesilla and Hueco Bolsons. According to Hutchison (2006), there was no fluvial deposition occurring around 5 Mya. Between 4 and 5 Mya the ancestral Rio Grande showed up within the region and terminated into a lake in the Hueco Bolson (Mack and Leeder, 1998; Hutchison, 2006). At this time playa lakes and alluvial fan environments deposited the basin fill sediments (Connell et al., 2005). Between 4 and 5 Mya the upper ancestral Rio Grande extended southwards into the Mesilla and Hueco Bolsons, but did not merge with the lower ancestral Rio Grande until around 1 Mya (Mack and Leeder, 1998; Hutchison, 2006).

Changes in topography (differentiated fault movement) shifted the course of the river around the region (Hutchison, 2006). Figure 5 shows the paleodrainages of the ancestral Rio Grande during the Pliocene and Early Pliestocene. According to Hutchison (2006), the Rio Grande shifted to its current course around 1 Mya. The river began down cutting the existing valley between 600 to 700 kya (Connell et al., 2005). The Franklin Mountains have uplifted about 30 feet and the Hueco Bolson has been down dropped by about 120 feet over the last 500,000 years (Langford, 2001).

Stratigraphy

The Hueco Bolson has deposits of Quaternary, Neogene, and Paleogene age (Ashworth

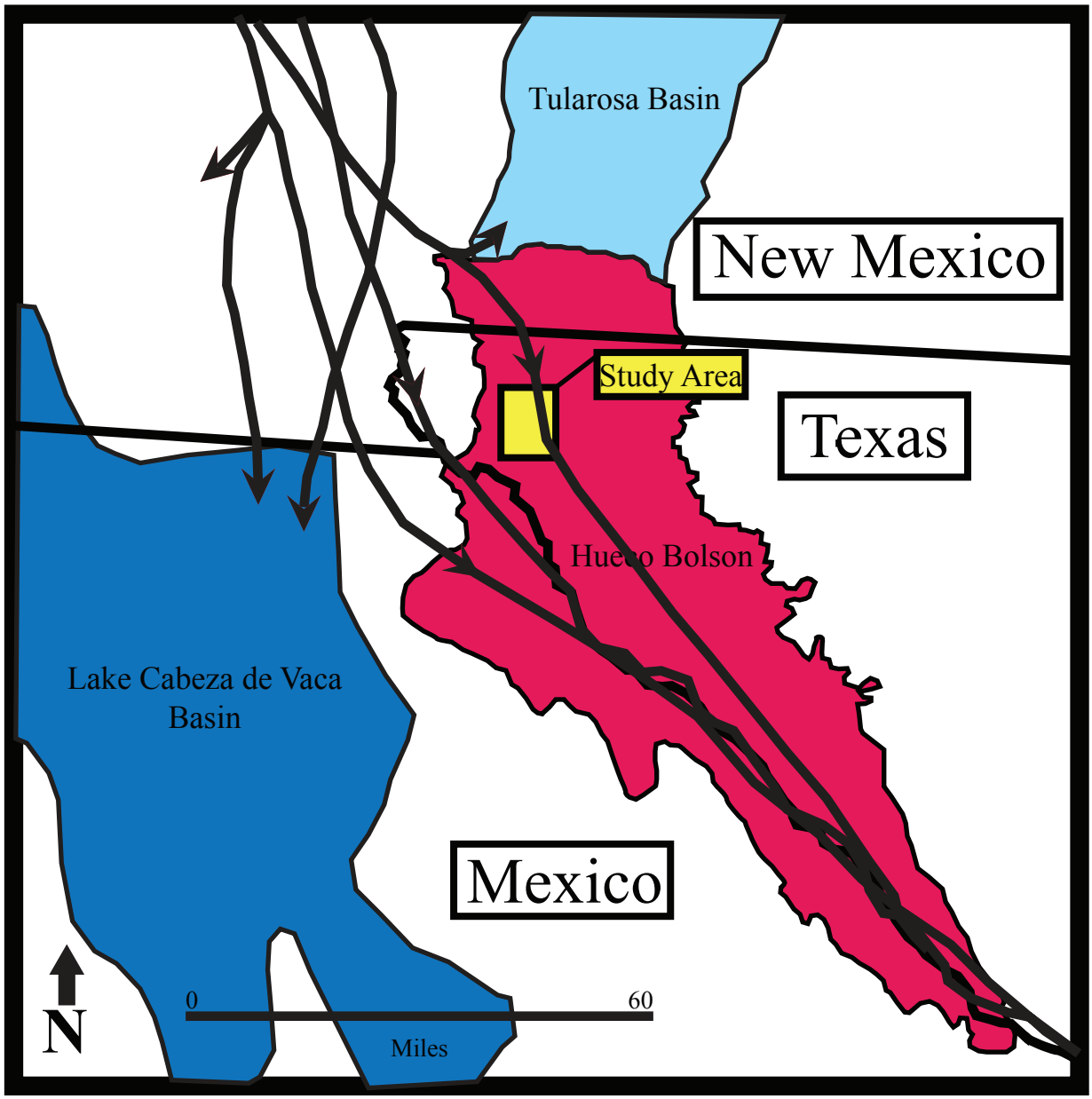

Figure 5. Modified from Hutchison (2006). This map shows paleodrainages (arrows show the direction of flow for the paleochannels) in the study region during the Pliocene and Early Pleistocene.

and Hopkins 1995). Not much is known about bolson deposits during most of the Neogene and late Paleogene due to the lack of outcrops showing more than several meters of deposits in the region (Collins and Raney, 1991). The studies completed in the region have shown that there are deposits of the Santa Fe group (20 Mya to 500 kya) in the Hueco Bolson (Hawley and Kennedy, 2004; Collins and Raney, 1991; Gile et al. 1981). Figure 6 shows that the Camp Rice (late Plioecene to early/middle Pleistocene) and Fort Hancock (Miocene to Pliocene) formations that comprise the Santa Fe Group were deposited within the Hueco Bolson.

Fort Hancock sediments were deposited primarily in lacustrine and alluvial fan depositional environments with local fluvial deposition (Collins and Raney, 1991). The Camp Rice sediments were deposited in alluvial fan, fluvial and lacustrine depositional environments (Collins and Raney, 1991). Albritton and Smith (1965) defined, mapped, and named five gravel units of Pleistocence age that stratigraphically lie above the Camp Rice and Fort Hancock formations near the Quittman Mountains. These units are named (oldest to youngest) Miser, Madden, Gills, Ramey, and Balluco gravels (see Figure 6). Albritton and Smith (1965) suggest these gravels were deposited on piedmont slope and arroyo terrace environments and range on average from 1.5 to 2.5 m thick (Albritton and Smith, 1965). The youngest units, which lie above these gravel units, are windblown, fluvial, and alluvial deposits (Figure 6). The gravel units are difficult to distinguish from the underlying Fort Hancock and Camp Rice Formations (Albirtton and Smith, 1965).

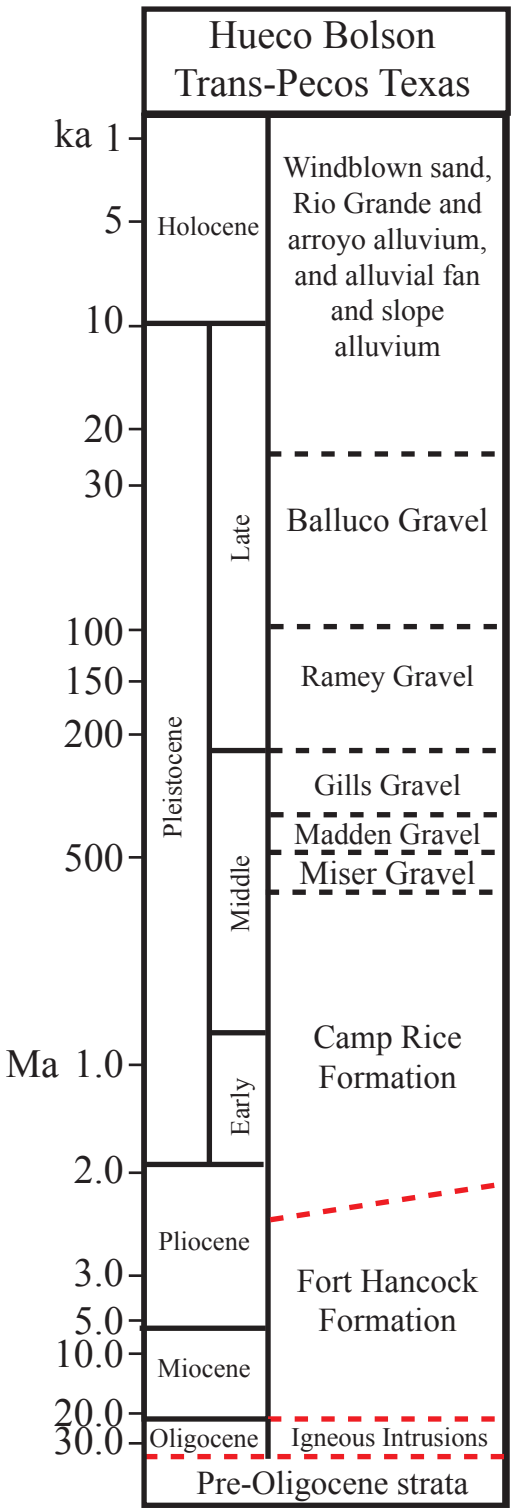

Figure 6. The red dashed lines indicate an unconformable contact and the dashed black lines indicate a conformable contact. The stratigraphic column modified from Collins and Raney (1991) showing the terminology of the gravels from Albritton and Smith (1965) and Strain (1966).

Methodology

Well cuttings were collected by EPWU at ten foot intervals in all the water wells. Wireline well-logs were acquired from EPWU and entered into log display and analysis software (Petra Log Analysis software and Kingdom Suites software). Logs are available down to approximately 900 ft below the surface of each well. Surface casing set from 60 to 100 ft obscured many of the logs in the uppermost part of the well.

The log suites for wells 601 to 610 included caliper, gamma ray, and spontaneous potential measurements as well as several resistivity logs, but only the gamma ray and resistivity curves were used for correlations (Plate 1). The log suites available for wells 611 through 616 and 509A through 515A had limited log curve and header data. The gamma ray log curves for these wells were of poor quality (Plate 1), so well log correlations were interpreted using the resistivity log curves for the wells that had them. The log suites from the MW wells were used to help correlate through the area of poorer log curve data between wells 610 to 616.

Grain-size analysis

The cuttings from five wells (601, 605, 610, 615, and 509A, Figure 2) were analyzed for grain-size distributions. These wells were spread across the study area to include the major regional lithological and salinity variations. Wells 601 and 605 were chosen in the fresh water section of the aquifer. Well 610 was analyzed along the west side of the faults located along the transition area, where the shift from fresh water to brackish water occurs. Wells 615 and 509A are located east of the transitional area where the cuttings are clay-rich and represent the high salinity areas.

The samples were initially weighed and then dried using a microwave until the sample weight changed by less than 0.05% as a dry weight using the procedures of Gee and Dodson

(1981). Particles larger than 1 mm were then sieved and fractions were measured at ½ phi (φ) intervals. The sieve mesh sizes were as follows from coarsest to finest: 3/8 (8 mm, -3 φ), 1/4 (5.7 mm, -2.5 φ), 5 (4 mm, -2 φ), 7 (2.8 mm, -1.5 φ), 10 (2 mm, -1 φ), 14 (1.4 mm, -0.5 φ), 18 (1 mm, 0 φ). All the sediment collected in each sieve was weighed and returned to the sample bag, except for the sediments finer than 1 mm that remained in the pan. The remaining sample was weighed, placed in a sample bottle, and dispersed for at least 24 hours in a solution of distilled water and sodium hexametaphosphate $(NaPO_3)_6$ (1 L of water and 5.5 g of $(NaPO_3)_6$, according to Gardner (1986) and Blake and Hartage (1986).

Once the sample was properly dispersed, it was analyzed using the Malvern Mastersizer 2000, which measures grain-sizes from 0.02 μm to 2000 μm. Samples that contained a large amount of clay were split into smaller volumes before analysis in the Malvern using a spinning riffler (Richard P.Langford, personal communication, September, 2007). Approximately every 3^{rd}-5^{th} sample was run as a triplicate sample to better determine the precision. Blanks were run every time a sample measurement was obscure to determine whether there was a background signal that might interfere with results. Standards were run throughout the measurement period to detect any calibration drift in the machine.

The results from the grain-size analysis were then input into an excel spreadsheet and combined with the sieve data. Sieve weights were added into the spreadsheet and divided by the total dry weight to convert to weight percents. The Malvern collected data in weight percent and then was multiplied by the percentage of the sample smaller than 1 mm to correct for the percent of coarse material. The median, mean, and standard deviation of the samples were estimated using the method of moments (Folk, 1966). The samples were divided into five classes: clay (>8 φ, 4 μ), silt (4 through 8 φ, 4 through 53 μ), fine grained sand (1.5 through 4 φ, 53 through 354

μ) coarse grained sand (-1 through -1.5 φ, 354 through 1000 μ) and gravel (> -1 φ, > 1000 μ). These data were then correlated to the midpoint depth for each cutting sample and entered as point log data into the Petra Log Analysis software and Kingdom Suites software.

Well Log Analysis

Well logs provide a detailed 2 ft scale record of stratigraphy. For water wells there are three common well logs run that estimate hydrogeological properties: natural gamma ray, resistivity, and spontaneous potential logs (Doser and Langford 2007).

Correlations were made from well 601 to well 509A using the gamma ray and resistivity log curves for all wells with high quality gamma log readings using Petra Log Analysis software and Kingdom Suites software. Only resistivity logs were used for well log correlation between wells 610-509A (Plate 1) for the wells lacking quality gamma readings. Changes in sequence patterns were used to correlate between wells and identify stratigraphy (e.g. coarsening upwards sequences, fining upwards sequences, aggradational sequences, etc.) using the gamma ray and resistivity logs. Wells that had both high quality gamma and resistivity logs have the most reliable correlations; wells that only had resistivity logs have less reliable correlations.

Cross-plots showing total percent clay on the y-axis and gamma ray activity on the x-axis were also created from this data to evaluate the analyzed wells (Figure 7). After creation of the cross-plots, a best-fit regression line was determined and the equation derived from this line was used to define the relationship between the gamma ray readings and the percentage of clay for all analyzed wells. Wells 601 and 605 had the best quality gamma curves, while the gamma ray quality of wells 610, 615, and 509A were poorer. The regression line equations for well 601 and 605 closely match, while the equations for the wells with poor data quality do not (Figure 7). Wells MW-6 and MW-4 are close to wells 610 and 615 and have excellent gamma ray data

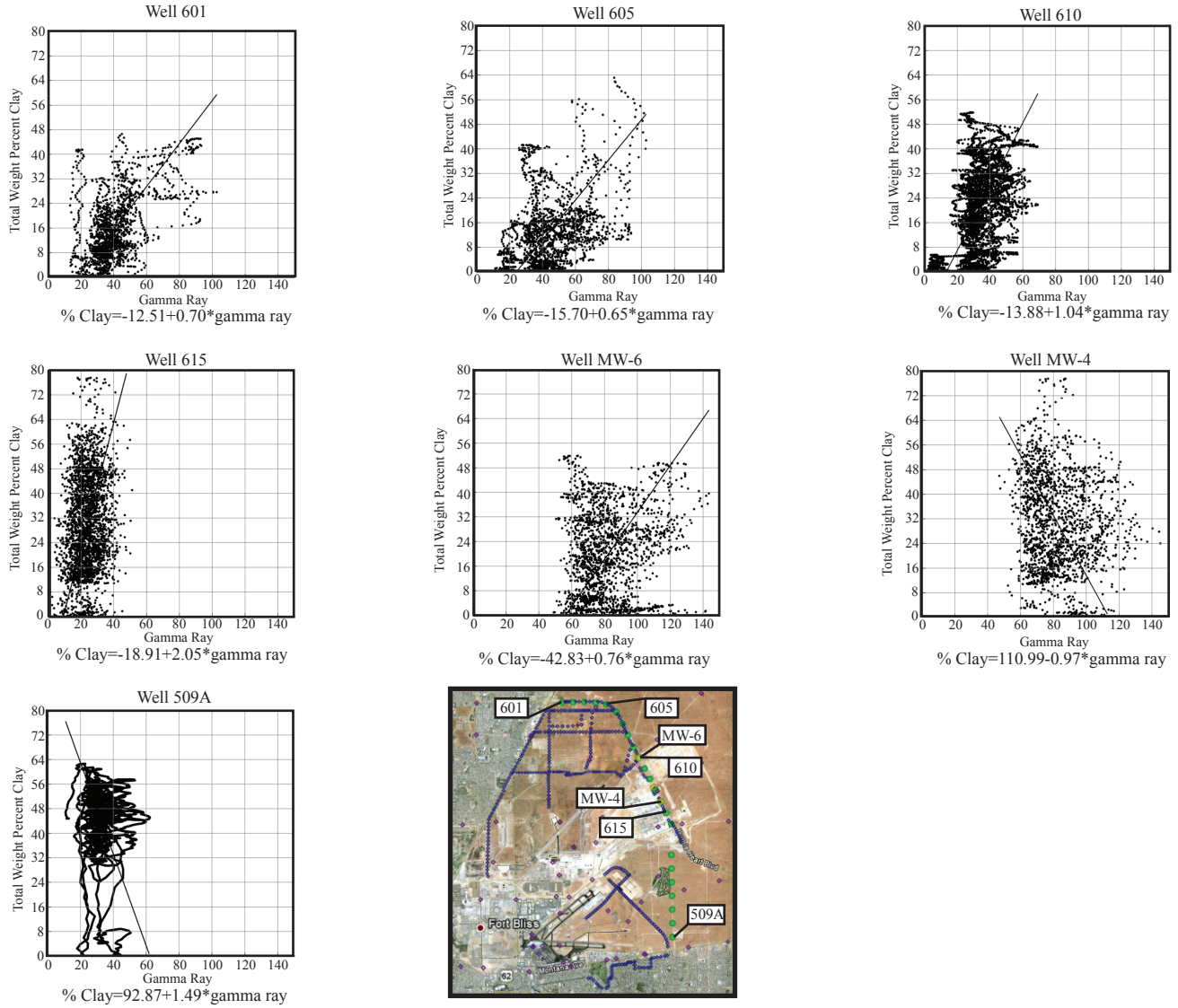

Figure 7. The cross-plots for wells 601 and 605 have similar and reliable best-fit curve equations (bfce) because of the gamma data quality. Well 610 has a similar bfce that closely matches wells 601 and 605, but the gamma data for well 610 is not of the same quality as wells 601 and 605. Wells 615, MW-6, MW-4, and 509A all have different bfce.

quality. Using the average of the regression line equation from the wells with good gamma ray readings, a Vshale (volume of shale) curve was created for all applicable wells to aid in the correlations. Cross-plots for wells MW-6 and MW-4 were created using the clay weight percent from wells 610 and 615, but the regression line equations of these cross-plots are dramatically different from wells 601 and 605. The equations from these wells were not used to create a Vshale curve.

Gravity Data

Gravity measurements were taken throughout the study area with 200 m to 100 m spacings to identify faults using a model G serial number 376 LaCoste and Romberg gravimeter. The gravity stations were taken along road sides (Figure 5) because of the complexities of access within the study area due to its location within a highly urbanized portion of the city of El Paso and on Fort Bliss.

Station positions were determined using a Topcon GB 1000 GPS with ground plane with <±3cm accuracy in elevation and to determine the latitude and longitude of each station. The gravity data collected during this survey were processed using elevations, latitudes, and longitudes.

Several corrections were applied to the gravity data before analysis. First, readings were corrected for instrumental drift and earth tidal effects by looping back to a base station every 2-3 hours. At the beginning and end of each day surveys were tied to the base station at the Kidd Memorial Seismological Observatory on the UTEP campus, where absolute gravity has been measured. Next, a latitude correction was applied to each station to account for the fact the earth is not a perfect sphere and distance to the center of the earth changes with latitude. Then a free-air correction is applied to correct for the difference between the station's elevation and a datum

(sea level). Then a free-air anomaly map was created in Oasis Montaj suites.

Creating a free-air anomaly map helps to identify subsurface gradients, which indicate changes in mass distribution below the surface that could be related to faulting and/or changes in lithology. A profile line was then selected for constructing a 2-D density model and using a forward modeling process to match modeled gravity to observed gravity values. The profile extended from the west side of the Franklin Mountains, across the study area in the Hueco Bolson, and into the Hueco Mountains.

My 2-D density model was based on mapped faults from Collins and Raney (2000) and the previous 2-D density models of Imana (2002). Blocks were created to represent individual lithologies and assigned representative densities, 2.18 g/cc for the Hueco and Mesilla Basin Fill (Bolson), 2.25 g/cc for the Permian, 2.3 g/cc for the Pennsylvanian, 2.4 g/cc for the Mississippian and Devonian, 2.5 g/cc for the Silurian and Ordovician, 2.55 g/cc for a syenite intrusion, 3.0 g/cc for a mafic intrusion (Imana, 2002; Hadi,1991), and 2.7g/cc for basement rock (Imana, 2002; Hadi,1991). After lithologic blocks were created, faults could then be inserted to decrease the error between observed and predicted gravity values to 1.966 mGal.

Hueco Bolson, West Texas Well 601-509A

Plate 1. Well log data from well 601 through 509A showing Gamma Ray (GR), Resistivity (16" and 64"), and Vshale (Vsh) data for applicable wells.

NW

505 ft | 480 ft | 382 ft | 600 ft | 611 ft | 573 ft | 545 ft | 577ft | 532ft | 29ft | 541ft | 549 ft | 399ft | 140ft | 548ft | 16ft | 539ft | 337 ft | 1551ft | 610ft | 609ft | 607ft | 611ft | 607ft | 608 ft

SE

601 | 602 | 603 | 604 | 605 | 606 | 607 | 608 | 609 | 610 | MW-6 | 611 | 612 | MW-5 | 613 | MW-4 | 614 | 615 | 616 | 515A | 514A | 513A | 512A | 511A | 510A | 509A

Results

Well cuttings for wells 601, 605, 610, 615, and 509A were loaned to the Geological Sciences Department at the University of Texas-El Paso by EPWU. The grain-size analysis yielded four defined zones, which can be correlated from well to well based on lithological changes. The changes in lithology are related to changes in grain-size, composition, and the abundance of grain-size classes within each bed. By separating zones marked by lithological changes I can then correlate between wells and identify topographic or environmental changes. The correlations for zones 1-4 for the wells 601 to 509A are shown in Figure 8.

Zones

Zone 1 consists largely of silty clays and clayey silts in various colors (shaded in blue in Figure 8). Silt and clay sized grains form 40-80 percent of all the cutting samples (Figure 8). Beds are typically 3-30 m (10-100 ft) thick. The clays have a reddish color and are compacted. White and tan cuttings are mostly cemented clayey silts. Thin beds of sand are intercalated into the interval in wells 601 and 605. In well 601, the sandy intervals are 10 m (30 feet) thick and appear to both coarsen upwards then fine upwards from 840-770 ft and 770-710 ft. The highest sandy interval then coarsens upwards and remains fairly consistent from 680-590 ft in well 601 (Figure 8). In well 605, the sandy intervals are 3-10 m (10-30 ft) thick and coarsen upwards from 770-740 ft and 710-680 ft, and from 680-600 ft the sands remain at a constant volume then suddenly fine upwards from 600-580 ft. The top of the unit is defined by the fining upwards sequence starting with a prominent coarse sand peak as seen at 480 ft (509A), 500 ft (615), 660 ft (610), 660 ft (605) and 620 ft (601) and is usually found in a red sandy mud bed. Zone 1 gradually thickens from northwest to southeast. This zone parallels bedding as inferred from log patterns.

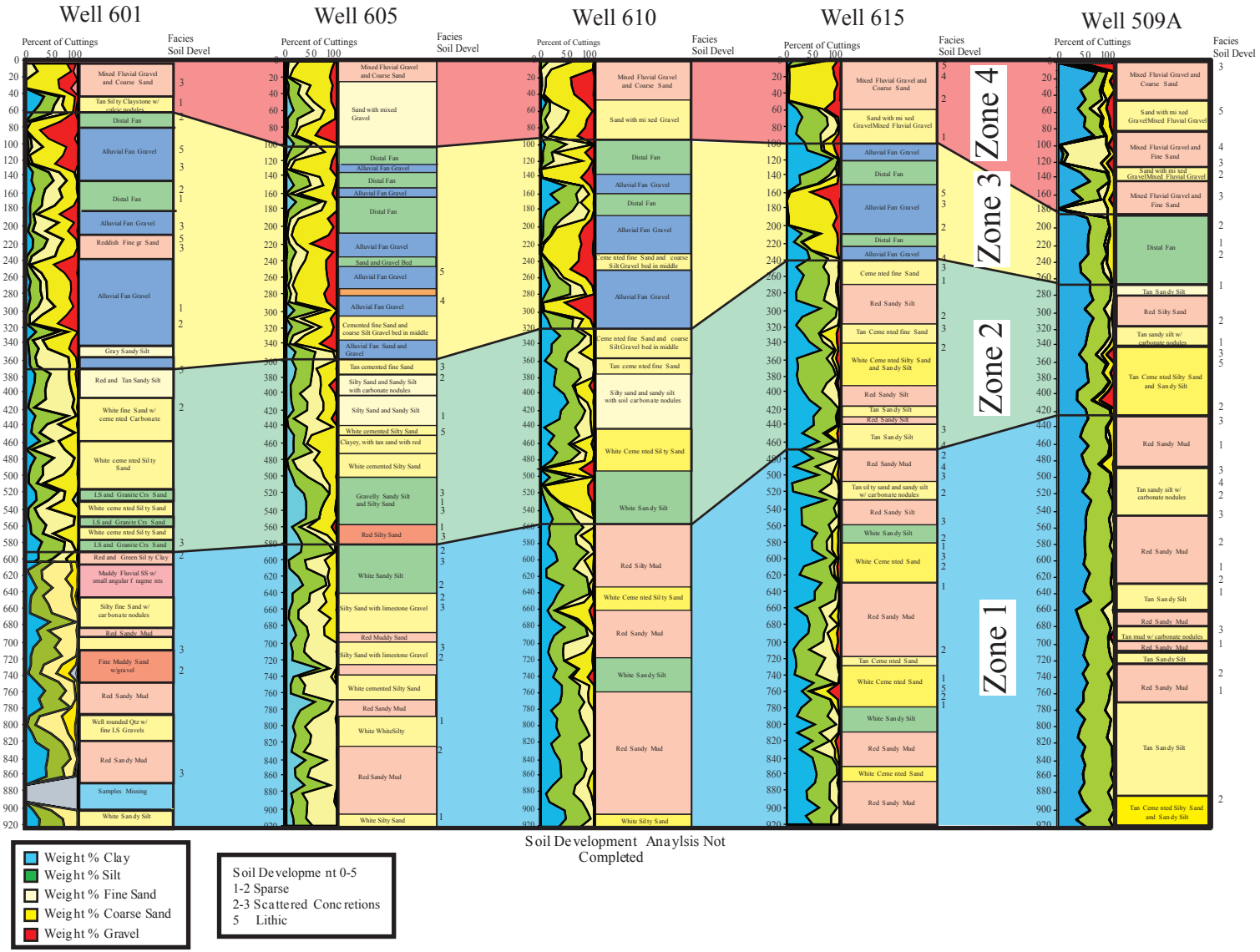

Figure 8. Well cutting grain-size analysis stratigraphy showing correlations for zones 1-4 for wells 601-509A.

Zone 2 consists primarily of clayey silts and silty clays in various colors (shaded in green in Figure 8) with larger quantities of sands and gravels than zone 1 contains. The base of zone 2 is marked by the coarsening upwards sequence with a prominent peak of sand or gravel (well 601 at 570 ft, well 605 at 560 ft, well 610 at 510 ft, well 615 at 470 ft, and well 509A at 410 ft). There are deposits of red clayey silts and silty sands in zone 2 found in wells 605, 615, and 509A. The white and tan cuttings here are mostly cemented sands with carbonate nodules. There are 3 m (10 ft) thick intercalated sand beds with coarse limestone and granite grains. Zone 2 has many alternating coarsening upwards and fining upwards sequences. Well 610 fines upwards from 490-450 ft, then both coarsen upwards and fines upwards from 490-380 ft. All of the wells have these alternating sequences. The top of this zone is defined by a clayey sandy silt fining upwards sequence found in most wells (610 to 509A). Zone 2 parallels bedding and gradually thickens from 220-240 ft from well 601 to 615 and then thins from well 615 to 509A.

Zone 3 is composed of 60-75 percent sands and gravels with the exception of well 509A which only has 27 percent (shaded in yellow in Figure 8). The base of zone 3 for wells 601-615 is identified by an apparent upwards coarsening from silty sands to coarse sands and gravels (well 601 from 370-340ft, well 605 from 360-340 ft, well 610 320-270 ft, and well 615 from 240-150 ft) and for well 509A the upwards coarsening from silty clays to sandy silty clays (270-240ft) (Figure 8). There are gravel beds from 3-30 m (10-100 ft) thick in wells 601 to 615. Well 509A does not have any gravel beds and instead has a sandy silty clay sheet deposit that is 24 m (80 ft) thick. There are alternating upwards fining and coarsening gravel and sand sequences for wells 601 to 615. Wells 605 (330-310 ft) and 610 (270-230 ft) both have a 6 m(20 ft) thick fine sand and coarse silt cemented gravel bed (Figure 8). Well 601 has a 10 m (30 ft) thick reddish

colored bed with upwards fining sand. Zone 3 parallels bedding (inferred from log patterns) and gradually thins from northwest to south east.

Zone 4 consists largely of sands with mixed gravels and rounded to well-rounded gravels and sands (shaded in red in Figure 8). The base of zone 4 is marked by the appearance of rounded to well-rounded sands and gravels (well 605-509A), or upwards coarsening silty clays (well 601) (Figure 8). There are 6-18 m (20-60 ft) thick beds of rounded to well-rounded (fluvial) coarse sands and gravels. Well 509 has intercalated 10-12 m (30-40 ft) thick beds of fluvial sands and gravels. The log patterns identified in zone 4 have upwards fining sequences that begin with an abrupt appearance of gravels and coarse sediments. The thickness of this zone remains consistent then thickens abruptly over nearly equal distances (9000 ft or 2745 m apart), with the exception of well 509A (16,400 ft or 5000 m) which is almost double the distance.

Grain-size Comparison

Figure 9 shows the overall average grain-size weight percentage distribution for the five analyzed wells. Well 509A has the highest weight percentages of clay and silt and well 615 has the second highest. This chart shows that there is a higher concentration of clay heading southeast towards wells 615 and 509A (Figure 9).

Well 601

Well 601 is located closest to the Franklin Mountains approximately 3.4 miles (5.5 km) away. Also, well 601 lies within the fresh water section of the HBA.

Zone 4 ranges from 0-60 ft (Figure 10 and Table 1). Zone 1 is largely sand (-1φ - 4φ) (63.2%) and gravel (<-1φ) (15.9%) with small amounts of silt (4φ - 8φ) (9.8%) and clay (>8φ) (11.1%).

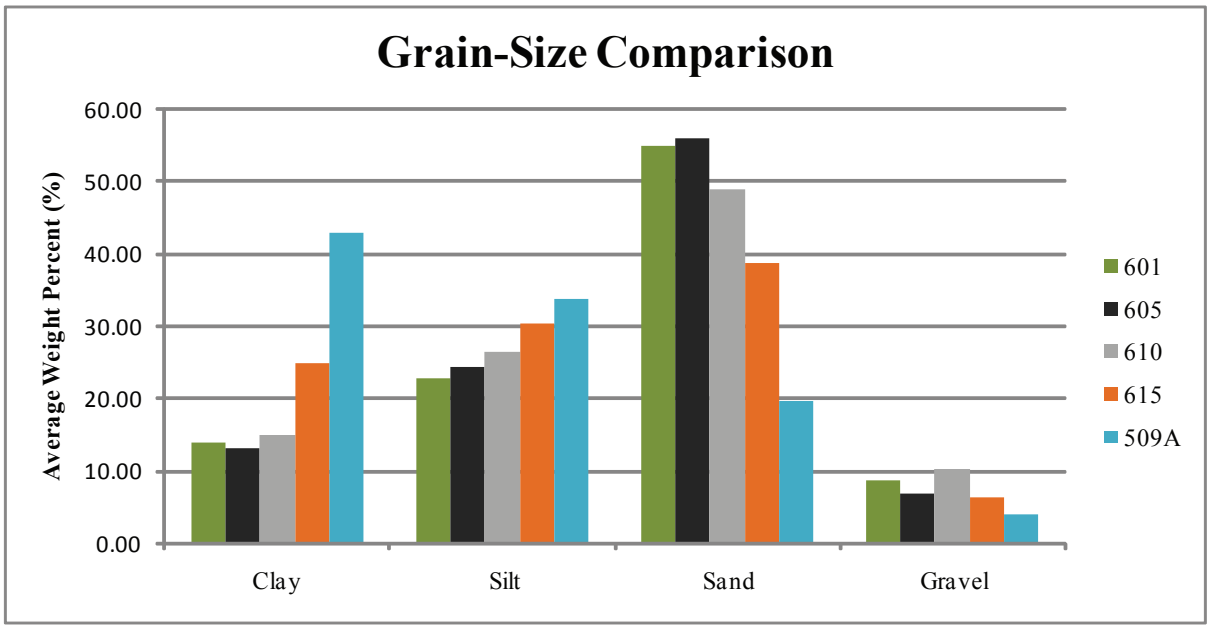

Figure 9. This graph shows the grain-size distribution for wells 601 (green), 605 (black), 610 (grey), 615 (orange), and 509A (blue) that were seived. Wells 615 and 509A have the highest concentrations of clay and silt.

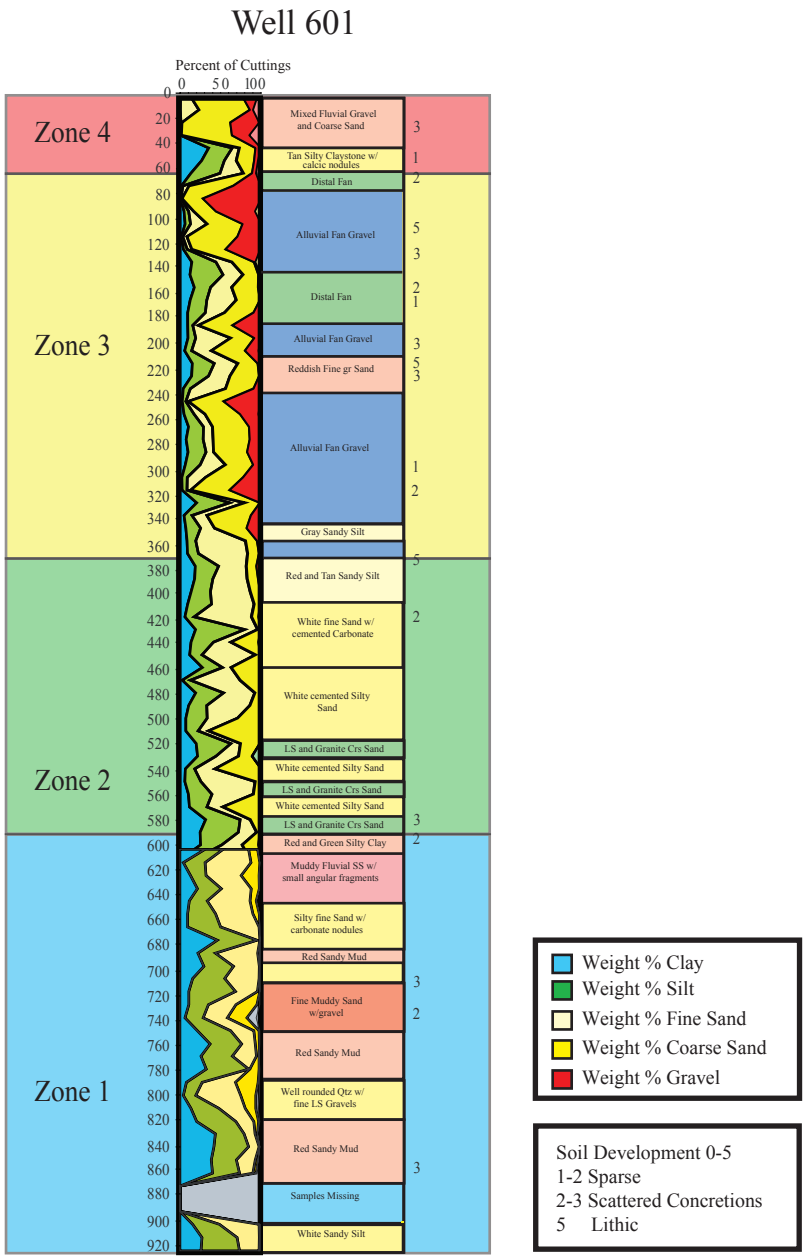

Figure 10. Well 601 is separated into four zones, which show the change in sediment size and upward coarsening.

Table 1. Weight percent distribution of grain sizes for well 601 from zones 1-4 and overall percentages.

Well 601	Depth (ft)	Weight % Clay (>8φ)	Weight % Silt (4φ-8φ)	Weight % Sand (-1φ - 4φ)	Weight % Gravel (< -1 φ)	Total % Sand and Gravel (<4φ)	Total % Silt and Clay (>4φ)
Zone 1	590-910	16.4	31.6	52.0	0.0		
Zone 2	370-590	14.5	26.6	58.0	0.9		
Zone 3	60-370	9.1	16.0	57.0	17.9		
Zone 4	0-60	11.1	9.8	63.2	15.9		
Overall	0-910	13.9	22.8	54.7	8.6	63.3	36.7

Zone 3 ranges from 60 ft to 370 ft with an average percent gravel (< -1 φ) of 17.9% and percent sand (-1φ - 4φ) of 57.0%. Zones 3 and 4 contain nearly all of the gravel within the well.

Zone 2 ranges from a depth of 370-590 ft. Clay (>8φ) and silt (4φ - 8φ) content increase in this zone with a combined weight percent average of 41.1% with a higher volume of silt than clay; while the weight percent gravel decreases to 0.9%.

Zone 1 ranges from 590-910 ft and is predominately fine-grained clays (>8φ) and silts (4φ - 8φ). The percent clay is highest in this zone at 16.4%. There was no gravel within this zone indicating that sediments are coarsening upwards in well 601. Overall, this well contains a higher percentage of gravel and sand (< 4φ) at 63.3% than silt and clay (> 4φ) at 36.7%.

Well 605

Well 605 is 6816 ft (2077.5 m) east of well 601 and located within the fresh water section of the aquifer. Figure 11 shows zones 1-4 in well 605 and Table 2 shows the total percentages of the distributed grain-sizes throughout the well.

Zone 4 ranges from 0-100 ft and thickens by 40 ft from well 601. This zone is largely sand (-1φ-4φ) and gravel (<-1φ) with percentages of 62.4% and 13.1% respectively. There is an increase of percent silt (4φ - 8φ) (18.1%) and a decrease in percent clay (>8φ) (6.4%) from well 601.

Zone 3 (100-360 ft) is 50 ft thinner than in well 601 and has the second highest gravel (<1φ) weight percentages for well 605, 12.3%. The weight percentages for zone 3 and 4 are very similar (Table 2).

Zone 2 ranges from depths of 360-580 ft and is primarily sand and silt averaging 79.3%. This zone has the same thickness of 220 ft from well 601 to 605. Zone 2 has higher clay content (17.7%) than zones 3 and 4 (12.9%) combined.

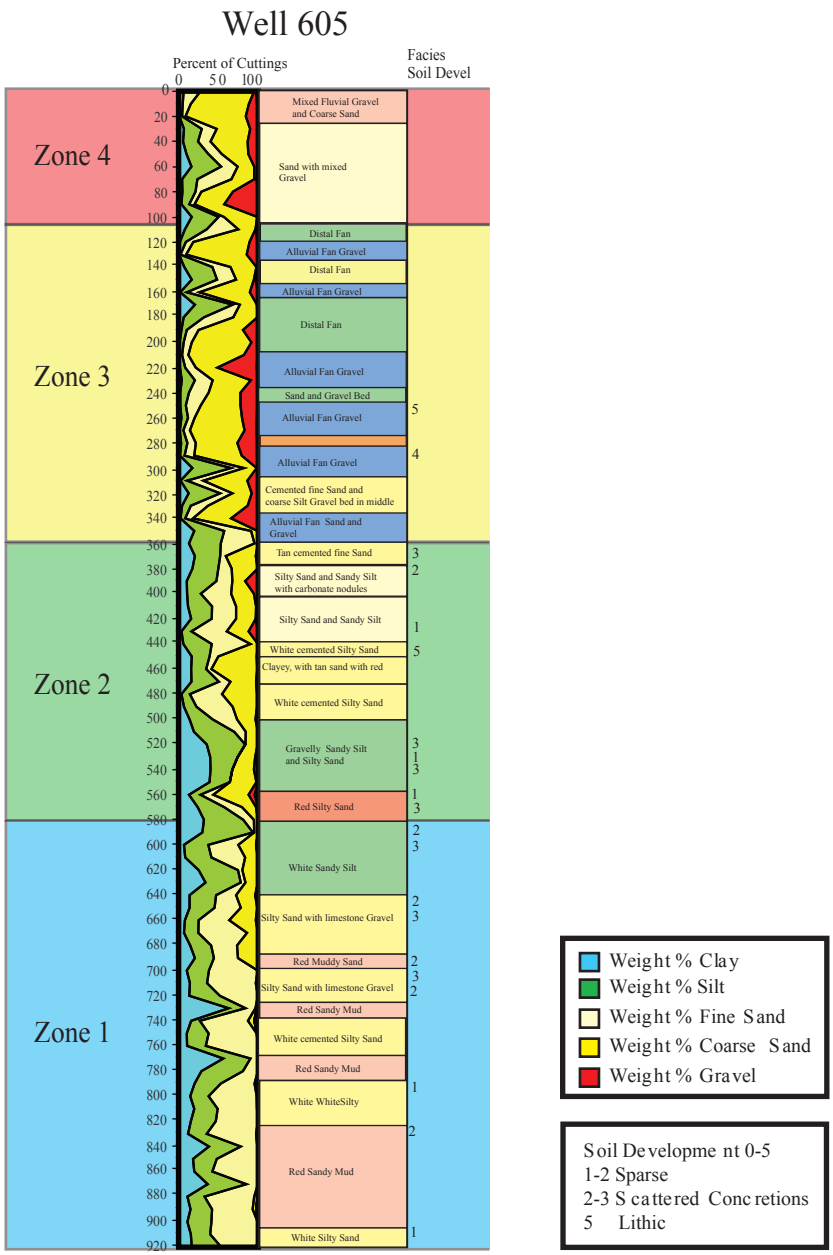

Figure 11. Well 605 is separated into four zones, which show the change in sediment size, upward coarsening, and several sequences of upwards fining.

Table 2. Weight percent distribution of grain sizes for well 605 from zones 1-4 and overall percentages.

Well 605	Depth (ft)	Weight % Clay (>8φ)	Weight % Silt (4φ-8φ)	Weight % Sand (-1φ - 4φ)	Weight % Gravel (< -1 φ)	Total % Sand and Gravel (<4φ)	Total % Silt and Clay (>4φ)
Zone 1	580-920	20.5	31.1	48.0	0.4		
Zone 2	360-580	17.7	29.2	50.1	3.0		
Zone 3	100-360	6.5	18.4	62.7	12.3		
Zone 4	0-100	6.4	18.1	62.4	13.1		
Overall	0-920	13.0	24.3	55.9	6.9	62.7	37.3

Zone 1 (580-920ft) has the highest percent clay average compared to the other three zones at 20.5% clay. The sand (-1φ - 4φ) weight percent average is 48.0%, silt (4φ - 8φ) is 31.1%, and there is almost no gravel (<1φ) in zone 1(0.4%).

In total, this well contains a higher weight percent of sand and gravel (<4φ) (62.7%) than silt and clay (>4φ) (37.3%), similar to well 601. The weight percent of silt and clay (>4φ) increases from well 601 to 605.

Well 610

Well 610 is located 9708 ft (2959 m) southeast from well 605. This well is not only located within a fault zone, but also within the transition boundary from fresh to brackish water. Figure 12 shows zones 1-4 in well 610 and Table 3 shows the total percentages of the distributed grain-sizes throughout the well.

Zone 4 ranges from 0-100 ft, which is the same thickness as well 605. This zone has 18.2% gravel (<-1φ) and is predominately comprised of sand (-1φ - 4φ, 69.4%). The percentage of gravel in this zone is higher than well 601 or 605. There are also lower concentrations of silt (4φ- 8φ, 9.4%) and clay (>8φ, 3.0%) in well 610 than wells 601 and 605.

Zone 3 ranges from 100-320 ft. Percent gravel is 12.70%, sand is 55.48%, and silt is 21.22%. The average percent of clay (10.60%) is increasing. Zones 3 thinned a total of 70 ft from well 605 to 610.

Zone 2 ranges from 270-580 ft thinning 40 ft from well 605 and contains a higher average weight percent of sand (-1φ - 4φ, 39.0%) than any other grain-size with almost the same volume of silt (4φ - 8φ, 35.1%). The volume of clay (>8φ) is 22.9%, and gravel (<-1φ) 3.0%. The clay volume for zone 2 is gradually increasing from well 601 to 610.

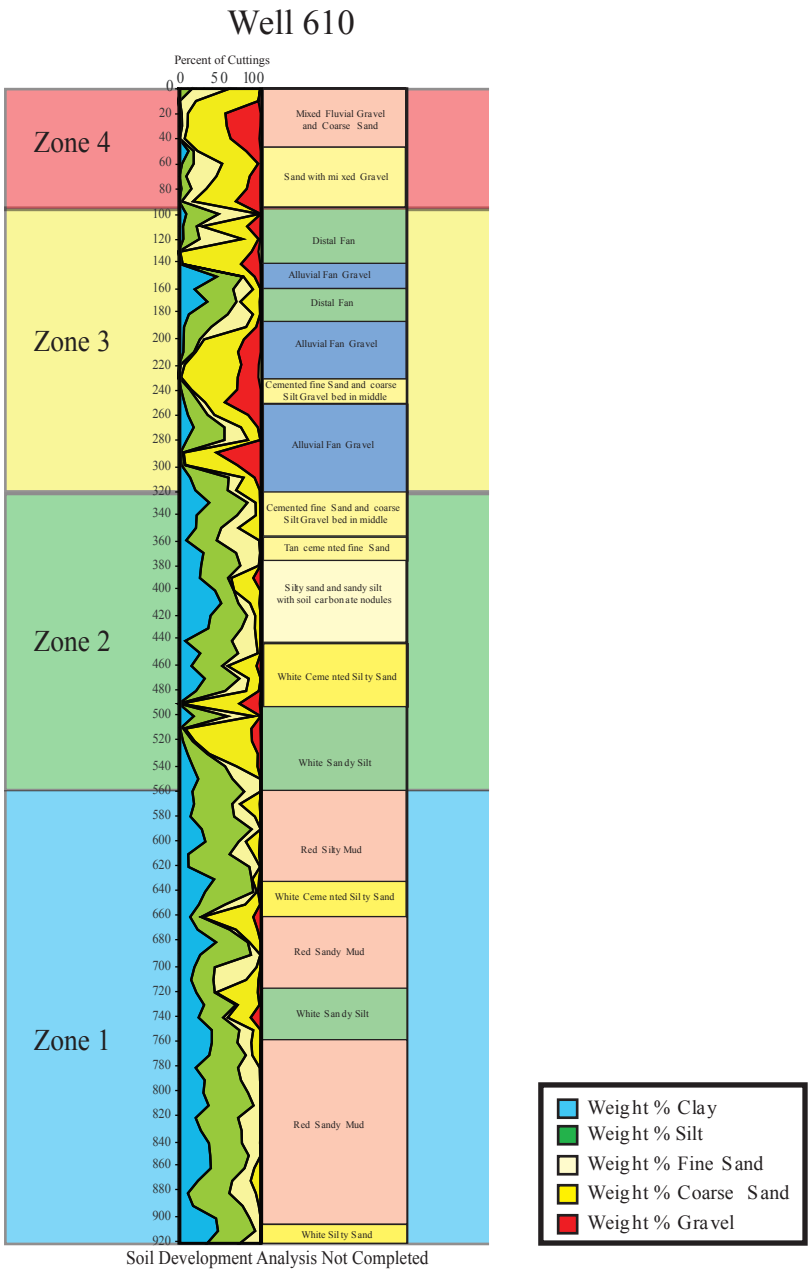

Figure 12. Well 610 is separated into four zones, which show the change in sediment size, upward coarsening, and several sequences of upwards fining. There is an increase in clay in this well compared to wells 601 and 605.

Table 3. Weight percent distribution of grain sizes for well 610 from zones 1-4 and overall percentages.

Well 610	Depth (ft)	Weight % Clay (>8φ)	Weight % Silt (4φ-8φ)	Weight % Sand (-1φ - 4φ)	Weight % Gravel (< -1 φ)	Total % Sand and Gravel (<4φ)	Total % Silt and Clay (>4φ)
Zone 1	560-920	26.8	44.8	27.3	1.2		
Zone 2	320-560	22.9	35.1	39.0	3.0		
Zone 3	100-320	10.7	23.3	51.0	15.0		
Zone 4	0-100	3.0	9.4	69.4	18.2		
Overall	0-920	14.8	26.3	48.7	10.1	58.9	41.1

Zone 1 ranges from 560-920 ft and silt (4φ - 8φ) is the dominant grain-size in this zone with a volume of 44.8% followed by sand (-1φ - 4φ) at 27.3% and clay (>8φ) at 26.8%. The volume of gravel is 1.2%, whereas wells 601 and 605 had almost all gravel in this zone. This is the first prominent appearance of interbedded muddy gravels.

Overall, this well contains a higher percentage of sediment <4φ (58.9%) than > 4φ (41.1%). The total percent clay (>8φ) increased by 0.9% from well 610 to 601 and silt (4φ - 8φ) by 3.5%. There is a steady decrease of the total weight percent of gravel (<-1φ) and sand (-1φ - 4φ) from well 601 to 610 and a gradual increase for silt (4φ - 8φ) and clay (>8φ).

Well 615

Well 615 is located 9204 ft (2806 m) southeast from well 610 and is located within the brackish section of the aquifer. Continuing with the trend, well 615 has an increase of clay (>8φ) content and contains more clay than the other analyzed 600 series wells. Zones 1-4 for well 601 are shown in Figure 13 and Table 4 shows the total percentages of the distributed grain-sizes throughout the well.

Zone 4 ranges from 0-100 ft maintaining the same thickness as in well 610. There is a high percentage of clay (>8φ) in this zone of 10.8% and the volume of gravel (<-1φ) is 9.2%. There is a higher volume of sand (-1φ - 4φ, 57.5%) and silt (4φ - 8φ, 21.9%) in this zone than clay and gravel. There is a dramatic decrease of gravel in this zone compared to wells 601 to 610, which indicates a decrease in energy for this region of the study area.

Zone 3 ranges from 100-240 ft thinning 80 ft from well 610 and has the highest gravel (<-1φ) volume of the well at 12.2%. This well shows a dramatic increase in clay (>8φ) volume for this zone compared to the other 600 series wells at 23.7%. This zone has a higher volume of clay and sand (44.8%) than silt (19.1%) and gravel.

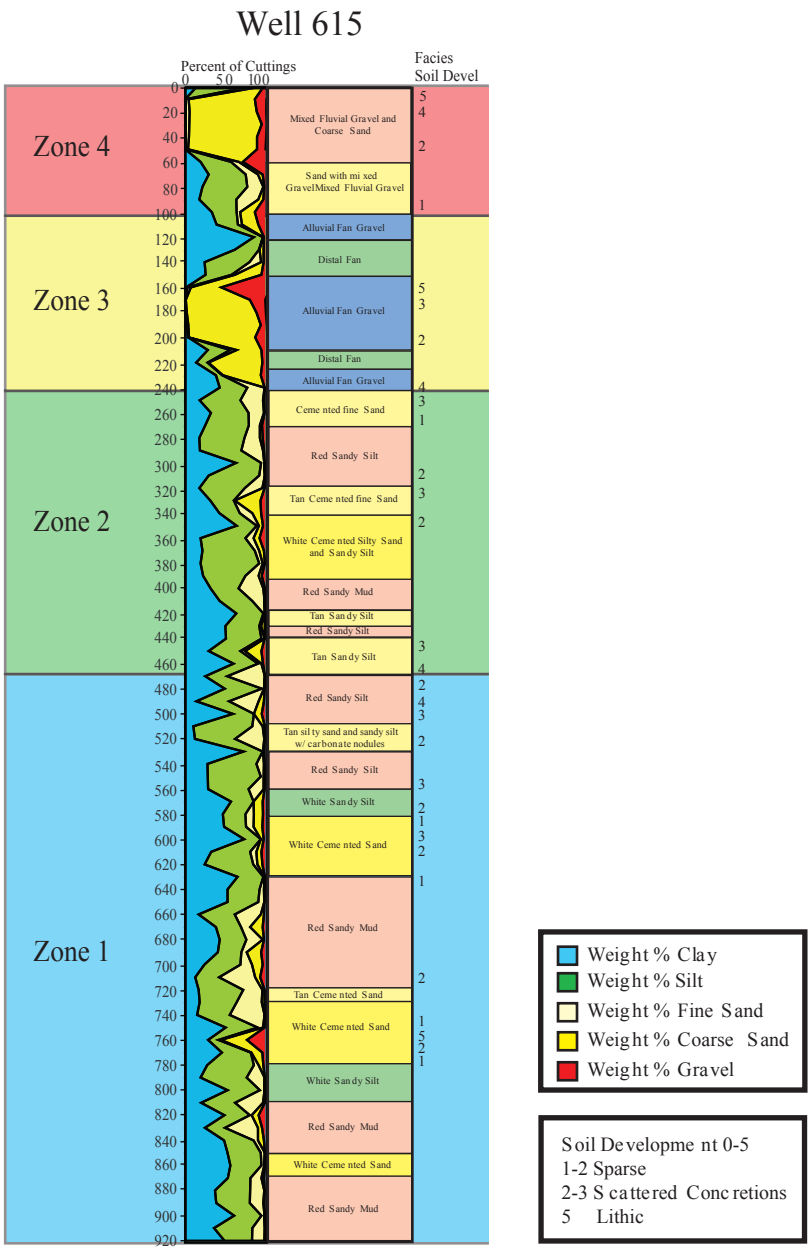

Figure 13. Well 615 is separated into four zones and shows the highest amounts of clay in the 600 series wells.

Table 4. Weight percent distribution of grain sizes for well 615 from zones 1-4 and overall percentages.

Well 615	Depth (ft)	Weight % Clay (>8φ)	Weight % Silt (4φ-8φ)	Weight % Sand (-1φ - 4φ)	Weight % Gravel (< -1 φ)	Total % Sand and Gravel (<4φ)	Total % Silt and Clay (>4φ)
Zone 1	470-920	33.3	38.7	26.4	1.5		
Zone 2	240-470	30.9	41.1	25.9	2.0		
Zone 3	100-240	23.7	19.1	44.8	12.2		
Zone 4	0-100	10.8	21.9	57.5	9.2		
Overall	0-920	24.7	30.2	38.7	6.2	44.9	54.9

Zone 2 ranges form 240-470 ft and has thinned 10 ft from well 610. This zone has a higher volume of silt (4φ - 8φ, 41.1%) and clay (>8φ, 30.9%) than sand (-1φ - 4φ, 25.9%) and gravel (<-1φ, 2.0%). This zone increased in the amount of clay compared to well 610 despite the decrease in thickness.

Zone 1 ranges from 470-920 ft and is largely comprised of silt (4φ - 8φ, 38.7%) and clay (>8φ, 33.3%). As in well 610, well 615 has a small volume of gravel (<-1φ) in zone 1 at 1.5%, where the muddy gravel deposits can still be correlated between the two wells.

Overall, well 615 has shown an increase of clay content by 9.9% compared to well 610. For well 615, the total volume of sediments >4φ is 54.9% and <4φ is 44.9%, where for wells 601-610 all had a higher volume of sediments <4φ. There is a transition from higher concentrations of gravel and sand in wells 601-610 to higher concentrations of silt and clay in well 615.

Well 509A

Well 509A is located 16,400 ft (5000 m) south of well 615 and in the brackish section of the HBA. This is the southernmost well in the study area and was the only well analyzed from the 500 series. Figure 14 shows zones 1-4 in well 601 and Table 5 shows the total percentages of the distributed grain-sizes throughout the well.

Zone 4 ranges from 0-190 ft and increases in thickness by 90 ft from well 615. The volume of clay (>8φ) in this well is the highest compared to all of the other analyzed wells at 36.1%. The gravel (<-1φ) content in this zone is 10.2%, which is the one of the lowest volumes of the analyzed wells for this zone. The sand (-1φ- 4φ) volume for this zone is 30.5% and has higher volumes of clay and sand.

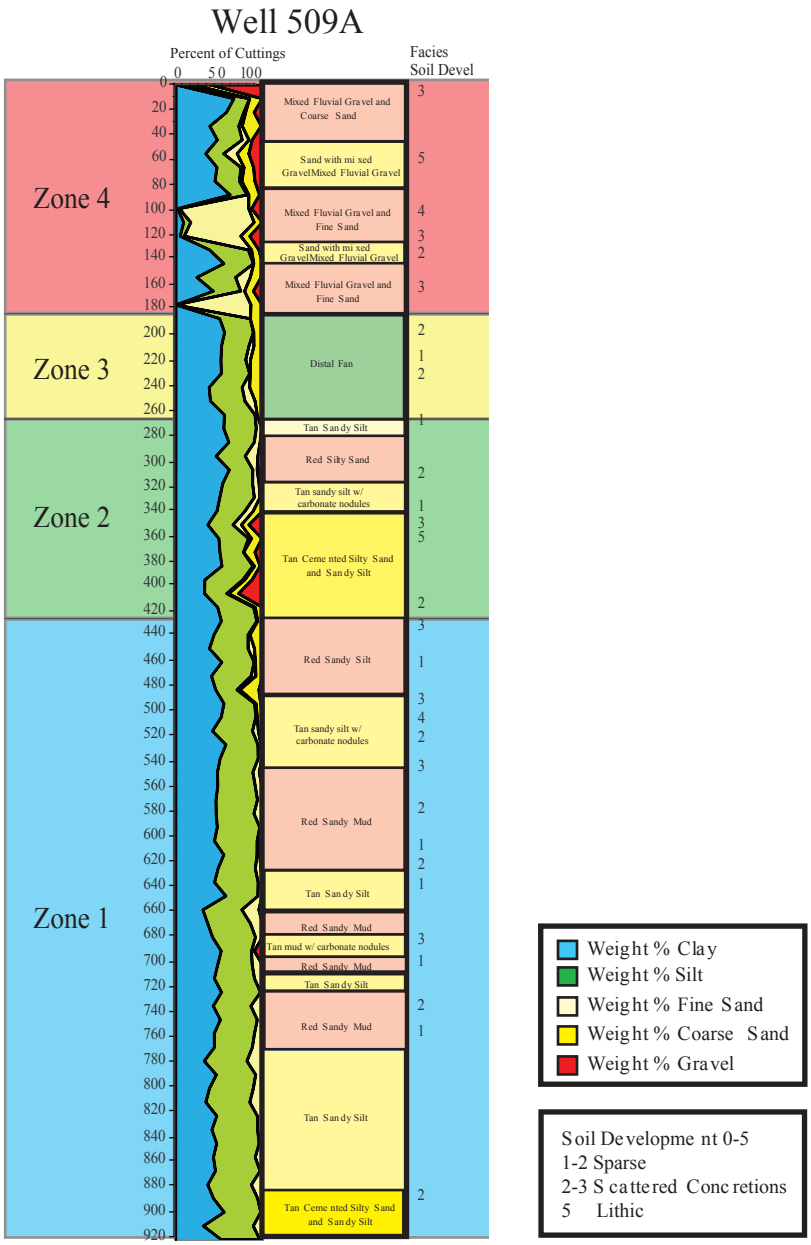

Figure 14. Well 509 A is separated into four zones and contains the highest amounts of clay of the wells analyzed.

Table 5. Weight percent distribution of grain sizes for well 509 A from zones 1-4 and overall percentages.

Well 509 A	Depth (ft)	Weight % Clay (>8φ)	Weight % Silt (4φ-8φ)	Weight % Sand (-1φ - 4φ)	Weight % Gravel (< -1 φ)	Total % Sand and Gravel (<4φ)	Total % Silt and Clay (>4φ)
Zone 1	430-900	45.8	44.8	9.0	0.4		
Zone 2	270-430	48.7	34.7	12.5	4.1		
Zone 3	190-270	40.8	31.7	26.2	1.2		
Zone 4	0-190	36.1	23.1	30.5	10.2		
Overall	0-900	42.9	33.5	19.6	4.0	23.5	76.4

Zone 3 ranges form 190-270 ft and thins about 60 ft from well 615. This zone has the lowest gravel (<-1φ) volume of all other analyzed wells at 1.2%. The clay (>8φ) content in this zone is 44.8% and is the highest for zone 3 compared to the other analyzed wells. This zone show a higher volume of sediments >4φ (72.5%) with silt at a volume of 31.7%.

Zone 2 ranges form 270-430 ft thinning about 70 ft from well 615. Just like zone 3, zone 2 has higher volumes of clay (>8φ, 48.7%) and silt (4φ - 8φ, 34.7%) than sand (-1φ- 4φ, 12.5%) and gravel (<-1φ, 4.1%). This zone has the highest concentration of clay compared to the other analyzed wells.

Zone 1 ranges from 430-900 ft and continues the trend of higher clay (>8φ, 45.8%) and silt (4φ - 8φ, 44.8%) volumes than sand (-1φ- 4φ, 9.0%) and gravel (<-1φ, 0.4%) seen in zones 2 and 3. Well 509A has the highest clay content for zone 1 compared to the other analyzed wells.

Overall, well 509A has the highest volume of clay (42.9%) compared to the other analyzed wells and the lowest gravel volume (4%). Well 601 contains a higher volume of gravel (8.6%) and a lower volume of clay (13.9%) in comparison to well 509A.

In summary, there is an increase in the volume of clay from the northwest section of the study area to the southeast. The wells in the fresh water part of the aquifer have a higher concentration of coarse-grained sediments (<4φ) and the wells in the brackish part have a higher concentration of fine- grained sediments (>4φ).

Well Log Analysis

The available log curves (recorded in electronic form) are gamma (GR), resistivity (shallow 16" and deep 64"), and spontaneous potential (SP). Volume shale (Vshale) log curves were created by creating cross-plots (Figure 7) plotting gamma ray readings against clay volume. The Vshale curve was used alongside the gamma ray and resistivity curves to help provide a

more accurate assessment of clay volume for the wells with good gamma ray curves that did not have grain-size analysis completed. The log curves were used to correlate between wells, and structural and stratigraphic cross-sections were then created to interpret the subsurface (Plates 2 and 3).

Gamma Ray Logs

Gamma logs detect radioactive decay within the different sediment layers of the well (Asquith and Krygowski, 2004). The higher the decay count the more radioactive elements are present in that layer. Usually, shales and clays have more radioactive minerals and higher decay counts than sands and gravels (Asquith and Krygowski, 2004). The El Paso region is an exception to this norm because the local source rocks that produce sand sized particles have higher concentrations of potassium and uranium (granite and rhyolite from the Franklin Mountains) (Doser and Langford, 2007). Grain-size analysis showed that within the study area clays can still be reliably identified by their higher gamma values.

The gamma ray log curves for wells 601-612, MW-6-MW-4, and 509A have good data quality that can be used for correlation and/or to create an accurate Vshale log curve. Wells 613-616 and 515A-510A have poorer data quality and could not be used for correlation or to create a Vshale log curve (Plate 1 and 2). The gamma logs are scaled from 0-150 API. Wells with high data quality have sands that correlate with gamma peaks that range from 15- 80 API units and shale peaks that range ranging from 80-148 API (Table 6 and 7). The data in both Table 6 and 7 were acquired from a cross-plot of Vshale on the x-axis and deep resistivity (64") and gamma ray activity on the x-axis.

Table 6. This table shows the gamma ray and deep resistivity values for sand at depths below the water table (400 ft) for all the wells with Vshale curves. The wells colored in light blue are located in the fresh water section of the aquifer. The wells colored in purple lie within the tranisition zone and brackish section of the aquifer.

Well	Grainsize	Gamma Ray	Resistivity (64")
601	SAND	20-50	15-50
602	SAND	20-50	11-51
603	SAND	20-50	15-40
604	SAND	20-50	15-36
605	SAND	20-45	11-41
606	SAND	20-50	11-41
607	SAND	20-50	15-40
608	SAND	20-50	15-39
609	SAND	20-50	12-30
MW-6	SAND	49-80	8-35
MW-5	SAND	50-80	8-40
MW-4	SAND	15-80	9-35
509A	SAND	20-35	1-30

Table 7. This table shows the gamma ray and deep resistivity values for clay at depths below the water table (400 ft) for all the wells with Vshale curves. The wells colored in light blue are located in the fresh water section of the aquifer. The wells colored in purple lie within the tranisition zone and brackish section of the aquifer.

Well	Grainsize	Gamma Ray	Resistivity (64")
601	CLAY	80-105	10-35
602	CLAY	65-80	11-25
603	CLAY	70-105	12-25
604	CLAY	70-105	11-30
605	CLAY	80-105	10-35
606	CLAY	65-95	9-25
607	CLAY	65-110	7-25
608	CLAY	65-110	9-31
609	CLAY	65-105	8-20
MW-6	CLAY	110-145	9-20
MW-5	CLAY	111-148	5-18
MW-4	CLAY	110-148	8-18
509A	CLAY	45-65	5-16

Resistivity Logs

Resistivity logs measure the ability of an interval to conduct electricity. There were two resistivity curves provided for these wells a shallow (16") and deep (64") resistivity. All of the wells provided have good quality resistivity logs and were used to help correlate between wells with poor gamma log curves. The correlations between resistivity values may have a higher correlation error because resistivity can change laterally within an interval if grain-size, salinity, or water saturation changes within the interval.

Resistivities are scaled from 1-200 Ohm-m. The water table is estimated to be around 400-450 ft deep within the study area (Hutchison, 2006). Since resistivity depends on grain-size and salinity, two different tables were created to reflect sand and clay resistivity values below the water table (Tables 6 and 7). The wells colored in blue lie in the fresh water section of the aquifer, wells in purple lie in the transition zone and the brackish water section of the aquifer. Over all, the trend in the range of resistivities in the fresh water wells are higher than the wells in the transition zone, and the range of resistivities in the transition zone are higher than in the brackish section of the aquifer. The same trend holds true for the clay intervals shown in Table 7. Water with higher salinities has lower resistivity values. Another trend identified in the cross-plots shows that resistivity values are lower at greater depths in the wells indicating a salinity increase with depth (Figure 15). The effect is particularly marked below 600 ft where each 100 ft interval is lower in resistivity that the preceding interval.

Interval Tops

T4 Unit

Interval tops were chosen using the stratigraphy identified through grain-size analysis and based on observed depositional changes seen in the gamma and resistivity logs (Plates 2 and 3).

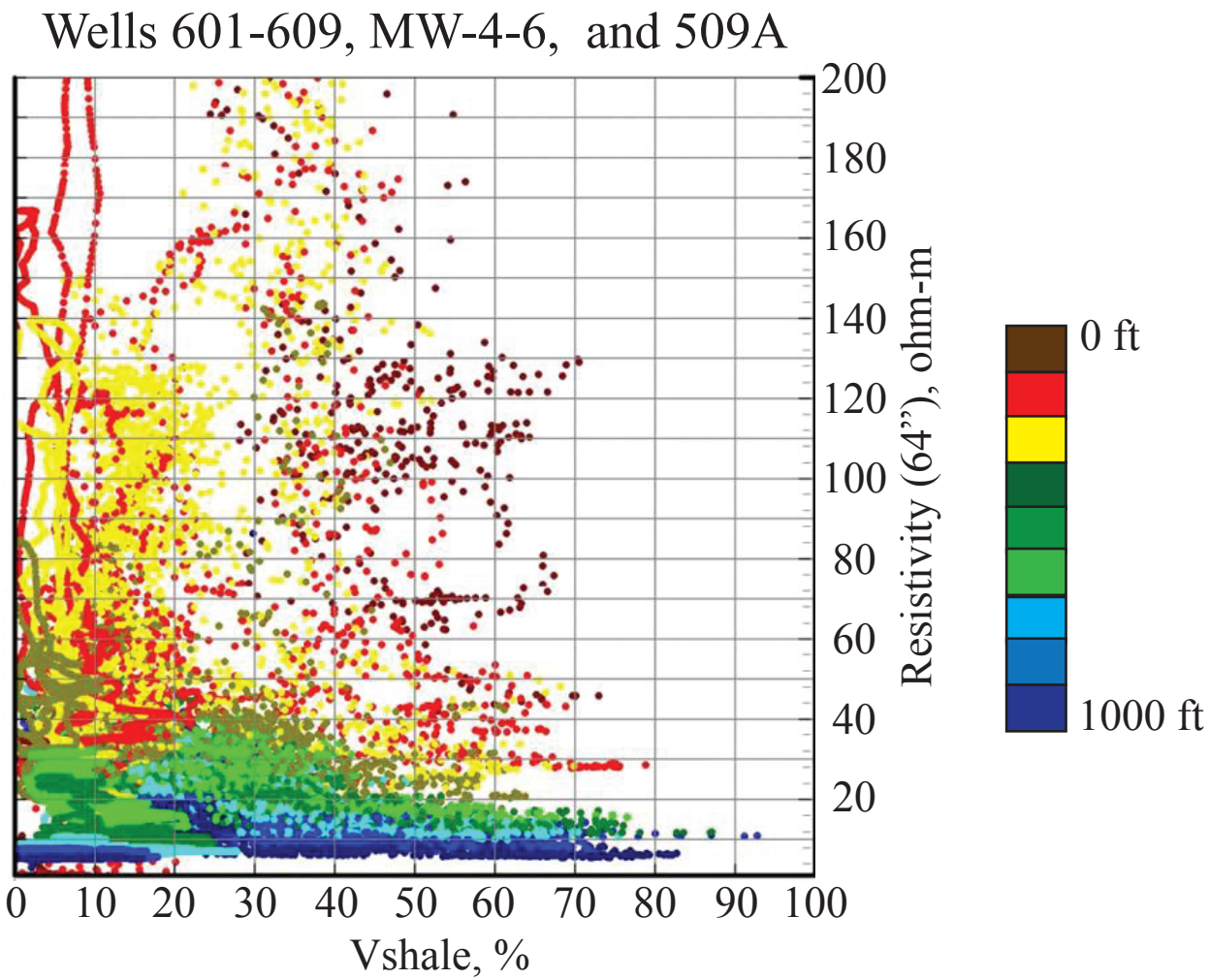

Figure 15. The Vshale values plotted were derrived from the grain-size analysis conducted on wells 601, 605, 610, 615, and 509A at 10 ft intervals. The corresponding resistivity values are at the given depth interval of the Vshale value. This cross-plot shows the decrease in resistivity with depth, where blue colors are at greater depths than brown and red colors.

The unit T4 (shaded in red in Plates 2 and 3) top (not identified in correlations) is the surface (0 ft) for each well. The T4 unit is equivalent to Zone 4 identified in Figure 8, which contains the Rio Grande River deposits as inferred from the cuttings. The base of T4 is not easily correlable between the log curves in the study area. In this interval, surface casing and hole collapse create an interval that provides unreliable log response in wells 511A-509A and MW-4-6. The lower boundary for the T4 interval was identified using the depths found through well cutting analysis (Figure 8) and correlated from well to well assuming an average of 100 ft depth for most wells. The T4 interval has an upwards fining sequence seen in gamma and resistivity curves from the base up as identified in wells 512A-509A and MW-4-6. In wells MW-4-6 the upwards fining sequence is followed by the abrupt appearance of blocky sand and only in MW-4 does it then fine upwards in the gamma log, while the resistivity log remains blocky. The base of the T4 interval going into the T3 interval shows a well defined funnel shape that is best expressed in wells 612 and MW-4. In the northwest, in wells 601 through 604, the logs are serrate, and an upward coarsening is not evident. The Vshale logs show an increase in shale with depth for T4 in wells MW-6 and MW-5.

The cuttings of T4 all contain gravel. In wells 601 through 610, this is a dominant component. However, gravel percentages decrease to 9.2% and 10.2% in wells 615 and 509A, respectively (Tables 4 and 5). Silt and clay percentages increase to the southeast from well 601 to 509A (Tables 1-5). Plate 3 shows the stratigraphic changes in thickness of the T4 unit, which remains nearly consistent in thickness until the 500 series wells. At well 515A T4 begins to gradually thicken until at well 511A where it becomes abruptly thicker. This signature of the well log curves, the grain-size analysis modeling creating log curves (Figure 8), composition of the cuttings, and the rounded to well-rounded sands (far travelled) and large sub-angular to

rounded gravel clasts indicate a channel fill or fluvial deposit. These were likely deposited by the ancestral Rio Grande River.

T3 Unit

The T3 unit (shaded in yellow in Plates 2 and 3) top is identified by two stacked funnel patterns in gamma and resistivity logs and interpreted as two upward coarsening sequences each with a flat top. The T3 unit is equivalent to Zone 3 indentified in Figure 8. The T3 unit has several stacked sequences showing upwards coarsening with gamma and resistivity logs best expressed in wells MW-5 and 4 between 100 and 300 ft. These sequences are best seen in the resistivity curves for most of the wells. Well MW-4 is a good representation of these sequences for both the gamma and resistivity logs. The lower sequence is barrel shaped in MW-4 as it is in most wells and generally seems coarser that the overlying sequence. The upper sequence is serrated and is inferred to contain discontinuous muds that cannot be correlated to adjacent wells. The base of the T3 unit is marked by a well defined inflection that is interpreted as a continuous shale bed. In some wells (612 and MW-4) the shale forms the base of a thin (5 m thick) well-defined upward coarsening sequence. The boundary between the base of the T3 interval going into the top of the T2 unit shows fining upwards sequence best expressed in well MW-4 in both gamma and resistivity logs. The Vshale curves show a fairly consistent volume of clay throughout the T3 unit with several increases in clay marking the tops of the upward coarsening sequence.

The well cuttings of T3 contain a higher ratio of sand and gravel to silt and clay in wells 601 to 615 and a higher ratio of silt and clay to sand and gravel in well 509A. This indicates a decrease in coarse grains (<4φ) from northwest to southeast (Tables 1-5). Plate 3 shows a gradual and nearly consistent decrease in thickness in unit T3 from well 601 to 509A. There is

an abrupt increase in thickness for well 609 and Plate 2 shows a down dropped block where well 609 was drilled. The signature of the log curves, the grain-size analysis modeling (Figure 8), composition of the cuttings (all local sediments found in the Franklin Mountains), and rounded to angular sediments indicate local fluvial transport most likely through alluvial fans. The upwards coarsening sequences formed during progradation of an alluvial fan environment, while the fining upwards sequences abandonment and deposition in a playa or axial stream environment.

T2 Unit

The T2 unit (shaded in green in Plates 2 and 3) top boundary is identified by a coarsening upwards sequence in most wells seen best in the resistivity logs and quality gamma logs. Zone 2 in Figure 8 is the unit equivalent to T2. The T2 unit has both upwards fining and coarsening sequences found in resistivity and quality gamma logs, where wells 603, 607, and MW-4 are good examples. The base of unit T2 is marked by an upwards coarsening sequence expressed best in wells MW-6 and MW-5, in both gamma and resistivity logs, with beds as thick as 60 ft (18 m) (Plates 2 and 3). The boundary between the base of unit T2 going into the top of the T1 unit is a laterally persistent clay interval, although often with poorly defined margins this gives an egg-shaped pattern best seen in wells 605 and 511A. The Vshale curves show a marked increase in clay in this interval relative to the overlying strata.

The well cuttings of T2 contain at least 10.9% more clay and silt than T3 did. There is a steady increase in clay and silt volume from northwest to southeast in the T2 unit; the inverse is true for sands and gravels (Tables 1-5). T2 maintains an even thickness throughout most of the study area (Plate 3) and thins by well 509A. The signature of the log curves, the grain-size analysis modeling (Figure 8), and composition of cuttings (gypsum grains begin to intermittently

appear in the clay in this unit) indicate a marginal playa setting. The upwards fining and coarsening sequences along with increase volumes of clay and silt indicate an unstable transitional environment, which can be found around the edges of a playa lake.

T1 Unit

The unit T1 (shaded in blue in Plates 2 and 3) top boundary is defined by a fining upwards signature and in some wells has an egg-shaped log signature best expressed in wells 605 and 511A. The stratigraphic unit T1 is the equivalent to Zone 1 in Figure 8. Resistivity values are lowest in the T1 unit and most wells show a decrease in values with depth. There is no defined base boundary for this unit and it is assumed to end below the total depth of the wells. There are beds of shale (high gamma log values) that appear to thicken from northwest to southeast (10 ft in well 602, 30 ft in well 608, 50 ft in well MW-6). It difficult to determine the shale beds in the wells with low quality gamma logs. The quality of Vshale curve is directly influenced by the quality of the gamma log, so the Vshale curve for well 509A does not have the same quality as the other Vshale curves. T1 has both upwards fining and coarsening sequences seen in the gamma and resistivity logs with thicker interbedded shales than T2.

The well cuttings of T1 contain the highest volumes of clay and silt compared to unit T2-T4 (Tables 1-5). Silt and clay dominate T1 in all of the analyzed wells with an increase in volume trending northwest to southeast. Sandy and gravel volumes decrease from northwest to southeast. There is no defined lower boundary for T1, so it is not possible to determine changes in thickness, but T1 appears at shallower depths from northwest to southeast (Plates 2 and 3). The signature of the log curves, grain-size analysis modeling (Figure 8), and composition of the cuttings (prominent gypsum grains found in the clay beds) indicate a playa lake/basin floor environment.

The depositional environments identified in this analysis are shown in Figure 16. This figure shows the interactions of the environments as inferred from the well log and cutting analysis.

Structure

Plate 2 is a structural cross-section created from the interpreted well log correlations made using the gamma, Vshale, and resistivity log curves. Faults were added in where there was an offset of the underlying strata. Faults 4 and 6 identified in this study have been previously mapped by Collins and Raney (2000) and extended into the urbanized neighborhoods of the city of El Paso from the data collected in this study. Faults 4-6 are located within the transitional boundary from fresh to brackish water in the HBA (Figure 2).

The farther the wells are from the Franklin Mountains, the shallower the strata (T1 and 2) become. Plate 2 shows the shape of the basin as a half graben structure, where the deepest section of the basin is closest to the Franklin Mountains (Figure 4).

Stratigraphy

A stratigraphic cross-section was created using the base of the T4 unit as the datum (Plate 3). The cross-section shows changes in depositional thickness of the intervals, which vary throughout the study area due to changes in topography and available sediment for deposition. Changes in thickness suddenly increase for units T2 and T3 due to a down dropped block where well 609 was drilled. Plate 2 shows the faults that lie on either side of well 509A. T3 becomes significantly thinner around well 511A where T4 becomes thicker. Unit T4 has more deposits from the ancestral Rio Grande River (Figure 8). The river cut into T3 in this area eroding it away and depositing the fluvial sediments.

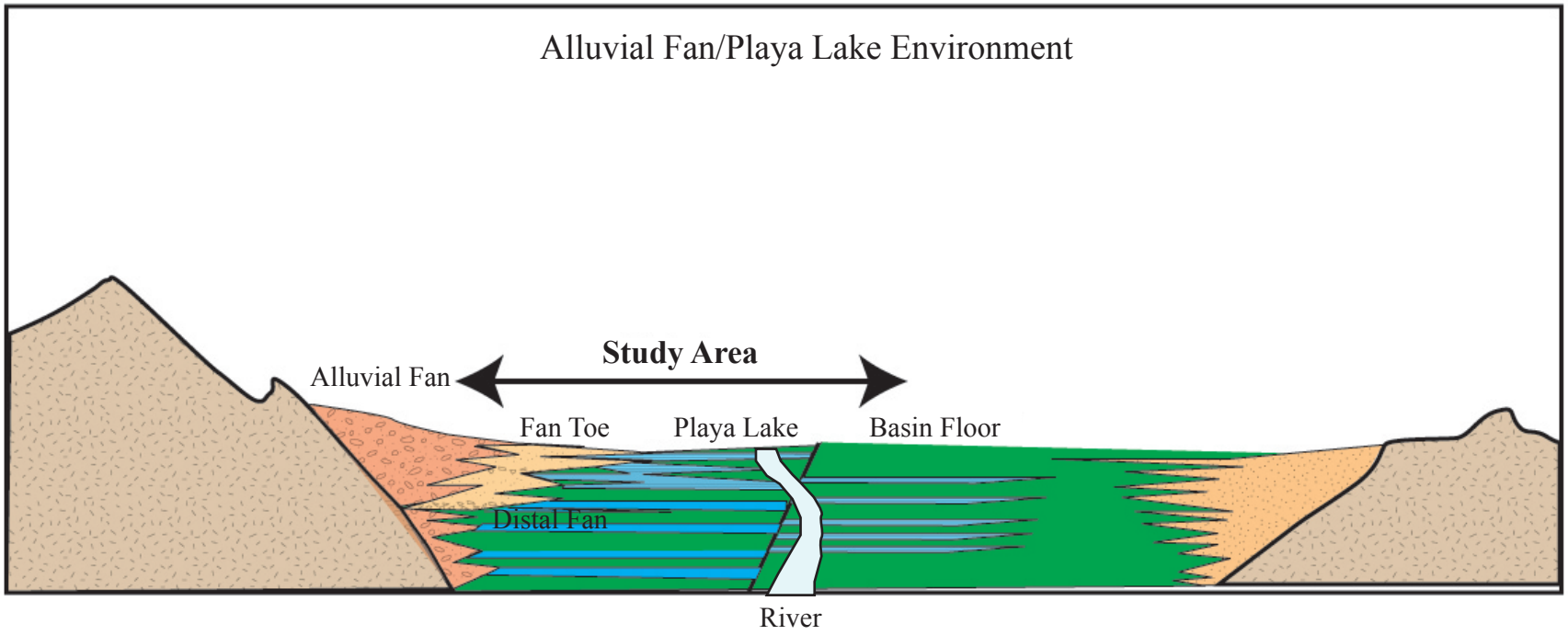

Figure 16. This figure shows the 4 depositional environments identified in grain-size analysis. This is an illustration of an alluvial fan system meeting a playa lake environment.

Structural Cross-Section
Hueco Bolson, West Texas
Well 601-509A

- T4 — Fluvial and River Deposits
- T3 — Alluvial Fan Deposits
- T2 — Playa Margin Deposits
- T1 — Playa lake
- Normal Fault

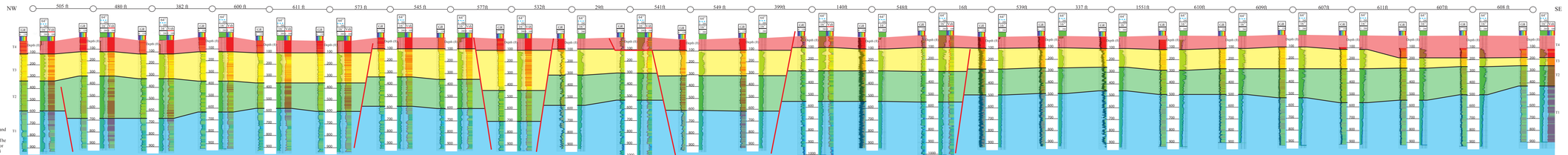

Plate 2. Correlations from well 601 to well 509A using Gamma Ray (GR), Resistivity (64" and 16"), and Vshale (Vsh) log curves. The faults are identified by the offset of the correlations. All faults are assumed to be normal because of the geologic tectonics of a rift environment. The major faults for the study area which have been identified by Collins and Raney (2000) and/or the free-air anomaly map are faults 1, 5, and 6. These three faults extend a minimum of 12.4 miles (21 km). The minor faults (2, 3, 4, and 7) extend a significantly shorter distance of about 1.2-2 km) across the study area as identified by the free-air anomaly map.

Stratigraphic Cross-Section
Hueco Bolson, West Texas
Well 601-509A

- T4 — Fluvial and River Deposits
- T3 — Alluvial Fan Deposits
- T2 — Playa Margin Deposits
- T1 — Playa lake

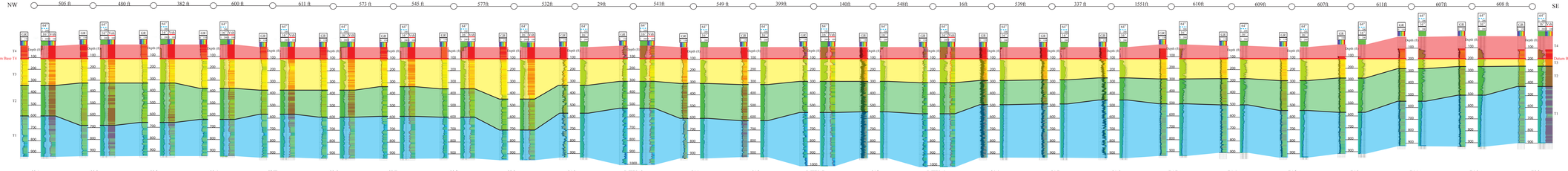

Plate 3. Correlations from well 601 to well 509A using Gamma Ray (GR), Resistivity (64" and 16"), and Vshale (Vsh) log curves. This cross-section shows the change in thickness of each correlated section. Thickness-deposition varies with proximity to faults (if deposition occured during active faulting), mountains (alluvial deposits), playa lakes, and the ancestral Rio Grande River.

Gravity

The free-air values processed for each station from the gravity data collected (500 new stations) in the study area were combined with gravity data collected from previous studies around the region from the following website: http://irpsrvgis00.utep.edu/repositorywebsite/. The free-air values were used to create a Free-Air anomaly map (Figure 17), which show color variations in milliGals (mGal) for the area. Higher gravity values correspond with high-density rocks like those found in the Franklin and Hueco Mountains. Lower gravity values are found in the basins between the two mountains (Hueco and Mesilla Bolson) where there are unconsolidated (low-density) deposits (thicker in the Hueco Bolson) covering the underlying consolidated strata.

The study area lies within the blue shaded regions (Figure 17), where some of the lowest gravity values are mapped. On the west side of the study area, the gradient rapidly increases from green to red and pink (higher gravity values). Abrupt changes in gravity values (sharp color gradient changes in Figure 17) indicate sudden changes in mass distribution below the surface, which correspond to faults. The East Franklin Boundary fault (the major fault located farthest west in the map, Figure 17) is a noticeable gradient in red on the eastside of the Franklin Mountains. The faults previously mapped by Collins and Raney (2000) are shown as solid red lines in Figure 17 and the faults identified from this study are dotted red lines.

A profile line (A-A', Figure 17) about 27.3 miles long (44 km) was selected to cut across the study area and interpreted using GM-SYS software (Figure 21). The profile created shows the half graben structure of the Hueco Bolson (Figure 21). This profile cuts across 3 of the faults identified in the well log correlations in Plate 2 (faults 1, 4, and 6). Faults 5 and 6 were previously mapped by Collins and Raney (2000) and fault 1 was identified from this study. The

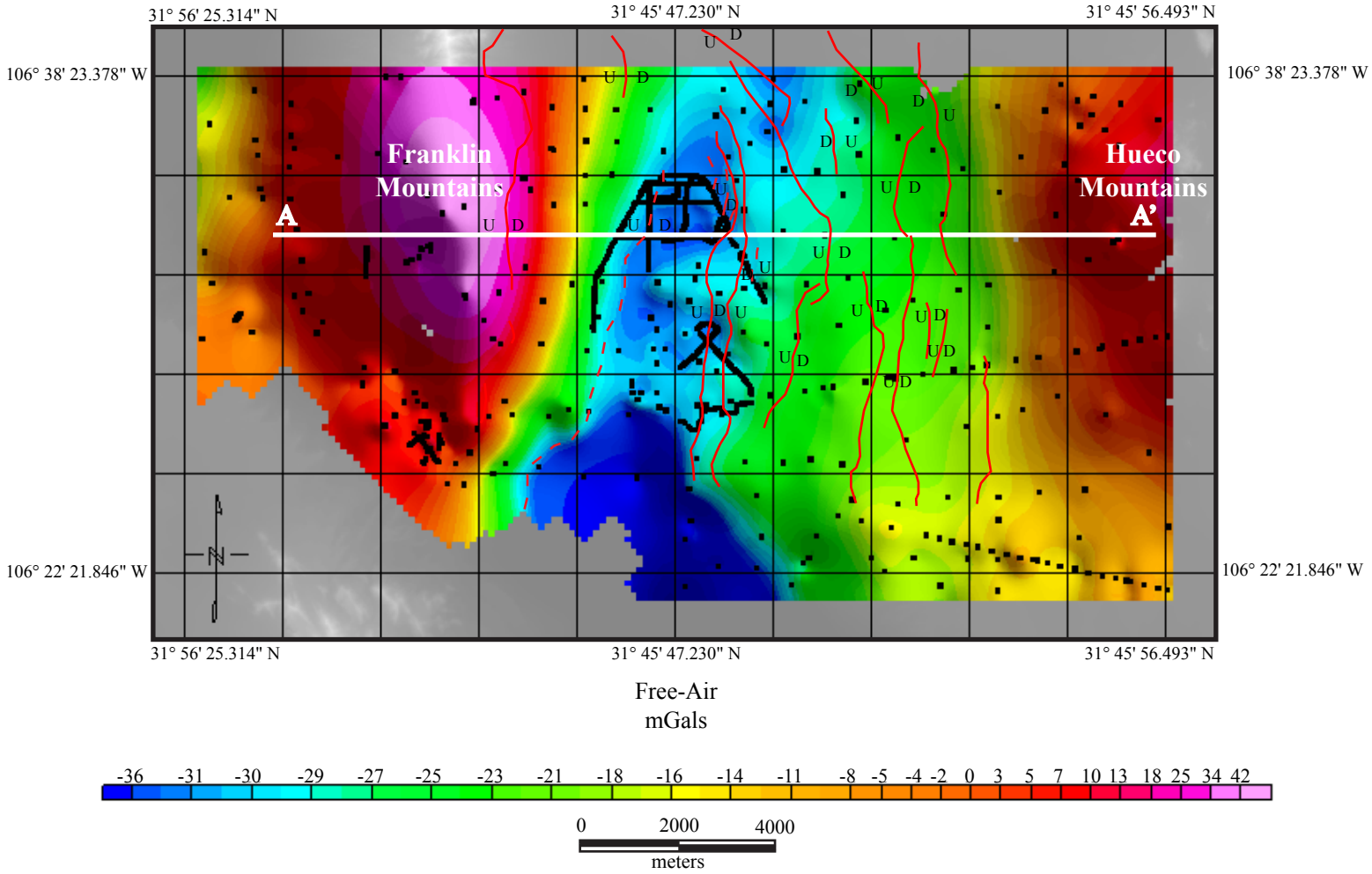

Figure 17. This is a free-air gravity anomaly map extending from the west side of the Franklin Mountains to the Hueco Mountains. The profile line A-A' is shown in Figure 18. The black dots are gravity stations. The solid red lines are normal faults mapped and modified from Collins and Raney (2000) and the dashed red lines are the faults interpreted from this study. The U's mark the up thrown block and the D's mark the down thrown block of the faults.

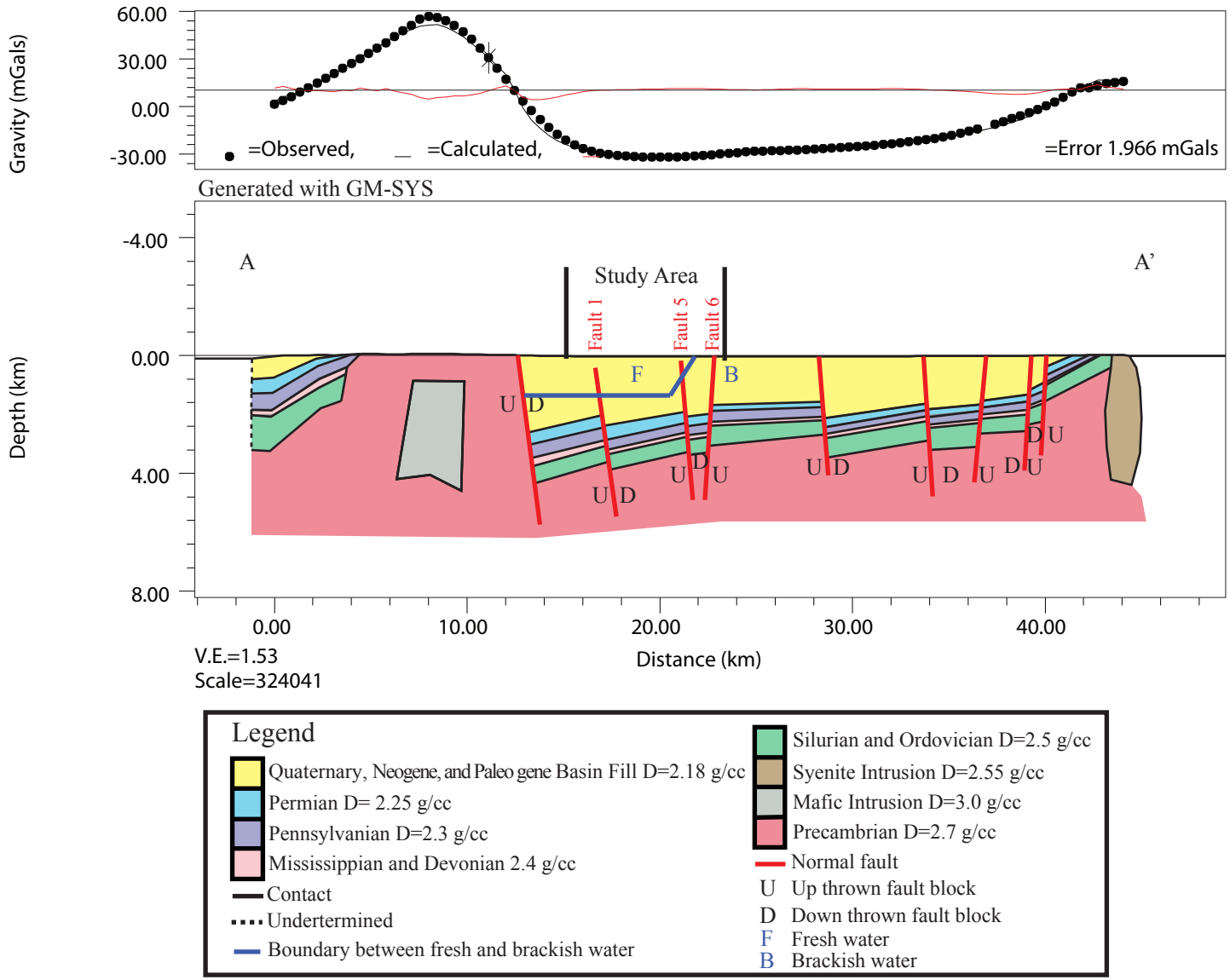

Figure 18. This is a profile line from A to A' in Figure 17. The boundary between the frsh and brackish water interpreted from Hutchison (2006). Modified from Collins and Raney (2000), Imana (2002), and Hadi (1991).

study area is located in one of the deepest sections of the Hueco Bolson. The fresh water section of the HBA lies between the Franklin Mountains (East Boundary Fault) and a line near fault 5 and 6 in the study area (Figure 19). The fresh water section in the study area lies within the compartment between faults 1 and 4 (from well 601 to well 610), where there is a lower volume of silt and clay (Tables 1-5).

Figure 20 is a free-air anomaly map showing only the study area. The faults shown in solid yellow are from Collins and Raney (2000), while the dashed yellow lines are normal faults identified in this study as seen in cross-section in Plate 2. The black dots are gravity stations and the U's mark the up thrown block of the faults and the D's are the down thrown blocks. Colors shaded in blue and green have low free-air values indicating less dense lithologies (e.g. unconsolidated sediments) and the pink and red colors have higher free-air anomaly values corresponding with higher density lithologies. The study area above 31°49'35.337"N (above label A) in Figure 20 shows a small closed basin system trending N-S. The study area below 31°49'35.337"N (between the numbers 1 and 5 in Figure 20) shows a potentially different closed basin system that may have fed sediment into a deeper basin (shaded in dark blue in Figure 17 and 20) in the area labeled with a white B in Figure 20. The faults labeled 1, 5, and 6 all trend parallel to the edges of these small isolated basins.

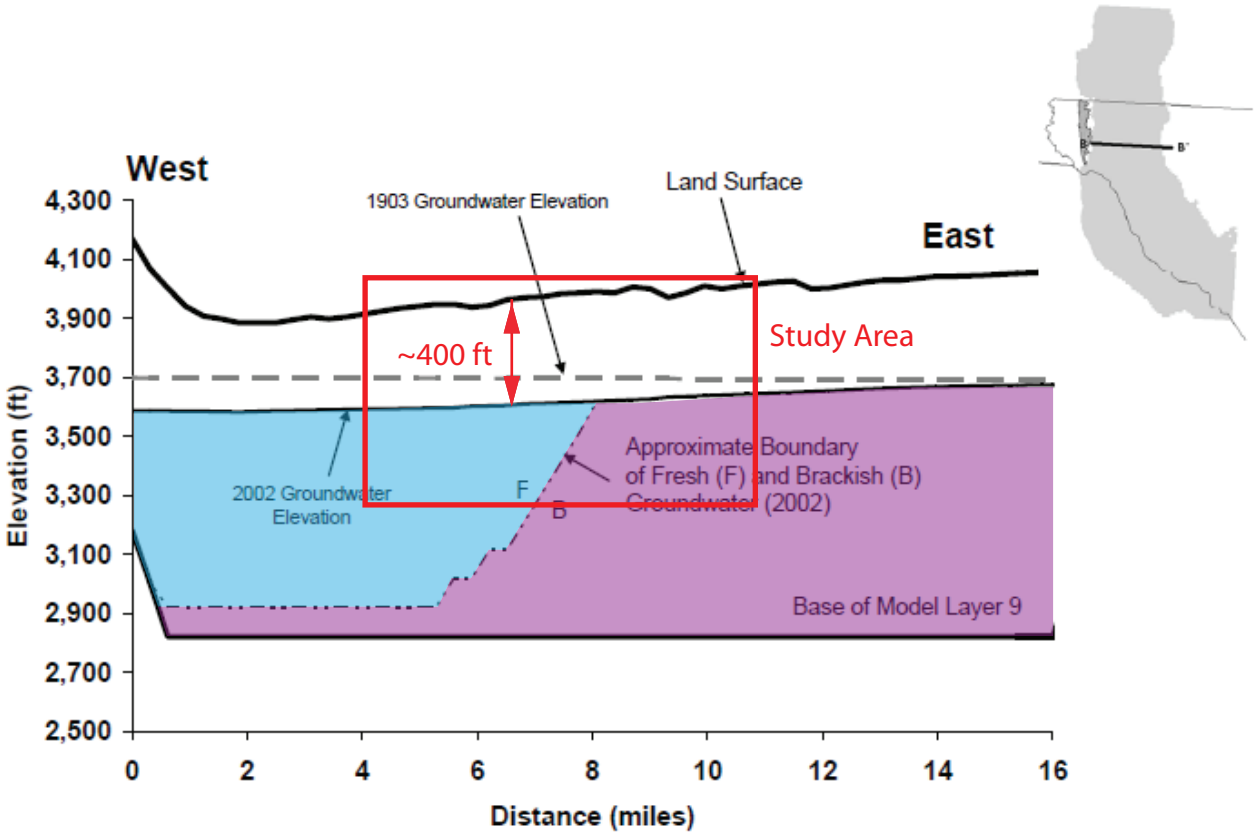

Figure 19. This illustration shows the profile line B-B' (top right of Figure) cutting through the study area (indicated in red). The fresh water section (shaded in blue) and the brackish water section (shaded in purple) transitional boundary lie within the study area about 400 ft below the surface. Modified from Hutchison (2006).

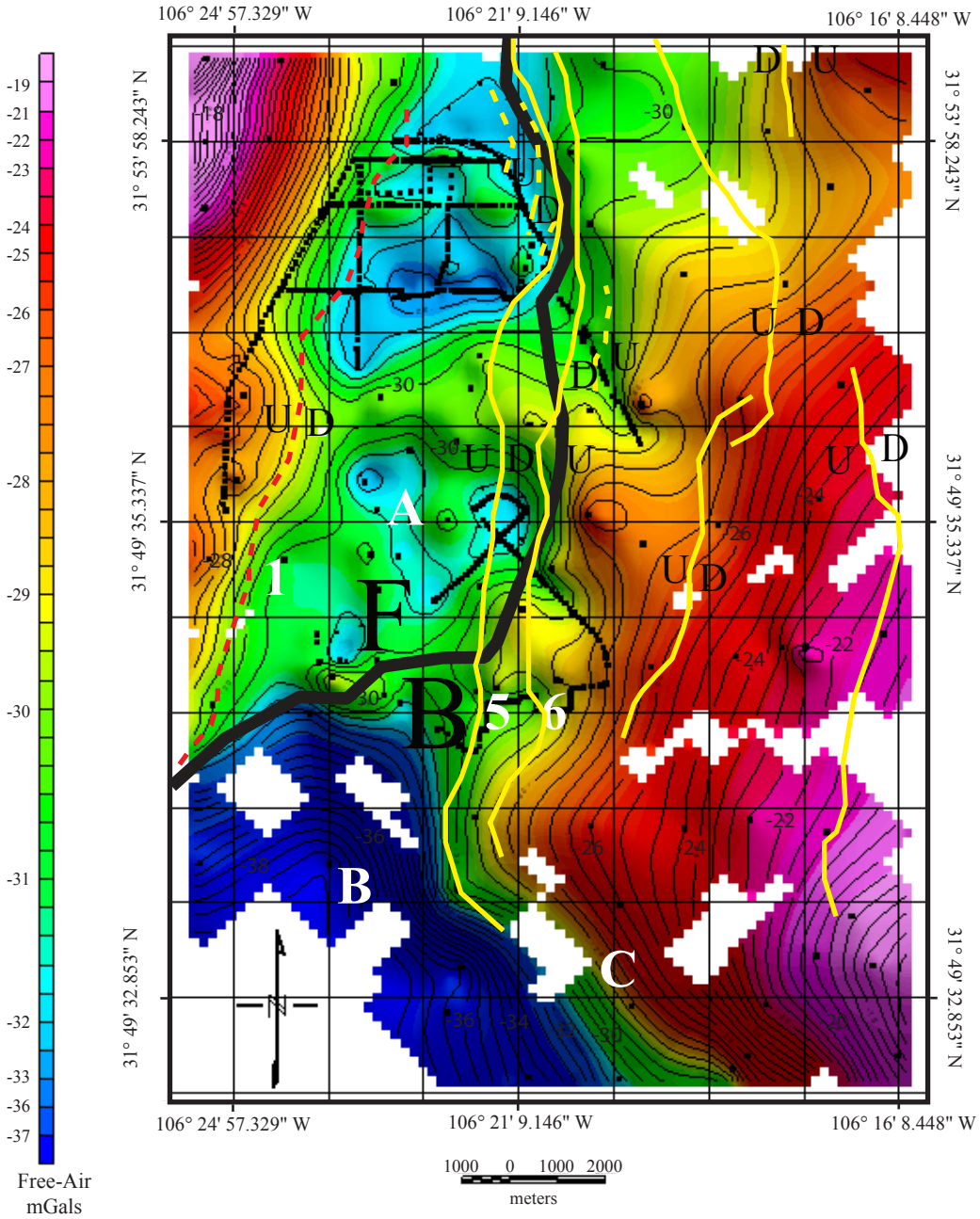

Hueco Bolson (Study Area) Free-Air Anomaly Map

Figure 20. This free-air anomaly map shows the study area where the black dots are gravity stations. Shades of pink and red have high free-air values corresponding with dense lithologies and shades of blue have low free-air values corredponding with less dense lithologies see scale to the left. Countour intervals are 0.5 mGals. The solid yellow lines are normal faults mapped and modified from Collins and Raney (2000). The red and yellow dashed lines on the map are normal faults identified and mapped from this study. The U's indicate the up thrown fault block and the D's indicate the down thrown fault block. Faults 1 5 and 6 are labeled in white numbers and areas labeled A-C are discussed in results and discussions. The solid black line is the boundary between the fresh (F) and brackish (B) water boundary.

Discussion

Research conducted in the Hueco Bolson has shown change in the aquifer's fresh and brackish water boundary over time since pumping of the HBA began. Salinity increases with depth (Figure 19). The brackish water corresponds to the playa lake deposits, which predate the deposition of the fresh water which corresponds to the ancestral Rio Grande river course (Hutchison, 2006).

Chloride concentration maps are can be used to map distributions in salinity throughout the aquifer. Chloride concentrations map images are superimposed on the study area maps (Bredehoeft, et al., 2004) (Figures 21-23). These maps were prepared by Bredehoeft et al. (2004) using data from three sources:

1) Sample wells and test holes drilled in 2002 and 2003
2) Water quality data from shallow wells located southeast of El Paso are from wells drilled by El Paso County Water Improvement District No. 1.
3) Electric conductivity data from wells in Juarez obtained from Juanta Municipal de Agua y Sandeamiento Juarez (JMAS).

The data used to create these concentration maps date to around 2003, at the earliest, and the data have changed due to pumping of the aquifer since that time. According to Hutchison (2006), pumping in 2002 was below 40,000 AF/yr, but increased in 2003 and 2004 because of drought conditions. Figure 3 shows TDS data taken in 2007 by EPWU for the 500 and 600 series wells. The updated fresh/brackish water boundary (modified from William R. Hutchison, personal communication, 2009; EPWU, 2009) from Figures 2 and 3 is shown alongside the chloride concentration data obtained from Bredehoeft et al. (2004).

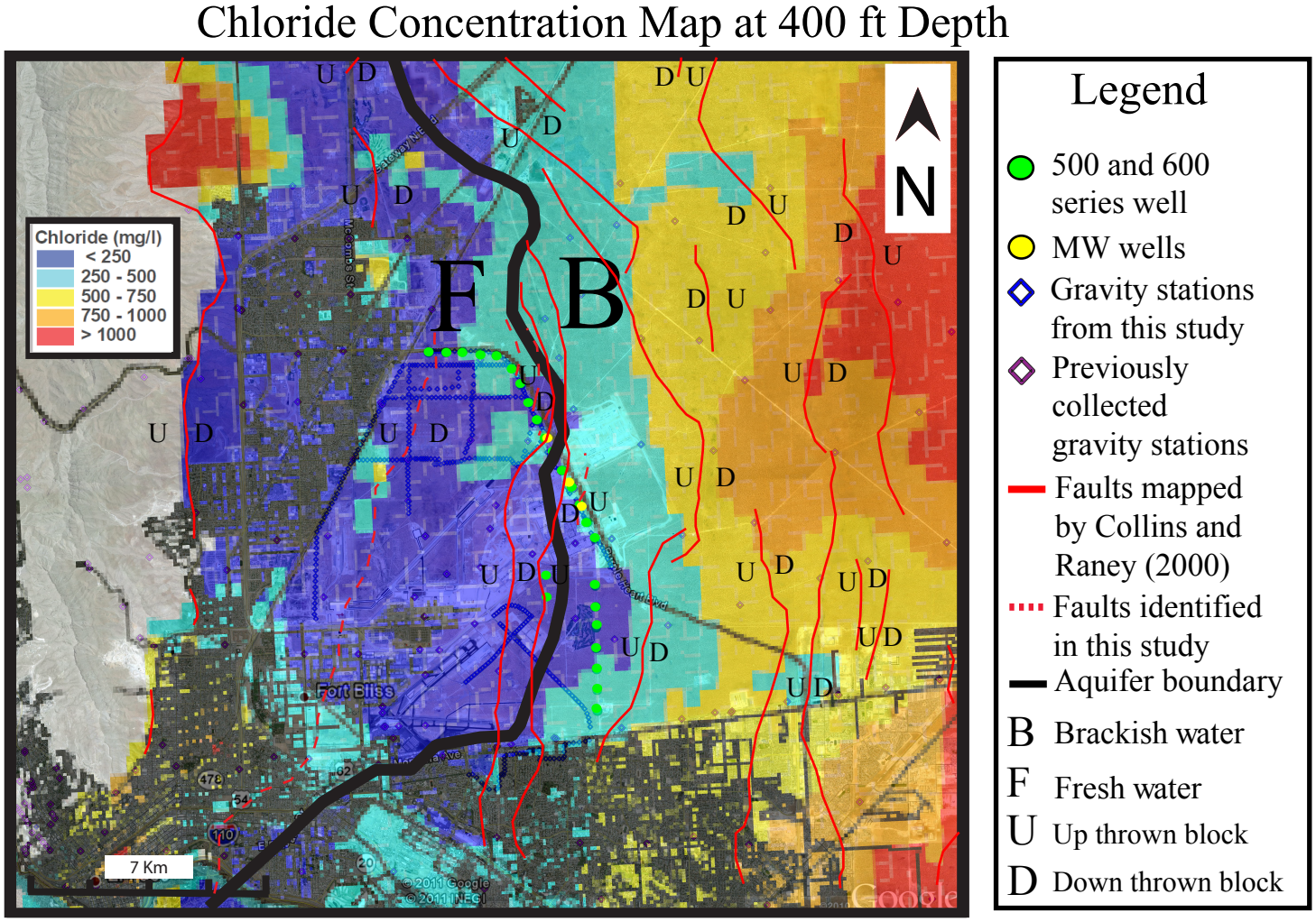

Figure 21. This figure shows a chloride map from EPWU superimposed onto a Google Earth image of El Paso, TX. The solid red lines are faults modified from Collins and Raney (2000) and the dashed red lines are faults interpreted from this study. The fresh and brackish water boundary is modified from Hutchison (2009). The green dots represent the 600 and 500 series wells, while the yellow dots are the MW wells. There are three MW wells, which are located within feet from an already existing 600 series well. The areas in blue show areas with lower concentrations of chloride and red show areas with higher concentrations. Chloride concentration map taken from Bredehoeft (2004).

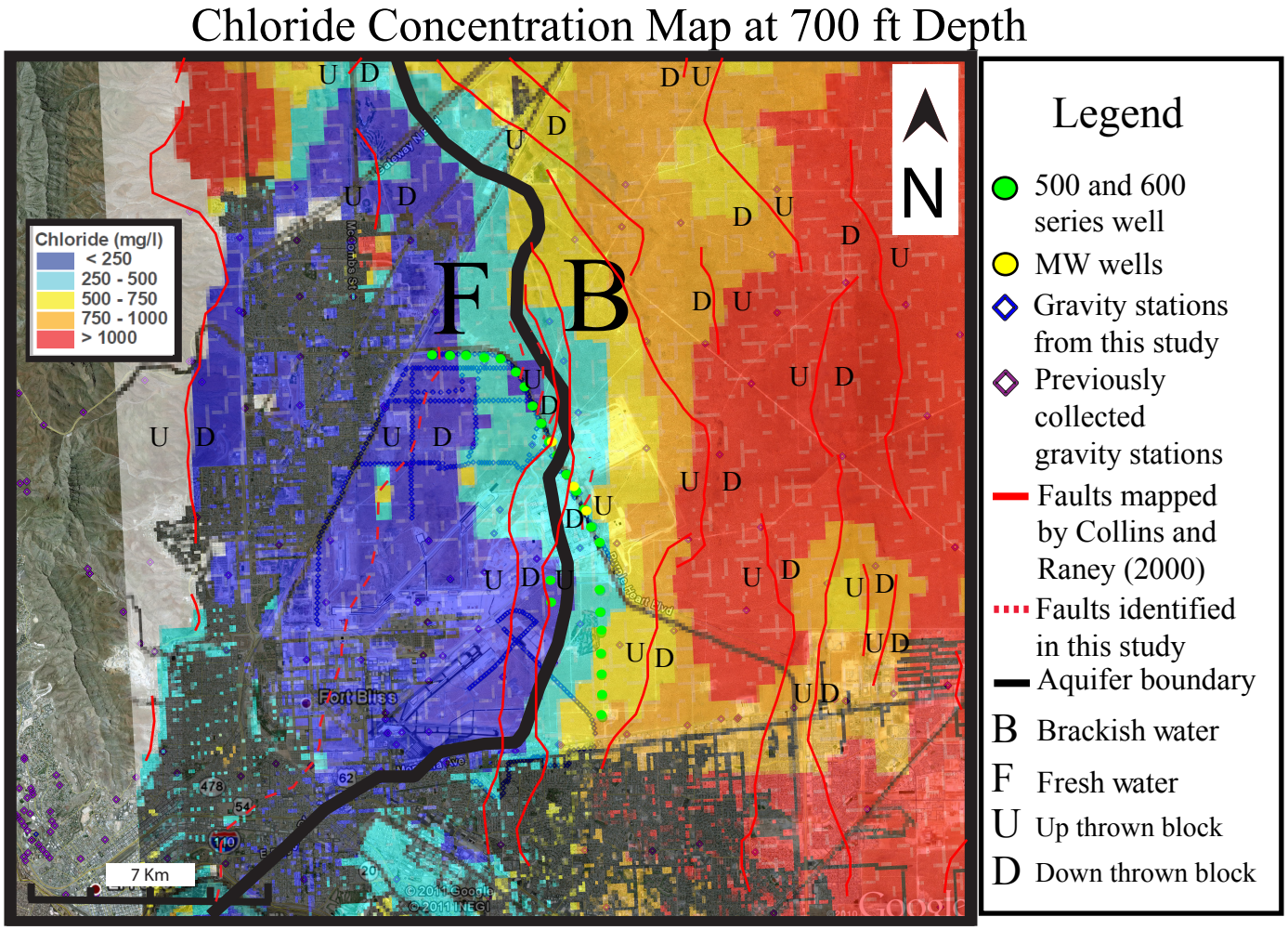

Figure 22. This figure shows a chloride map from EPWU superimposed onto a Google Earth image of El Paso, TX. The solid red lines are faults modified from Collins and Raney (2000) and the dashed red lines are faults interpreted from this study. The fresh and brackish water boundary is modified from Hutchison (2009). The green dots represent the 600 and 500 series wells, while the yellow dots are the MW wells. There are three MW wells, which are located within feet from an already existing 600 series well. The areas in blue show areas with lower concentrations of chloride and red show areas with higher concentrations. Chloride concentration map taken from Bredehoeft (2004).

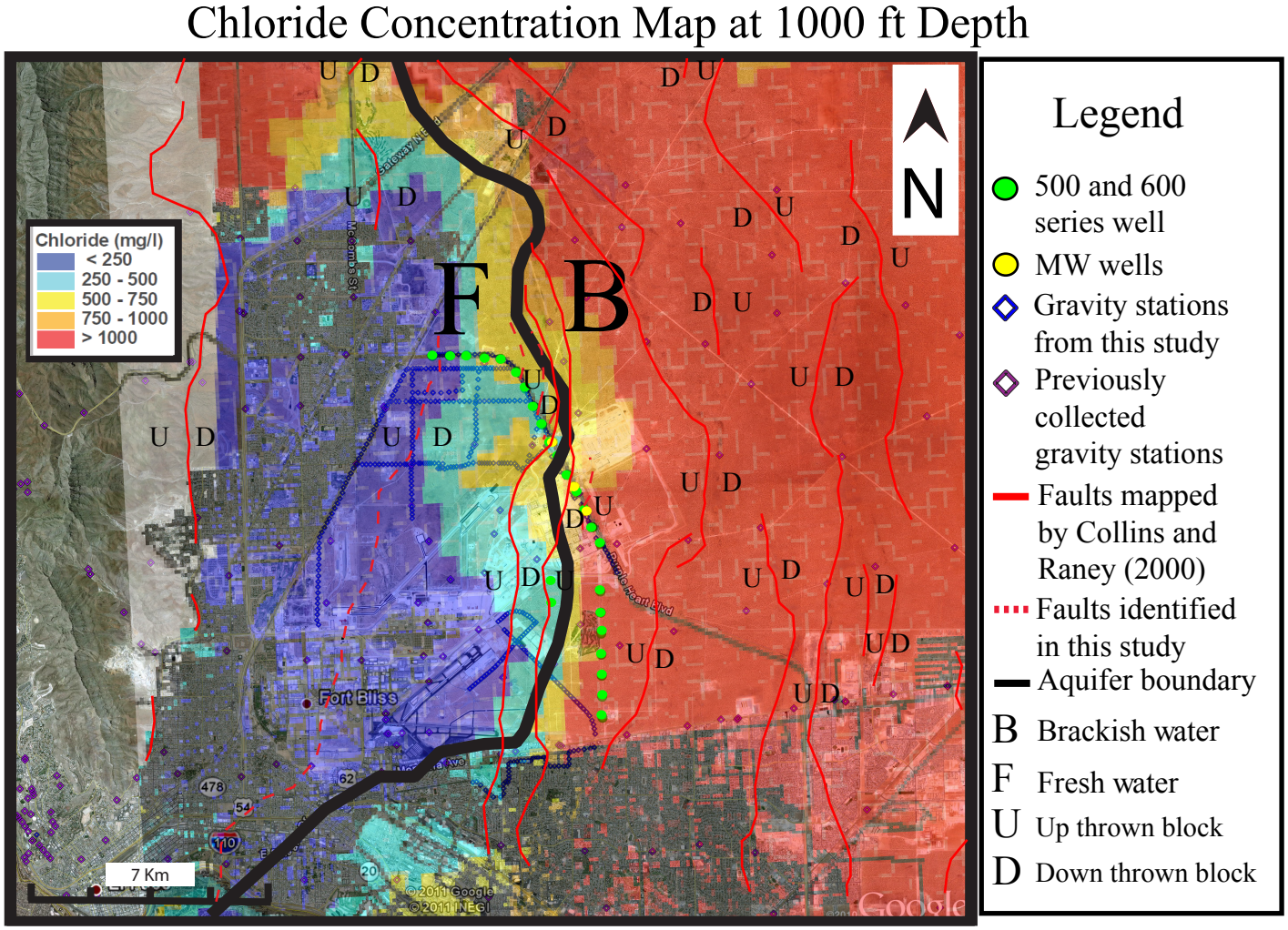

Figure 23. This figure shows a chloride map from EPWU superimposed onto a Google Earth image of El Paso, TX. The solid red lines are faults modified from Collins and Raney (2000) and the dashed red lines are faults interpreted from this study. The fresh and brackish water boundary is modified from Hutchison (2009). The green dots represent the 600 and 500 series wells, while the yellow dots are the MW wells. There are three MW wells, which are located within feet from an already existing 600 series well. The areas in blue show areas with lower concentrations of chloride and red show areas with higher concentrations. Chloride concentration map taken from Bredehoeft (2004).

Three depths were selected from the available chloride maps (400, 700, and 1000 ft, Figures 21-23). The lower chloride concentrations are in blue (<250 mg/l) and the higher concentrations are in red (>1000 mg/l), where mg/l are analogous to TDS. Chloride concentration values between 250 and 500 TDS (shaded in turquoise in Figures 21-23) mark the transition zone between fresh and brackish water. At 400 ft this transition zone is within the study area and there are pockets of brackish water which may be fault controlled. Figure 21 shows the changes in chloride concentrations across the study area at a depth of 400 ft below the surface where the water table is. Figure 22 shows the chloride concentrations at 700 ft and Figure 23 shows the concentrations at 1000 ft. The chloride concentration maps show a sharp vertical gradient boundary between the fresh and brackish water sections of the HBA. This vertical boundary can also be seen in Figure 19. The updated boundary between the fresh and brackish section of the aquifer parallels the chloride concentration gradient with depth (Figures 24-26).

The transitional boundary between the two sections of the aquifer (fresh and brackish) lies between wells 608 and MW-5 where there is a series of four faults (Figure 3 and Plate 2). On the west side of the boundary, wells 601 and 605 have higher volumes of sand and gravel (Tables 1-5) than silt and clay. On the east side of the boundary, wells 615 and 509A gradually increase in clay volume throughout the well and have higher volumes of silt and clay (Tables 1-5) than sand and gravel. Coarse-grained sediments in the aquifer have a faster flow velocity than the fine-grained sediments sections of the aquifer (Hutchison, 2006). Clay also absorbs more water than other grain-sizes. The higher volume of clay on the east side of the boundary (brackish water section) hinders the flow of fluid into the fresh water section (west side) of the aquifer.

Four faults lie within the transitional boundary zone between the fresh and brackish water between wells 609 and MW-5. Faults 5 and 6 have an obvious scarp mappable on the surface, are parallel to one another, and extend at least 12.4 miles (21 km) (Figure 2). Faults have been known to act as conduits or barriers to horizontal fluid flow in an aquifer system (Bense and Person, 2006). Depth of burial (Fulljames et al., 1997; Fisher and Knipe, 1998; Rawling et al., 2001; Bense et al. 2003), fault throw (Wiek et al., 1995; Mailloux et al., 1999) and secondary mineralization along a fault plane (Fisher and Knipe, 1998) all affect the permeability of a fault zone. Hydraulic anisotropy in a fault can be caused by clay-smearing, sand drag, and re-orientation of grains along the fault plane (Bense and Person, 2006). The volume of clay increases from well 601 to well 610 (Tables 1-3) and well 610 has about 50% volume of sand. This could be enough to create hydraulic anisotropy in the faults within the transition zone and act as a barrier impeding the incursion of the brackish water into the fresh water section of the aquifer. Quaternary age faults (which include all faults in the study area) are likely to act as barriers, impeding the flow of ground-water across fault planes (Heywood and Yager 2003; Nwaneshiudu, 2007).

Free-Air Anomaly Maps

Figure 17 shows a N-S trending basin (shaded in blues in Figure 17 and in blues and green in Figure 20) where faults 1, 5, and 6 appear to be step over faults that bound this basin. This basin appears to be fault controlled and may have formed because of different activation times and amount of slip between faults 1, 5, and 6.

Figure 20 shows two small isolated basin systems within the study area. There is a gravity high separating the two basins (labeled A in Figure 20), which may be controlled by some other cross fault within the area. The isolated basin between the labels identifying Faults 1

and 5 in the southern area of the study area may have been feeding sediment into the deeper basin to the south. The topography seen in these basins (Figure 20) may have controlled the differences in grain-size distribution occurring between well 509A and the 600 series wells. The boundary between the fresh and brackish water trends parallel to faults 5 and 6 and then makes a sharp left above the deepest isolated basin area (labeled B in Figure 20).

Faults

Faults were identified during well log correlations and can be seen in the structural cross-section (Plate 2). Two of these faults were previously mapped by Collins and Raney (2000) (faults 5 and 6) and identified during well log analysis and in the gravity maps (Figures 17 and 20), which run about 12.4 miles and trend N-S. Fault 1 was initially identified during well log analysis and can be seen in Plate 2. Gravity analysis showed a sharp gradient in free-air values cutting into well 601 that trends N-S and can be followed into the southern area of Figures 17 and 20. Faults 2, 3, 4, and 7 are not as apparent in the gravity maps (Figures 17 and 20), but offset of strata is apparent in the structural cross-section (Plate 2).

During gravity analysis with GM-SYS faults were added into the profile line A-A' (Figure 18) to reduce error. The East Franklin Boundary fault (located farthest left in Figure 18) shows the most offset of the faults mapped. Faults 5 and 6 can be seen on the surface, whereas fault 1 is located in a more urbanized area and is not easily seen on the surface or it may not reach the surface. Faults 2, 3, 4, and 7 are masked by faults 5 and 6 in the data set because they lie so close and are smaller faults.

Depositional Environments

Most of the deposits in zone 1 (unit T1) were deposited in a low energy system. This zone is dominated by red silts and muds, with some deposits of tan silts and muds, and the

occasional deposit of white sandy silt and silty sands. Silts and clays extend across the area and close to the Franklin Mountains. Individual red-colored clays can be correlated across faults and represent continuous areas of low-relief, low-energy deposition and are interpreted as deposits of ephemeral lakes (playas). The presence of extensive playas close to the mountains indicates that deposition in the basin exceeded the rate of deposition on the alluvial fans. This is interpreted as being the result of either a large intrabasinal stream, or an ancestral Rio Grande terminating in the Northern Hueco Basin. Since the base of zone 1 cannot be constrained, the thickness of the unit is unknown.

Zone 2 (unit T2) is characterized by coarser grained and less continuous beds (Figure 8 and Plates 2 and 3). The Vshale curves show coarser sediment in wells 601 and 601 (Plates 2 and 3) and then little consistent change from well to well. Individual beds are difficult to correlate, but a relatively sandy upward coarsening unit forms the bottom 150 to 200 ft (50 to 75 m) of the unit. This is overlain by a finer grained that contains several 30 m upward fining intervals. The entire unite maintains nearly the same thickness across the study area. However, it thickens in the internal grabens between faults 3 and 4 and faults 5 and 6. This interval is interpreted to represent deposition on a relatively flat basin floor that extended almost across the study area. The upward coarsening interval is interpreted as the filling of the large playa and its replacement with small playas and playa margin deposits. Zone 2 was deposited in higher energy system than zone 1. This zone is a transition zone between the playa environment of zone 1 and the alluvial fan environment of zone 3. The playa margin deposits are characterized by the gravelly mud deposits.

Zone 3 (unit T3) was deposited in a high energy system. This unit is characterized by the upwards coarsening sand to gravel sequences (Figure 8). The gravel clasts identified in this zone

are all sourced from the Franklin Mountains where individual beds are difficult to correlate from well to well and the average thickness of the upwards coarsening beds range from 10 to 100 ft (3.1 m to 30.5 m) in thickness. These beds are interpreted to be alluvial fan deposits. This zone is also characterized by the upwards fining gravel to sand deposits. These beds also contain sediments from the Franklin Mountains. These beds are interpreted to be from alluvial fan toe and distal fan deposits. These beds are difficult to correlate from well to well and range in thickness from 20 to 90 ft (6.1 to 27.5 m) in thickness. The alluvial fan, alluvial fan toe, and distal fan deposits are thickest in the northwest section of the study area in the 600 series wells (Figure 2 and Plates 2 and 3) then slowly begin to pinch out into the basin from wells 615 to 509A. However, it thickens in the internal grabens between faults 3 and 4 and faults 5 and 6. It took many years to build a fan large enough to deposit coarse-grained sediments out into the basin reaching as far as well 509A.

Zone 4 (unit T4) is characterized by the rounded to well rounded exotic sediments (sediments that are far travelled and not sourced from the Franklin Mountains). While unit 4 contains a high volume of sands and gravels (similar to unit 3, Figure 8), these deposits show upward fining sequences that can be correlated from well to well (Figure 8 and Plates 2 and 3). The fluvial sandy gravel beds range in thickness from 20 to 60 ft (6.1 to 18.3 m), while the fluvial gravelly sand beds range in thickness from 20 to 70 ft (6.1 to 21.4 m). This unit is interpreted to be fluvial deposits from the Ancestral Rio Grande which were deposited in a high energy environment. Differentiated fault movement in the basin slowly closed off the basin, where the playa lake began drying up and a river began flowing through the area.

In summary, a change in energy can be identified with the different depositional environments identified in this study. The energy changes from the low energy needed to

deposit the older playa and playa margin units to the younger higher energy needed to deposit the alluvial fan and fluvial units.

Conclusion

Twenty-six wells within the Hueco Bolson were used for this study (Figure 2). The 600 series wells were drilled in order to provide brackish water to the Kay Bailey Hutchinson Desalination Plant and to create a trough in the ground water to help prevent the incursion of the brackish water into the fresh water aquifer.

A total of five wells were selected for grain size analysis: wells 601,605, 610, 615, and 509A. Four different depositional environments are inferred from well cuttings analysis from zones 1-4 and units T1-4: playa lake, playa margin, alluvial fan, and fluvial ancestral Rio Grande deposits. The depositional beds were shifted and thickened across the faults indicating deposition and growth of strata during faulting.

Based on cuttings and well log analysis there is an increase in the volume of clay and silt from northwest to south east and a decrease in the volume of sand and gravel from northwest to southeast. The transition zone between the fresh and brackish water section of the HBA lies between well 609 and MW-5 where three faults are located. Two of these faults run at least 12.4 miles (21 km) across the basin which act as barriers to water mixing. The increases in clay on the eastern side of the boundary, coupled with the barrier faults create a natural seal impeding the incursion of brackish water into the fresh water section of the aquifer.

Fault 1 was identified in this study first through well log correlations. When the free-air anomaly map was created, a sharp gradient was seen in the data near well 601 along the western most side of the study area which identified this same fault extending about 12 .4 miles (~21 km). Fault 1 belongs to a series of step-over faults heading east into the basin from the Franklin Mountains. Several other shorter faults (faults 2-4) lie within a region of the aquifer that

contains pockets of brackish water within the fresh water section of the HBA. These faults may help control the flow and location of these brackish pockets of water.

A change in depositional energy was identified within the study area from the total depth of the wells to the surface. Where lower energy deposits are located deeper in the wells and the depositional energy increases from zone 1 to zone 4 (Figure 8).

Future Work

Fault 1 in Figures 17 and 23 may connect with a fault mapped and identified by Collins and Raney (2000) that lie 1000 meters to the north. A gravity survey between the faults would need to be conducted in order to determine the relationship between the faults. Grain-size analysis on the wells located near the fault mapped by Collins and Raney (2000) north of fault 1 would extend the cross-section (Plates 2 and 3) and help identify structural and stratigraphic constraints on groundwater flow and quality/quantity in the northern section of the basin.

The gravity stations in Figure 20 near the letter A are scarce and taking a few more data points in this area would help define an additional fault or other structures that may be constraining the two small isolated basins in the study area. Biggs Army Airfield lies over that area, so collecting more gravity reading would not be possible. More gravity stations can be obtained where the B and C labels on Figure 20 are located. These areas lie within the urban city of El Paso. More gravity data collection around the area around label B on Figure 20 would help define the edges/geometry of the isolated deep basin in that area. More gravity data collection around the label C in Figure 20 would constrain faults 5 and 6.

Figure 24 shows the map of the study area where other wells (orange dots) are located and where potential gravity stations (pink diamonds) can be collected. It would be beneficial to conduct grain-size analysis on wells within the brackish water section of the HBA that lie within the deepest isolated basin (labeled B in Figure 20) to identify the dominant grain-size for that area.

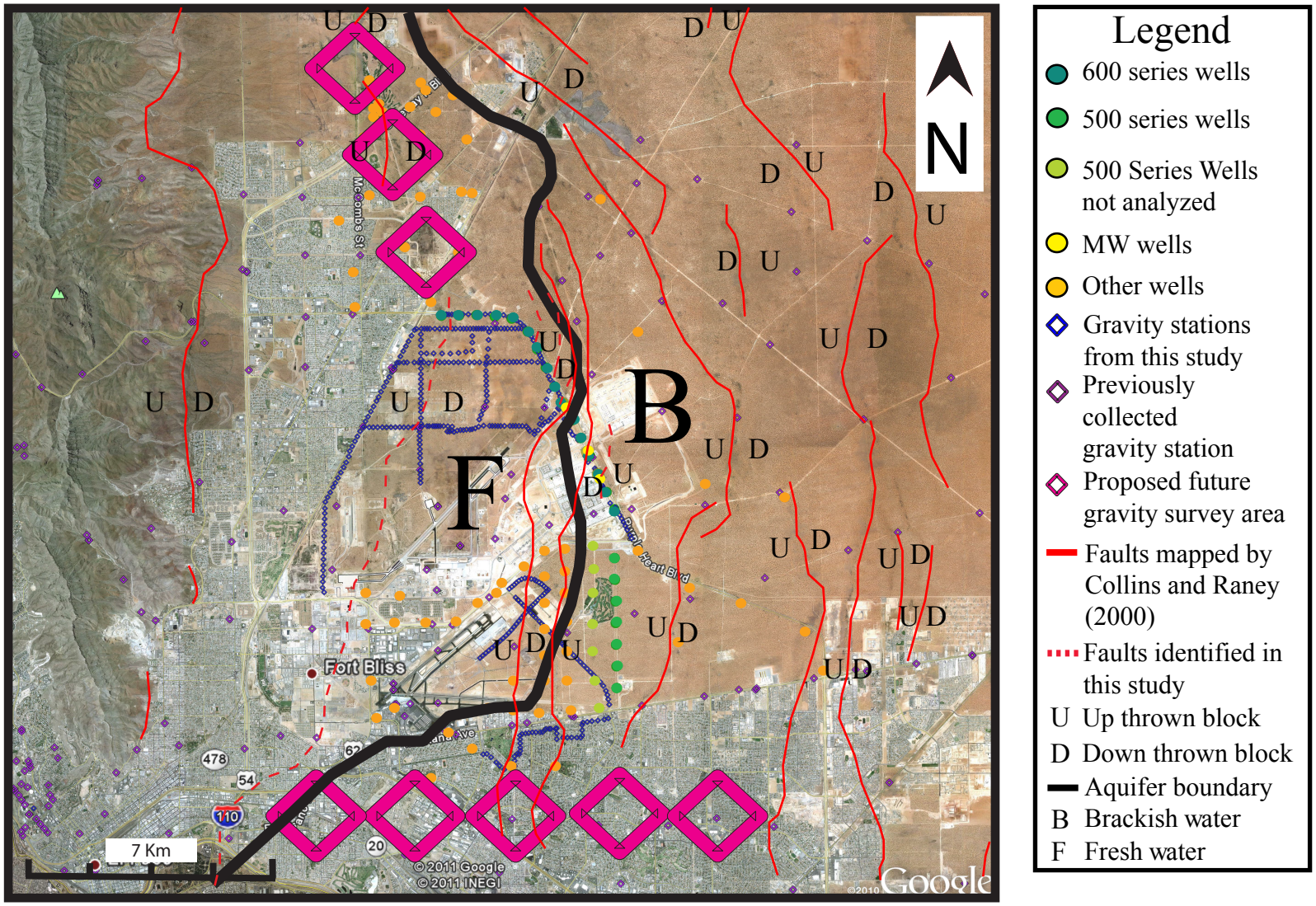

Figure 24. Well map from EPWU superimposed onto a Google Earth image of El Paso, TX. The faults in solid red lines are modified from Collins and Raney (2000) and the dashed red lines are faults interpreted from this study. The fresh and brackish water boundary is modified from Hutchison (2009). Aquifer boundary modified from Hutchison, 2006.

Bibliography

Ashworth, J.B., Hopkins, J., 1995, Aquifers of Texas: TDWR Report. 345, 69 p.

Asquith, G., Krygowski, D., 2004, Gamma Ray, in G. Asquith and D. Krygowski, Basic Well Log Analysis: AAPG Methods in Exploration 16, p. 31-35.

Albritton, C.C., Jr., Smith, J.F. Jr., 1965, Geology of the Sierra Blanca area, Hudspeth County, Texas: U.S. Geological Survey Professional Paper 479, 131 p.

Bense, V. F., Van den Berg, E. H., and Van Balen, R. T., 2003b, Deformation mechanisms and hydraulic properties of fault zones in unconsolidated sediments; the Roer Valley Rift System, the Netherlands: Hydrogeology, v. 11, 319-332, doi: 10.1007/s10040-003-2062-8.

Bense, V.F., and M.A. Person, 2006, Faults as conduit-barriers to fluid flow in siliclastic Sedimentary aquifers: Water Resources Research, v. 42, W05421, doi: 10.1029/2005WR004480.

Blake, G.R., and Hartage, K.H., 1986, "Bulk Density", p. 363-375, in Methods of Soil Analysis, Part I. Physical and Mineralogical Methods, A. Klute, ed. Agronomy Monograph no. 9 (2nd ed.), Soil Science Society of America, Madison, Wis.

Boyle Engineering Corporation, 1991, El Paso Water Resource Management Plan, 1991–2040: Report prepared for El Paso Water Utilities Public Service Board and El Paso County Water Improvement District No. 1.

Bredehoeft, J., Ford, J., Harden, B., Mace, R., Rumbaugh, J., III., 2004, Review and interpretation of the Hueco Bolson groundwater model: Prepared for El Paso Water Utilities Report 39 p.: www.epwu.orp/water/hueco_bolson.html (January 2009).

Chapin, C. E., 1971, The Rio Grande rift part 1: modifications and additions: New Mexico

Geological society, Annual Field Conference Guidebook No.22, p.191-201.

Chapin, C.E., 1979, Evolution of the Rio Grande rift, in Reicker, R.E., ed., Rio Grande rift: Tectonics and magmatism: Washington, D.D., American Geophysical Union, p.1-5.

Cliett, T.E., 1969. Groundwater occurrence of the El Paso area and its Related Geology, in Guidebook 20th Field Conference, New Mexico Geological Society, Border Region, Chihuahua, Mexico, and United States, p.209-214.

Collins, E. W., and Raney, J. A., 1991, Tertiary and Quaternary Structure and Paleotectonics Of the Hueco Basin, Trans-Pecos Texas and Chihuahua, Mexico: The University of Texas at Austin, Bureau of Economic Geology, Geological Circular 91-2, 44-p. text.

Collins, E. W., and Raney, J. A., 2000, Geologic map of West Hueco Bolson, El Paso Region, Texas: The University of Texas at Austin, Bureau of Economic Geology, Miscellaneous Map No. 40, scale 1:100,000, 24 p. text.

Connell, S.D., Hawley, J.W., and Love, D.W., 2005, Late Cenozoic drainage development in the southeastern Basin and Range of New Mexico, southeastern most Arizona and western Texas, in Lucas, S. G., Morgan, G., and Zeigler, K.E., eds., 2005, New Mexico's Ice Ages: New Mexico Museum of Natural History & Science Bulletin No. 28, p. 125-150.

Cordell, L., 1978, Regional geophysical setting of the Rio Grande rift: Geological Society Of America Bulletin, v.89, no.7,p.1073-1090.

Doser, D.I., Langford, R.P.,2007, Characterization of Aquifer Extent and Quality for Desalination and Brine Disposal Projects: Report W-06-04.

Eastoe, C.J., Hibbs, B.J., et.al, 2008, Isotopes in the Hueco Bolson Aquifer, Texas (USA) and Chihuahua (Mexico): local and general implications for recharge sources in alluvial Basins: Hydrogeology, v. 16, p. 737-747.

El Paso Water Utilities, 2004, Hueco Bolson Groundwater Conditions and Management Report: http://www.epwu.org/water/hueco_bolson.html (February 2009).

El Paso Water Utilities, 2009, Analytical Report: Internal Laboratory, Unpublished Document.

Folk, R.L., 2006. A Review of Grain-Size Parameters: Sedimentology, v.6, 73-93.

Fisher, Q., and Knipe, R., 1998, Fault sealing processes in siliciclastic sediments, in Faulting, Fault Sealing and Fluid Flow in Hydrocarbon Reservoirs: Geological Society London Special Publication, v. 147, p. 117– 134, doi: 10.1144/GSL.SP.1998.147.01.21.

Fulljames, J. R., Zijerveld, J.J., and Franssen, R. C. M. W., 1997, Fault seal processes: systematic analysis of fault seals over geological and production time scales, in Hydrocarbon Seals - Importance for Exploration and Production: Norwegian Petroleum Society Special Publication, v. 7, p. 51-59, doi: 10.1016/S0928-8937(96)80006-9.

Gardner, W. H., 1986, "Water content", p. 493-545, in Methods of Soil Analysis, part 1, Physical and Mineralogical Methods, A. Klute, ed. Agronomy Monograph no. 9 (2nd ed.), Soil Science Society of America, Madison, Wis.

Gee, G.W., and Dodson, M.E., 1981, Soil water content by microwave drying: a routine procedure: Soil Science Society of America Journal, v. 45, no. 6, p. 1234-1237, doi: 10.2136/sssaj1981.03615995004500060045x.

Geology, physiography, and groundwater resources: http://www.tceq.state.tx.us/assets/Public/permitting/watersupply/groundwater/pgma/hudspeth2.pdf (February 2009).

Gile, L.H., Hawley, J.W., and Grossman, R.B., 1981, Soils and Geomorphology in a Basin and Range Area of Southern New Mexico, Guide book to the Desert Project, Memoir 39, NM Bureau of Mines and Mineral Resources, Socorro, NM, p. 222.

Hadi, J., 1991, A Study of the Structure and Subsurface Geometry of the Hueco Bolson Texas

[M.S. thesis]: El Paso, University of Texas at El Paso, 88 p.

Hawley, J.W., Kernodle, J.M., 2000, Overview of the hydrology and geo hydrology of the Northern Rio Grande basin: Colorado, New Mexico and Texas. In Ortega-Klett, CT (ed) The Rio Grande Compact: It's the law! Proceedings of the 44th Annual New Mexico Water conference, New Mexico Water Resources Research Institute Report 312, 79-102 p.

Hawley, J. W., and Kennedy J.F., 2004, Creation of a Digital Hydrogeological Framework Model of the Mesilla Basin and Southern Jornada del Muerto Basin: WRRI Technical Completion Report. 332, 105 p.

Henry, C.D., and Price, J.G., 1985, Summary of the tectonic development of Trans-Pecos Texas: The University of Texas at Austin, Bureau of Economic Geology Miscellaneous Map No. 36, 8 p.

Henry, C.D., and Price, J.G., 1986, Early Basin and Range development in Trans-Pecos Texas and adjacent Chihuahua: magamatism and orientation, timing, and style of extension; Journal of Geophysical Research, v. 91, no. B6, p. 6213-6224.

Heywood, C.E., and Yager, R.M., 2003, Simulated ground-water flow in the Hueco Bolson, an Alluvial-basin aquifer system near El Paso, Texas: Water-Resources Investigations Report 02-4108, 73 p.

Hutchison, W.R., 2006, Groundwater Management in El Paso, Texas [Ph.D. thesis]: El Paso, University of Texas at El Paso, 329 p.

Imana, E.M.C., 2002, The Mesilla Bolson: An Intergrated Geophysical, Hydrological, and Structural Analysis Utilizing Free Air Anomalies [PhD. Thesis]: El Paso, University of Texas at El Paso, 152 p.

Kottloswki, F.E., 1958, Geological history of the Rio Grande near El Paso, Guidebook of Franklin and Hueco Mountains, Texas, West Texas Geological Society, Field Trip Guidebook, p. 46-64.

Langford, R. P., 2001, Segmentation of the Rio Grande Alluvial Surface and Evolution of the Rio Grande Rift: Rocky Mountain (53rd) and South-Central (35th) Sections, GSA, Joint Annual Meeting (April 29–May 2, 2001).

Mack, G.H., and Leeder, M.R., 1998, Channel shifting of the Rio Grande, southern Rio Grande rift: implications for alluvial stratigraphic models: Sedimentary Geology, v.117, p.207-219.

Mack, G.H., Seager, W.R,. and Kieling, J., 1994, Late Oligocene and Miocene faulting and sedimentation, and evolution of the southern Rio Grande rift, New Mexico, USA: Sedimentary Geology, v. 92, p. 79-96, doi: 10.1015/0037-0738(94)900055-8.

Mailloux, B. J., M. Person, S. Kelley, N. Dunbar, S. Cather, L. Strayer, and P. Hudleston, 1999, Tectonic controls on the hydrogeology of the Rio Grande Rift, New Mexico: Water Resources Research, v.35, p. 2641-2659.

Muehlberger, W.R., 1980, Texas lineament revisited, in Dickerson, P.W., Hoffer, J.M., and Callender, J.F., eds., Trans-Pecos region, southeastern New Mexico and West Texas: New Mexico Geological Society Annual Field Conference guidebook, no. 31, p. 113-121.

Muller, D. A., and Price, R. D., 1979, Ground-Water Availability in Texas, Estimates and Projections through 2030: Texas Department of Water Resources Report 238.

Nwaneshiudu, O., 2007, Modeling and assessment of flow and transport in the Hueco Bolson, a transboundary groundwater system: The El Paso/Ciudad Juarez Case [Ph.D. thesis]: El Paso, University of Texas at El Paso, 197 p.

Rawling, G. C., Goodwin, L. B., and Wilson, J. L., 2001, Internal architecture, permeability structure, and hydrologic significance of contrasting fault zone types: Geology, v. 27, p. 43– 46.

San Diego County Water Authority, 2005, Sea Water Desalination: http://www.sdcwa.org/manage/sources-desalintaion.phtml (December 2005).

Stevens, J.B., and Stevens, M.S., 1985, Basin and range deformation and depositional timing, Trans-Pecos Texas, in Dickerson, P.W., and Muehlberger, W.R., Structure and tectonics of Trans-Pecos Texas: West Texas Geological Society Field Conference Publication 85-81p. 157-163.

Strain, W.S., 1966, Blancan mammalian fauna and Pleistocene formations, Hudspeth County, Texas: Texas Memorial Museum Bulletin, no.10, 55 p.

Veatch, S. W., The Rio Grande Rift: http://home.att.net/~sgeoveatch/rio_grande_rift.htm (February 2006).

Wieck, J., Person, M., and Strayer, L., 1995, A finite element method for simulating fault block motion and hydrothermal fluid flow within rifting basins, Water Resources Research, v. 31, p. 3241– 3258.

Appendix A

Well Locations

Well Number	Elevation (m)	Longitude	Latitude
509A	3979	-106.33	31.80
510A	3975	-106.33	31.81
511A	3975	-106.33	31.81
512A	3974	-106.33	31.82
513A	3977	-106.33	31.83
514A	3970	-106.33	31.83
515A	3974	-106.33	31.84
601	3925	-106.38	31.90
602	3957	-106.38	31.90
603	3933	-106.37	31.90
604	3956	-106.37	31.90
605	3926	-106.36	31.90
606	3923	-106.36	31.89
607	3954	-106.35	31.89
608	3949	-106.35	31.89
609	3946	-106.35	31.88
610	3944	-106.35	31.88
611	3944	-106.34	31.87
612	3954	-106.34	31.87
613	3960	-106.34	31.86
614	3964	-106.34	31.86
615	3970	-106.33	31.85
616	3967	-106.33	31.85
MW-6	3955	-106.35	31.88
MW-5	3970	-106.34	31.86
MW-4	3973	-106.34	31.86

Appendix B

New Gravity Readings (Hueco Bolson, West Texas)

Free-Air Anomaly Values				
Station	Elevation (m)	Latitude	Longitude	Values (mGals)
Kidd	1246.60	31.77	-106.51	26.23
W601	1196.33	31.90	-106.38	-30.77
WJ02	1199.21	31.83	-106.35	-31.12
1	1197.39	31.89	-106.39	-29.63
2	1197.38	31.89	-106.39	-29.58
3	1197.12	31.89	-106.39	-29.64
4	1196.97	31.89	-106.39	-29.54
5	1196.98	31.89	-106.39	-29.41
6	1196.82	31.89	-106.40	-29.49
7	1196.03	31.89	-106.40	-29.49
8	1195.43	31.89	-106.40	-29.48
9	1195.00	31.88	-106.40	-29.46
10	1194.78	31.88	-106.40	-29.38
11	1194.63	31.88	-106.40	-29.31
12	1193.74	31.88	-106.40	-29.28
13	1193.08	31.88	-106.40	-29.27
14	1192.37	31.88	-106.40	-29.28
15	1191.71	31.88	-106.40	-29.32
16	1190.67	31.88	-106.40	-29.27
17	1189.68	31.87	-106.40	-29.26
18	1188.80	31.87	-106.40	-29.17
19	1188.06	31.87	-106.41	-29.11
20	1187.46	31.87	-106.41	-29.12
21	1186.39	31.87	-106.41	-29.12
22	1185.76	31.87	-106.41	-29.06
23	1185.17	31.87	-106.41	-28.97
24	1184.76	31.87	-106.41	-28.77
25	1184.48	31.86	-106.41	-28.65
26	1184.79	31.86	-106.41	-28.54
27	1184.38	31.86	-106.41	-28.40
28	1183.95	31.86	-106.41	-28.20
29	1183.44	31.86	-106.41	-27.97
30	1182.82	31.86	-106.41	-27.76
31	1182.51	31.86	-106.41	-26.50
32	1182.20	31.85	-106.42	-27.36
33	1182.14	31.85	-106.42	-27.06
34	1182.26	31.85	-106.42	-26.81
35	1181.90	31.85	-106.42	-26.55
36	1181.36	31.85	-106.42	-26.59
37	1181.03	31.85	-106.42	-25.64

Free-Air Anomaly Values				
Station	Elevation (m)	Latitude	Longitude	Values (mGals)
38	1180.84	31.85	-106.42	-26.75
39	1180.66	31.85	-106.42	-26.96
40	1180.69	31.84	-106.42	-26.99
41	1180.30	31.84	-106.42	-26.07
42	1180.38	31.84	-106.42	-27.25
43	1180.46	31.84	-106.42	-27.37
44	1180.39	31.84	-106.42	-27.45
45	1180.35	31.84	-106.42	-27.51
46	1180.83	31.84	-106.42	-27.53
47	1180.45	31.83	-106.42	-27.77
48	1180.52	31.83	-106.42	-27.90
49	1180.94	31.83	-106.42	-27.97
50	1180.99	31.83	-106.42	-28.08
51	1181.33	31.83	-106.42	-28.33
52	1196.54	31.90	-106.38	-31.15
53	1196.94	31.90	-106.38	-31.21
54	1197.40	31.90	-106.38	-31.24
55	1197.79	31.90	-106.38	-31.32
56	1198.17	31.90	-106.38	-31.41
57	1198.87	31.90	-106.38	-31.49
58	1199.84	31.90	-106.37	-31.60
59	1200.62	31.90	-106.37	-31.58
60	1201.36	31.90	-106.37	-31.27
61	1201.93	31.90	-106.37	-31.78
62	1202.36	31.90	-106.37	-31.81
63	1203.19	31.90	-106.37	-31.86
64	1203.48	31.90	-106.37	-31.90
65	1205.48	31.90	-106.36	-31.71
66	1205.58	31.90	-106.36	-31.70
67	1206.11	31.90	-106.36	-31.65
68	1206.23	31.90	-106.36	-31.67
69	1208.07	31.90	-106.36	-31.50
70	1207.20	31.90	-106.36	-31.58
71	1208.39	31.89	-106.36	-31.52
72	1196.63	31.90	-106.38	-31.36
73	1208.18	31.89	-106.36	-31.70
74	1208.72	31.89	-106.36	-31.57
75	1209.13	31.89	-106.36	-31.49
76	1209.60	31.89	-106.35	-31.43
77	1210.11	31.89	-106.35	-31.37

Free-Air Anomaly Values				
Station	Elevation (m)	Latitude	Longitude	Values (mGals)
78	1209.21	31.89	-106.35	-31.49
79	1209.22	31.89	-106.35	-31.47
80	1209.38	31.89	-106.35	-31.51
81	1208.79	31.89	-106.35	-31.39
82	1208.00	31.89	-106.35	-31.36
83	1207.48	31.88	-106.35	-31.45
84	1206.64	31.88	-106.35	-31.27
85	1206.17	31.88	-106.35	-31.25
86	1205.56	31.88	-106.35	-31.39
87	1205.27	31.88	-106.35	-31.40
88	1204.11	31.88	-106.35	-31.48
89	1203.23	31.88	-106.35	-31.44
90	1203.31	31.88	-106.35	-31.31
91	1203.29	31.88	-106.35	-31.33
92	1203.07	31.88	-106.35	-31.33
93	1204.17	31.87	-106.35	-31.36
94	1204.31	31.87	-106.35	-31.31
95	1202.97	31.87	-106.35	-31.47
96	1202.62	31.87	-106.35	-31.50
97	1203.03	31.87	-106.36	-31.51
98	1202.40	31.87	-106.35	-31.43
99	1204.73	31.87	-106.35	-31.21
100	1203.59	31.87	-106.35	-31.30
101	1202.58	31.87	-106.35	-31.30
102	1202.10	31.87	-106.35	-31.36
103	1200.66	31.87	-106.36	-32.32
104	1202.28	31.87	-106.36	-31.96
105	1202.04	31.87	-106.36	-32.26
106	1201.91	31.87	-106.36	-32.41
107	1202.67	31.87	-106.36	-32.22
108	1202.61	31.87	-106.36	-32.17
109	1202.37	31.87	-106.36	-32.26
110	1203.05	31.87	-106.36	-31.96
111	1202.15	31.87	-106.37	-32.14
112	1201.26	31.87	-106.37	-32.42
113	1201.64	31.87	-106.37	-32.29
114	1201.42	31.87	-106.37	-32.46
115	1202.27	31.87	-106.37	-32.27
116	1201.43	31.87	-106.37	-32.25
117	1201.68	31.87	-106.37	-32.14

Free-Air Anomaly Values				
Station	Elevation (m)	Latitude	Longitude	Values (mGals)
118	1199.89	31.87	-106.37	-32.58
119	1198.76	31.87	-106.37	-32.62
120	1199.54	31.87	-106.37	-32.20
121	1198.96	31.87	-106.38	-32.01
122	1198.73	31.87	-106.38	-32.07
123	1196.83	31.87	-106.38	-32.62
124	1196.42	31.87	-106.38	-32.56
125	1197.79	31.87	-106.38	-31.81
126	1194.52	31.87	-106.38	-32.65
127	1196.35	31.87	-106.38	-32.22
128	1196.64	31.87	-106.38	-32.10
129	1196.13	31.87	-106.38	-32.37
130	1195.14	31.87	-106.38	-32.62
131	1195.70	31.87	-106.38	-32.31
132	1195.05	31.87	-106.38	-31.82
133	1195.14	31.87	-106.38	-31.61
134	1195.23	31.87	-106.38	-31.40
135	1194.52	31.87	-106.38	-31.58
136	1194.65	31.87	-106.39	-31.48
137	1193.81	31.87	-106.39	-31.56
138	1194.06	31.87	-106.39	-31.47
139	1193.40	31.87	-106.39	-31.39
140	1193.11	31.87	-106.39	-31.50
141	1202.35	31.87	-106.35	-31.13
142	1202.26	31.87	-106.35	-31.03
143	1203.28	31.87	-106.35	-30.86
144	1204.24	31.87	-106.34	-30.75
145	1204.65	31.87	-106.34	-30.67
146	1205.89	31.87	-106.34	-30.51
147	1206.18	31.87	-106.34	-30.53
148	1209.56	31.86	-106.34	-30.08
149	1208.78	31.86	-106.34	-30.14
150	1208.04	31.86	-106.34	-30.29
151	1208.11	31.86	-106.34	-30.23
152	1208.24	31.86	-106.34	-30.18
153	1209.36	31.86	-106.34	-30.06
154	1209.63	31.86	-106.34	-29.97
155	1209.47	31.86	-106.34	-29.92
156	1208.90	31.86	-106.34	-29.99
157	1208.62	31.86	-106.34	-29.98

Free-Air Anomaly Values				
Station	Elevation (m)	Latitude	Longitude	Values (mGals)
158	1209.52	31.86	-106.33	-29.85
159	1209.81	31.85	-106.33	-29.83
160	1209.60	31.85	-106.33	-29.81
161	1209.53	31.85	-106.33	-29.68
162	1209.28	31.85	-106.33	-29.69
163	1209.63	31.85	-106.33	-29.55
164	1209.25	31.85	-106.33	-29.44
165	1210.29	31.85	-106.33	-29.33
166	1210.88	31.85	-106.33	-29.21
167	1211.00	31.85	-106.33	-29.13
168	1210.97	31.84	-106.33	-29.09
169	1211.61	31.84	-106.33	-28.92
170	1211.78	31.84	-106.33	-28.77
171	1211.70	31.84	-106.33	-28.71
172	1192.21	31.87	-106.39	-31.66
173	1191.43	31.87	-106.39	-31.45
174	1191.07	31.87	-106.39	-31.43
175	1190.85	31.87	-106.39	-31.28
176	1190.79	31.87	-106.39	-31.08
177	1189.96	31.87	-106.40	-30.90
178	1189.29	31.87	-106.40	-30.70
179	1189.12	31.87	-106.40	-30.58
180	1188.92	31.87	-106.40	-30.35
181	1189.49	31.87	-106.40	-30.09
182	1189.79	31.87	-106.40	-29.82
183	1189.68	31.87	-106.40	-29.56
184	1189.30	31.87	-106.40	-29.29
185	1188.19	31.87	-106.41	-29.01
186	1192.23	31.87	-106.39	-31.55
187	1192.25	31.87	-106.39	-31.58
188	1192.07	31.87	-106.39	-31.58
189	1191.82	31.87	-106.39	-31.62
190	1191.74	31.87	-106.39	-31.64
191	1191.59	31.86	-106.39	-31.72
192	1191.33	31.86	-106.39	-31.74
193	1190.95	31.86	-106.39	-31.81
194	1190.94	31.86	-106.39	-31.86
195	1191.66	31.86	-106.39	-31.78
196	1192.16	31.86	-106.39	-31.76
197	1192.59	31.86	-106.39	-31.70

Free-Air Anomaly Values				
Station	Elevation (m)	Latitude	Longitude	Values (mGals)
198	1193.07	31.86	-106.39	-31.74
199	1193.65	31.90	-106.39	-30.98
200	1194.97	31.90	-106.39	-30.98
201	1197.80	31.90	-106.39	-30.36
202	1196.01	31.90	-106.39	-30.90
203	1197.57	31.90	-106.39	-30.50
204	1196.59	31.90	-106.38	-30.70
205	1197.62	31.90	-106.38	-30.48
206	1198.12	31.90	-106.38	-30.47
207	1197.23	31.90	-106.38	-30.97
208	1198.70	31.90	-106.38	-30.95
209	1199.85	31.90	-106.38	-30.68
210	1199.93	31.90	-106.38	-30.93
211	1200.21	31.90	-106.38	-31.02
212	1201.52	31.90	-106.38	-30.72
213	1202.70	31.90	-106.37	-30.48
214	1203.22	31.90	-106.37	-30.59
215	1203.46	31.90	-106.37	-30.62
216	1205.34	31.90	-106.37	-30.23
217	1204.99	31.90	-106.37	-30.49
218	1206.00	31.90	-106.37	-30.33
219	1206.58	31.90	-106.37	-30.24
220	1207.00	31.90	-106.37	-30.44
221	1205.31	31.90	-106.37	-31.01
222	1205.58	31.90	-106.37	-31.01
223	1206.31	31.90	-106.36	-30.95
224	1206.62	31.90	-106.36	-30.91
225	1206.53	31.90	-106.36	-30.94
226	1206.09	31.90	-106.36	-30.95
227	1206.34	31.90	-106.36	-30.92
228	1206.72	31.90	-106.36	-30.91
229	1207.52	31.90	-106.36	-30.83
230	1208.46	31.90	-106.36	-30.75
231	1209.23	31.89	-106.35	-30.54
232	1208.39	31.89	-106.35	-30.50
233	1208.07	31.89	-106.36	-30.48
234	1208.15	31.89	-106.36	-30.47
235	1208.31	31.89	-106.36	-30.55
236	1207.54	31.89	-106.36	-30.62
237	1207.34	31.89	-106.36	-30.66

Free-Air Anomaly Values				
Station	Elevation (m)	Latitude	Longitude	Values (mGals)
238	1207.10	31.89	-106.36	-30.69
239	1206.32	31.89	-106.36	-30.82
240	1204.99	31.89	-106.37	-30.98
241	1203.90	31.89	-106.37	-31.01
242	1203.36	31.89	-106.37	-31.00
243	1202.67	31.89	-106.37	-31.05
244	1201.75	31.89	-106.37	-30.98
245	1201.08	31.89	-106.37	-30.94
246	1200.67	31.89	-106.37	-30.85
247	1199.95	31.89	-106.38	-30.88
248	1199.01	31.89	-106.38	-30.79
249	1198.32	31.89	-106.38	-30.75
250	1197.47	31.89	-106.38	-30.71
251	1196.74	31.89	-106.38	-30.56
252	1195.96	31.89	-106.38	-30.55
253	1195.18	31.89	-106.38	-30.45
254	1194.92	31.89	-106.39	-30.26
255	1194.98	31.89	-106.39	-30.94
256	1195.34	31.89	-106.39	-30.73
257	1195.63	31.89	-106.39	-30.55
258	1196.80	31.89	-106.39	-30.08
259	1196.80	31.89	-106.39	-29.89
260	1196.50	31.89	-106.40	-29.73
261	1205.98	31.82	-106.35	-30.02
262	1203.48	31.82	-106.35	-30.27
263	1202.29	31.82	-106.35	-30.40
264	1202.70	31.82	-106.35	-30.45
265	1201.84	31.82	-106.35	-30.62
266	1202.43	31.82	-106.35	-30.58
267	1203.12	31.82	-106.35	-30.51
268	1201.77	31.82	-106.35	-30.67
269	1200.17	31.82	-106.35	-30.89
270	1199.53	31.82	-106.35	-31.03
271	1200.55	31.82	-106.35	-31.05
272	1199.70	31.82	-106.36	-31.16
273	1199.23	31.82	-106.36	-31.22
274	1198.74	31.82	-106.36	-31.29
275	1198.30	31.82	-106.36	-31.23
276	1197.89	31.83	-106.36	-31.30
277	1197.54	31.83	-106.35	-31.34

Free-Air Anomaly Values				
Station	Elevation (m)	Latitude	Longitude	Values (mGals)
278	1198.02	31.83	-106.35	-31.50
279	1198.03	31.83	-106.35	-31.28
280	1197.58	31.83	-106.35	-31.32
281	1197.79	31.83	-106.35	-31.24
282	1198.50	31.83	-106.35	-31.16
283	1198.20	31.83	-106.35	-31.24
284	1197.78	31.83	-106.35	-31.25
285	1197.60	31.83	-106.35	-31.26
286	1197.94	31.83	-106.35	-31.28
287	1198.33	31.83	-106.35	-31.29
288	1198.87	31.83	-106.35	-31.33
289	1199.17	31.83	-106.36	-31.34
290	1199.81	31.83	-106.36	-31.33
291	1201.23	31.83	-106.36	-31.28
292	1202.73	31.83	-106.36	-31.14
293	1202.75	31.83	-106.36	-31.16
294	1202.61	31.83	-106.36	-31.20
295	1202.17	31.83	-106.36	-31.20
296	1202.03	31.83	-106.36	-31.24
297	1202.37	31.83	-106.36	-31.22
298	1202.95	31.81	-106.37	-31.25
299	1203.44	31.81	-106.37	-31.17
300	1203.97	31.81	-106.37	-31.09
301	1204.52	31.81	-106.37	-31.05
302	1205.10	31.81	-106.37	-31.00
303	1205.66	31.81	-106.37	-30.95
304	1206.06	31.82	-106.37	-30.94
305	1205.84	31.82	-106.37	-30.89
306	1205.26	31.82	-106.36	-30.82
307	1204.72	31.82	-106.36	-30.83
308	1204.15	31.82	-106.36	-30.82
309	1203.69	31.82	-106.36	-30.94
310	1203.09	31.82	-106.36	-30.98
311	1202.53	31.82	-106.36	-31.11
312	1202.00	31.82	-106.36	-31.08
313	1201.45	31.82	-106.36	-31.07
314	1200.47	31.82	-106.36	-31.12
315	1199.48	31.82	-106.36	-31.23
316	1212.44	31.80	-106.33	-27.44
317	1211.58	31.80	-106.33	-27.59

Free-Air Anomaly Values				
Station	Elevation (m)	Latitude	Longitude	Values (mGals)
318	1210.06	31.80	-106.34	-27.96
319	1207.43	31.80	-106.34	-28.29
320	1206.53	31.80	-106.34	-28.35
321	1205.21	31.80	-106.34	-28.59
322	1205.56	31.79	-106.34	-28.28
323	1204.45	31.79	-106.34	-28.57
324	1204.52	31.79	-106.34	-28.63
325	1204.52	31.79	-106.34	-28.58
326	1202.46	31.79	-106.34	-29.14
327	1203.10	31.79	-106.34	-28.83
328	1203.13	31.79	-106.35	-28.91
329	1202.90	31.79	-106.35	-29.01
330	1201.79	31.79	-106.35	-29.34
331	1201.20	31.79	-106.35	-29.58
332	1200.73	31.79	-106.35	-29.60
333	1200.65	31.79	-106.35	-29.59
334	1201.31	31.79	-106.35	-29.69
335	1201.38	31.79	-106.35	-29.69
336	1201.17	31.79	-106.35	-29.75
337	1201.08	31.79	-106.35	-29.74
338	1201.39	31.79	-106.35	-29.78
339	1201.65	31.79	-106.35	-29.73
340	1202.18	31.79	-106.35	-29.69
341	1202.90	31.79	-106.36	-29.74
342	1203.09	31.79	-106.36	-29.80
343	1203.23	31.79	-106.36	-29.90
344	1203.49	31.79	-106.36	-29.92
345	1203.51	31.79	-106.36	-29.92
346	1203.56	31.79	-106.36	-29.91
347	1203.70	31.79	-106.36	-29.86
348	1204.84	31.79	-106.36	-29.56
349	1204.32	31.79	-106.36	-29.75
350	1205.20	31.79	-106.36	-29.70
351	1205.94	31.79	-106.36	-29.81
352	1206.29	31.79	-106.36	-29.76
353	1206.88	31.79	-106.36	-29.68
354	1206.67	31.78	-106.36	-29.60
355	1206.16	31.78	-106.36	-29.70
356	1206.94	31.78	-106.36	-29.99
357	1206.98	31.78	-106.37	-30.10

Free-Air Anomaly Values				
Station	Elevation (m)	Latitude	Longitude	Values (mGals)
358	1207.05	31.79	-106.37	-30.20
359	1206.62	31.79	-106.37	-30.45
360	1205.83	31.79	-106.37	-30.56
361	1205.51	31.79	-106.37	-30.69
362	1192.69	31.87	-106.39	-31.51
363	1193.11	31.87	-106.39	-31.40
364	1193.06	31.87	-106.39	-31.36
365	1193.08	31.88	-106.39	-31.38
366	1193.36	31.88	-106.39	-31.38
367	1193.79	31.88	-106.39	-31.31
368	1194.22	31.88	-106.39	-31.17
369	1194.64	31.88	-106.39	-31.16
370	1194.80	31.88	-106.39	-31.04
371	1195.03	31.88	-106.39	-31.00
372	1195.04	31.89	-106.39	-30.83
373	1194.90	31.89	-106.39	-30.75
374	1195.30	31.89	-106.39	-30.72
375	1195.51	31.89	-106.39	-30.60
376	1196.27	31.89	-106.39	-30.41
377	1197.40	31.89	-106.39	-30.24
378	1198.41	31.89	-106.39	-30.10
379	1195.06	31.89	-106.39	-30.89
380	1195.55	31.89	-106.39	-31.14
381	1196.71	31.89	-106.38	-31.18
382	1198.52	31.89	-106.38	-31.34
383	1200.07	31.89	-106.38	-31.41
384	1201.41	31.89	-106.38	-31.39
385	1201.44	31.89	-106.37	-31.44
386	1202.36	31.89	-106.37	-31.36
387	1201.66	31.89	-106.37	-31.36
388	1202.87	31.89	-106.37	-31.65
389	1203.28	31.88	-106.37	-31.61
390	1203.42	31.88	-106.37	-31.67
391	1202.60	31.88	-106.37	-31.65
392	1202.33	31.88	-106.37	-31.66
393	1203.15	31.88	-106.37	-31.62
394	1203.94	31.88	-106.37	-31.58
395	1203.26	31.88	-106.37	-31.66
396	1203.04	31.88	-106.37	-31.66
397	1202.83	31.87	-106.37	-31.67

Free-Air Anomaly Values				
Station	Elevation (m)	Latitude	Longitude	Values (mGals)
398	1201.80	31.87	-106.37	-31.83
399	1201.72	31.87	-106.37	-31.93
400	1204.36	31.87	-106.35	-31.06
401	1204.39	31.87	-106.35	-31.18
402	1205.32	31.87	-106.35	-31.05
403	1205.92	31.88	-106.35	-31.01
404	1206.56	31.88	-106.35	-30.91
405	1204.14	31.89	-106.37	-31.32
406	1204.24	31.89	-106.37	-31.33
407	1203.70	31.89	-106.37	-31.27
408	1204.95	31.89	-106.37	-31.21
409	1213.51	31.80	-106.33	-27.48
410	1213.64	31.80	-106.33	-27.59
411	1214.62	31.80	-106.33	-27.59
412	1213.92	31.80	-106.33	-27.69
413	1213.46	31.80	-106.33	-27.94
414	1213.70	31.81	-106.34	-28.03
415	1211.96	31.81	-106.34	-28.31
416	1210.98	31.81	-106.34	-28.53
417	1211.10	31.81	-106.34	-28.66
418	1211.16	31.81	-106.34	-28.81
419	1211.18	31.81	-106.34	-28.91
420	1210.25	31.81	-106.34	-29.07
421	1209.31	31.81	-106.34	-29.26
422	1208.37	31.81	-106.34	-29.49
423	1208.31	31.81	-106.34	-29.57
424	1209.15	31.81	-106.35	-29.66
425	1207.32	31.81	-106.35	-29.85
426	1198.78	31.82	-106.36	-31.37
427	1201.24	31.82	-106.36	-31.23
428	1202.82	31.83	-106.36	-31.19
429	1204.00	31.83	-106.36	-31.07
430	1204.02	31.83	-106.36	-30.97
431	1203.63	31.83	-106.36	-31.15

Appendix C

Grain-Size Analysis (Hueco Bolson, West Texas)

Well 601

Sample Number Depth (ft)	Weight % Clay	Weight % Silt	Weight % Sand	Weight % Fine Sand	Weight % Coarse Sand	Weight % Gravel	Mean Grain-Size (Phi)	Mean Grain-Size (microns)
10-20	0.66	0.00	80.82	13.66	67.16	18.52	1.04	486.57
20-30	0.43	0.00	95.37	25.60	69.77	4.19	0.58	667.60
30-40	1.06	0.14	62.44	1.33	61.11	36.36	0.06	961.16
40-50	1.06	0.00	73.99	1.02	72.97	24.95	2.35	195.97
50-60	35.60	29.18	28.57	8.59	19.97	6.65	1.86	274.91
60-70	27.87	29.19	38.11	15.19	22.92	4.84	2.90	134.13
70-80	14.36	38.42	42.07	30.65	11.41	5.15	4.34	49.43
80-90	1.76	1.86	62.29	7.59	54.70	34.09	2.68	156.01
90-100	1.04	0.19	27.22	1.44	25.78	71.55	1.04	485.59
100-110	5.48	6.16	36.37	6.61	29.76	51.99	0.30	814.17
110-120	6.35	6.69	64.19	20.43	43.76	22.78	3.93	65.47
120-130	1.96	1.57	68.72	5.25	63.46	27.76	3.53	86.35
130-140	4.39	4.70	47.88	5.75	42.13	43.03	0.74	598.64
140-150	15.78	32.09	50.25	20.98	29.26	1.89	0.08	943.75
150-160	12.38	40.97	43.59	24.62	18.97	3.06	3.32	100.14
160-170	17.96	20.34	59.07	26.24	32.83	2.63	4.15	56.15
170-180	12.78	20.76	66.19	36.67	29.52	0.27	0.86	552.64
180-190	9.61	21.94	59.73	23.79	35.94	8.73	5.14	28.35
190-200	9.79	6.36	50.03	7.00	43.03	33.82	3.16	111.87
200-210	9.92	9.56	72.38	43.07	29.30	8.14	0.80	572.85
210-220	6.01	8.89	67.92	25.11	42.82	17.17	0.56	678.23
220-230	15.32	27.20	53.45	29.02	24.43	4.03	0.18	880.02
230-240	14.42	20.93	62.46	26.41	36.06	2.18	0.08	944.92
240-250	4.04	8.75	78.04	43.47	34.57	9.17	1.77	293.63
250-260	2.88	4.44	47.01	3.20	43.82	45.67	1.11	463.38
260-270	5.17	12.81	58.65	13.91	44.73	23.38	0.79	579.49

Well 601

Sample Number Depth (ft)	Weight % Clay	Weight % Silt	Weight % Sand	Weight % Fine Sand	Weight % Coarse Sand	Weight % Gravel	Mean Grain-Size (Phi)	Mean Grain-Size (microns)
270-280	10.58	18.47	56.06	11.05	45.01	14.89	0.73	604.90
280-290	7.77	21.35	58.25	12.38	45.87	12.63	0.36	781.01
290-300	9.99	22.22	50.60	9.16	41.43	17.19	0.61	653.57
300-310	6.60	18.46	65.30	30.99	34.31	9.64	0.52	696.41
310-320	2.33	6.66	68.82	22.50	46.32	22.19	5.05	30.18
320-330	2.72	6.07	52.92	4.62	48.30	38.29	1.10	467.91
330-340	20.75	40.97	37.25	18.58	18.67	1.02	3.85	69.32
340-350	5.11	9.95	73.28	18.45	54.83	11.66	1.46	363.88
350-360	7.26	18.28	56.66	17.02	39.64	17.80	0.23	850.23
360-370	8.74	10.84	75.73	61.50	14.23	4.69	5.01	30.94
370-380	9.38	13.48	74.96	60.87	14.09	2.18	4.77	36.67
380-390	19.03	28.93	46.59	34.11	12.48	5.45	4.26	52.19
390-400	18.26	22.68	56.01	42.50	13.50	3.05	4.19	54.65
400-410	13.95	23.95	61.46	49.19	12.27	0.64	3.34	98.60
410-420	9.56	29.61	60.15	52.71	7.44	0.68	3.09	117.20
420-430	6.18	11.50	79.52	70.86	8.66	2.80	3.79	72.39
430-440	19.37	61.04	19.59	15.87	3.72	0.00	4.00	62.48
440-450	13.69	27.77	55.42	21.45	33.97	3.11	2.09	235.34
450-460	12.06	15.37	72.16	66.09	6.07	0.41	4.13	57.20
460-470	27.73	24.92	45.55	10.53	35.02	1.80	3.26	104.46
470-480	2.97	10.18	86.85	61.57	25.29	0.00	3.00	125.17
480-490	19.51	34.62	45.87	38.62	7.24	0.00	4.02	61.85
490-500	10.99	22.77	66.23	54.16	12.07	0.00	2.03	245.01
500-510	7.44	27.01	65.55	38.22	27.33	0.00	2.83	140.65
510-520	7.25	15.20	77.54	12.75	64.80	0.00	3.92	66.06
520-530	20.43	43.61	35.96	11.85	24.11	0.00	5.20	27.28

Well 601

Sample Number Depth (ft)	Weight % Clay	Weight % Silt	Weight % Sand	Weight % Fine Sand	Weight % Coarse Sand	Weight % Gravel	Mean Grain-Size (Phi)	Mean Grain-Size (microns)
530-540	24.52	25.63	49.86	31.30	18.55	0.00	6.57	10.54
540-550	6.64	11.54	81.83	25.11	56.71	0.00	6.09	14.63
550-560	6.07	19.96	73.97	67.14	6.83	0.00	5.68	19.56
560-570	10.55	29.22	60.23	51.14	9.09	0.00	5.54	21.44
570-580	11.71	21.69	66.60	19.62	46.98	0.00	2.50	176.84
580-590	31.84	42.85	25.31	12.26	13.05	0.00	4.94	32.65
590-600	25.42	48.20	26.37	22.83	3.55	0.00	6.45	11.42
600-610	26.29	27.03	46.68	25.92	20.76	0.00	6.82	8.88
610-620	3.47	18.60	77.93	63.21	14.72	0.00	3.52	87.04
620-630	11.22	18.74	70.04	36.28	33.77	0.00	3.96	64.38
630-640	18.31	30.27	51.42	31.03	20.39	0.00	5.66	19.77
640-650	9.90	19.87	70.23	50.10	20.14	0.00	6.18	13.76
650-660	8.04	25.28	66.68	54.81	11.88	0.00	4.13	57.20
660-670	7.82	29.35	62.83	59.19	3.63	0.00	4.13	57.23
670-680	37.92	53.83	8.25	8.00	0.25	0.00	2.85	139.04
680-690	19.11	19.83	61.07	51.21	9.85	0.00	3.47	90.27
690-700	24.94	36.16	38.90	36.07	2.82	0.00	3.94	65.24
700-710	12.51	35.19	52.30	47.27	5.03	0.00	4.39	47.81
710-720	8.62	48.12	43.26	39.15	4.10	0.00	4.34	49.25
720-730	29.30	21.12	13.96	12.63	1.33	0.00	8.50	2.76
730-740	9.29	11.26	68.45	60.70	7.75	0.00	8.19	3.41
740-750	23.85	27.50	61.28	60.95	0.33	0.00	4.92	33.14
750-760	39.71	23.74	65.77	65.77	0.00	0.00	5.05	30.19
760-770	26.80	34.24	9.53	9.53	0.00	0.00	6.11	14.52
770-780	56.52	23.27	62.12	60.57	1.56	0.00	7.20	6.82
780-790	10.79	29.59	50.63	49.36	1.26	0.00	7.76	4.60

Well 601

Sample Number Depth (ft)	Weight % Clay	Weight % Silt	Weight % Sand	Weight % Fine Sand	Weight % Coarse Sand	Weight % Gravel	Mean Grain-Size (Phi)	Mean Grain-Size (microns)
790-800	5.03	31.34	53.18	53.18	0.00	0.00	6.58	10.49
800-810	16.37	23.69	64.62	62.14	2.48	0.00	6.02	15.42
810-820	22.74	29.84	52.15	51.19	0.96	0.00	7.18	6.92
820-830	42.94	21.66	67.28	62.62	4.66	0.00	6.21	13.52
830-840	42.66	27.07	55.59	51.51	4.08	0.00	7.01	7.73
840-850	39.03	30.40	58.60	58.38	0.22	0.00	5.24	26.51
850-860	41.52	24.58	60.17	59.40	0.77	0.00	6.97	7.99
860-870	N/A	N/A	N/A	N/A	N/A	N/A	N/A	N/A
870-880	N/A	N/A	N/A	N/A	N/A	N/A	N/A	N/A
880-890	N/A	N/A	N/A	N/A	N/A	N/A	N/A	N/A
890-900	15.62	36.83	46.64	46.64	0.00	0.00	5.83	17.60
900-910	21.43	36.83	46.64	46.64	0.00	0.00	N/A	N/A
910-920	26.75	36.83	46.64	46.64	0.00	0.00	N/A	N/A

Well 605

Sample Number Depth (ft)	Weight % Clay	Weight % Silt	Weight % Sand	Weight % Fine Sand	Weight % Coarse Sand	Weight % Gravel	Mean Grain-Size (Phi)	Mean Grain-Size (microns)
0-10	1.08	5.23	91.75	22.08	69.67	1.95	1.04	486.57
10-20	1.30	3.76	84.38	10.53	73.85	10.56	0.58	667.60
20-30	0.81	3.40	80.43	4.51	75.92	15.36	0.06	961.16
30-40	6.65	22.71	61.89	19.31	42.58	8.75	2.35	195.97
40-50	5.59	19.02	62.81	15.80	47.01	12.57	1.86	274.91
50-60	9.97	27.33	50.52	16.97	33.55	12.18	2.90	134.13
60-70	15.96	37.59	41.79	20.99	20.80	4.66	4.34	49.43
70-80	4.47	19.51	73.17	43.78	29.40	2.85	2.68	156.01
80-90	4.70	16.60	47.14	7.38	39.76	31.55	1.04	485.59
90-100	3.52	9.99	43.92	6.63	37.29	42.57	0.30	814.17
100-110	16.71	33.61	48.83	6.82	42.01	0.84	3.93	65.47
110-120	7.97	28.27	62.77	40.72	22.05	0.99	3.53	86.35
120-130	1.74	7.20	80.93	9.70	71.23	10.12	0.74	598.64
130-140	0.46	2.02	84.08	7.15	76.94	13.45	0.08	943.75
140-150	6.91	35.52	55.62	22.93	32.68	1.95	3.32	100.14
150-160	16.98	32.74	48.19	24.84	23.35	2.09	4.15	56.15
160-170	2.06	8.22	79.55	15.55	64.00	10.17	0.86	552.64
170-180	20.82	48.20	30.76	9.01	21.76	0.22	5.14	28.35
180-190	6.29	25.75	67.97	37.34	30.63	0.00	3.16	111.87
190-200	3.59	6.54	71.57	15.11	56.45	18.31	0.80	572.85
200-210	1.34	5.13	86.52	10.27	76.24	7.01	0.56	678.23
210-220	0.86	3.66	78.31	7.75	70.56	17.17	0.18	880.02
220-230	1.78	6.43	41.50	13.87	27.63	50.29	0.08	944.92
230-240	3.74	16.76	70.47	22.57	47.90	9.03	1.77	293.63
240-250	2.11	11.06	64.83	24.78	40.04	22.00	1.11	463.38
250-260	2.06	7.26	69.44	19.00	50.44	21.24	0.79	579.49

Well 605

Sample Number Depth (ft)	Weight % Clay	Weight % Silt	Weight % Sand	Weight % Fine Sand	Weight % Coarse Sand	Weight % Gravel	Mean Grain-Size (Phi)	Mean Grain-Size (microns)
260-270	3.71	8.25	69.13	8.41	60.72	18.91	0.73	604.90
270-280	1.18	4.83	78.90	8.64	70.26	15.09	0.36	781.01
280-290	3.24	7.75	64.01	11.03	52.99	25.00	0.61	653.57
290-300	1.53	6.20	72.85	12.07	60.77	19.42	0.52	696.41
300-310	17.15	49.09	32.33	16.08	16.25	1.42	5.05	30.18
310-320	2.27	8.27	76.49	20.77	55.72	12.98	1.10	467.91
320-330	12.73	39.48	39.77	15.35	24.43	8.02	3.85	69.32
330-340	4.30	11.21	71.93	21.67	50.26	12.56	1.46	363.88
340-350	2.29	6.08	58.05	9.68	48.37	33.58	0.23	850.23
350-360	19.70	38.03	42.27	34.13	8.14	0.00	5.01	30.94
360-370	13.09	39.95	46.97	42.63	4.34	0.00	4.77	36.67
370-380	20.50	32.02	44.57	7.07	37.50	2.91	4.26	52.19
380-390	17.32	32.78	49.69	16.97	32.72	0.21	4.19	54.65
390-400	10.15	37.37	36.28	20.08	16.21	16.20	3.34	98.60
400-410	10.47	17.45	67.11	38.14	28.97	4.98	3.09	117.20
410-420	11.97	30.05	55.60	30.50	25.09	2.38	3.79	72.39
420-430	16.20	26.61	57.19	31.61	25.58	0.00	4.00	62.48
430-440	3.41	12.79	72.32	44.62	27.70	11.48	2.09	235.34
440-450	6.04	35.58	58.38	48.95	9.43	0.00	4.13	57.20
450-460	16.40	22.65	59.44	10.85	48.58	1.52	3.26	104.46
460-470	15.83	18.80	64.44	6.54	57.89	0.93	3.00	125.17
470-480	16.03	34.66	47.06	14.59	32.47	2.26	4.02	61.85
480-490	3.38	10.67	84.86	40.67	44.19	1.09	2.03	245.01
490-500	6.70	15.83	76.30	45.59	30.71	1.17	2.83	140.65
500-510	13.75	29.04	54.21	31.07	23.15	3.00	3.92	66.06
510-520	19.35	50.67	29.78	14.64	15.15	0.19	5.20	27.28

Well 605

Sample Number Depth (ft)	Weight % Clay	Weight % Silt	Weight % Sand	Weight % Fine Sand	Weight % Coarse Sand	Weight % Gravel	Mean Grain-Size (Phi)	Mean Grain-Size (microns)
520-530	35.34	48.69	15.40	0.27	15.13	0.57	6.57	10.54
530-540	39.61	34.63	22.11	0.06	22.06	3.65	6.09	14.63
540-550	40.24	27.38	27.42	0.16	27.26	4.97	5.68	19.56
550-560	39.14	25.43	33.60	0.02	33.58	1.83	5.54	21.44
560-570	13.68	15.06	63.49	16.79	46.70	7.77	2.50	176.84
570-580	23.97	33.41	40.32	22.50	17.82	2.30	4.94	32.65
580-590	31.96	49.46	18.58	13.62	4.96	0.00	6.45	11.42
590-600	29.84	63.91	6.25	1.48	4.78	0.00	6.82	8.88
600-610	6.94	31.02	61.48	38.66	22.83	0.56	3.52	87.04
610-620	8.25	33.21	58.13	42.45	15.68	0.41	3.96	64.38
620-630	25.38	49.43	25.20	5.32	19.88	0.00	5.66	19.77
630-640	33.75	44.57	21.69	5.85	15.83	0.00	6.18	13.76
640-650	14.35	34.12	50.52	26.11	24.41	1.02	4.13	57.20
650-660	13.91	31.31	53.87	33.17	20.70	0.91	4.13	57.23
660-670	7.92	17.47	73.30	39.17	34.13	1.31	2.85	139.04
670-680	6.60	18.06	75.34	61.57	13.77	0.00	3.47	90.27
680-690	14.48	26.40	59.12	32.88	26.24	0.00	3.94	65.24
690-700	20.61	24.06	55.32	30.30	25.02	0.00	4.39	47.81
700-710	10.04	28.24	61.72	61.35	0.36	0.00	4.34	49.25
710-720	14.01	21.94	64.05	61.25	2.80	0.00	4.36	48.81
720-730	13.21	38.92	47.87	47.87	0.00	0.00	4.88	33.98
730-740	64.30	21.49	14.21	12.85	1.36	0.00	8.02	3.86
740-750	16.33	11.82	71.85	63.72	8.13	0.00	3.85	69.33
750-760	10.25	27.80	61.95	61.61	0.33	0.00	4.37	48.44
760-770	10.49	23.74	65.77	65.77	0.00	0.00	4.32	50.22
770-780	56.23	34.24	9.53	9.53	0.00	0.00	8.01	3.87

Well 605

Sample Number Depth (ft)	Weight % Clay	Weight % Silt	Weight % Sand	Weight % Fine Sand	Weight % Coarse Sand	Weight % Gravel	Mean Grain-Size (Phi)	Mean Grain-Size (microns)
780-790	28.91	52.18	18.91	18.91	0.00	0.00	6.46	11.34
790-800	20.50	33.49	46.01	43.10	2.91	0.00	5.11	28.97
800-810	14.60	23.27	62.12	60.57	1.56	0.00	4.43	46.30
810-820	19.79	29.59	50.63	49.36	1.26	0.00	5.05	30.26
820-830	15.47	31.34	53.18	53.18	0.00	0.00	4.76	36.97
830-840	11.63	23.70	64.67	62.19	2.48	0.00	4.16	55.77
840-850	38.17	40.09	21.74	20.96	0.77	0.00	6.79	9.04
850-860	18.00	29.84	52.15	51.19	0.96	0.00	4.86	34.44
860-870	19.54	22.79	57.67	57.67	0.00	0.00	4.89	33.82
970-880	36.75	48.71	14.54	14.50	0.04	0.00	6.79	9.05
880-890	10.88	21.70	67.42	62.74	4.67	0.00	3.97	63.67
890-900	15.30	27.74	56.97	52.78	4.18	0.00	4.46	45.35
900-910	11.00	30.40	58.60	58.38	0.22	0.00	4.40	47.34
910-920	15.25	24.58	60.17	59.40	0.77	0.00	4.57	42.21
920-930	16.53	36.83	46.64	46.64	0.00	0.00	5.11	29.01

Well 610

Sample Number Depth (ft)	Weight % Clay	Weight % Silt	Weight % Sand	Weight % Fine Sand	Weight % Coarse Sand	Weight % Gravel	Mean Grain-Size (Phi)	Mean Grain-Size (microns)
0-10	1.76	14.14	83.83	47.45	36.38	0.27	1.04	486.57
10-20	0.00	1.58	98.42	20.40	78.03	0.00	0.58	667.60
20-30	1.61	2.50	53.13	7.47	45.66	42.76	0.06	961.16
30-40	2.11	2.24	54.63	6.77	47.85	41.03	2.35	195.97
40-50	0.83	0.93	62.64	5.97	56.67	35.60	1.86	274.91
50-60	7.45	4.64	69.89	9.02	60.87	18.01	2.90	134.13
60-70	4.24	14.46	78.24	34.59	43.64	3.06	4.34	49.43
70-80	1.31	8.08	77.71	36.73	40.98	12.90	2.68	156.01
80-90	3.48	12.30	67.50	18.08	49.42	16.72	1.04	485.59
90-100	0.89	2.95	66.35	14.14	52.21	29.80	0.30	814.17
100-110	9.51	39.46	51.04	48.89	2.15	0.00	3.93	65.47
110-120	5.48	16.50	61.72	6.87	54.84	16.31	3.53	86.35
120-130	5.90	19.92	71.81	52.01	19.79	2.37	0.74	598.64
130-140	0.06	0.15	91.36	2.00	89.35	8.44	0.08	943.75
140-150	1.95	2.69	71.57	0.73	70.84	23.79	3.32	100.14
150-160	46.60	31.40	14.33	1.00	13.33	7.67	4.15	56.15
160-170	19.77	47.02	33.20	23.67	9.53	0.00	0.86	552.64
170-180	34.86	35.54	28.48	4.95	23.53	1.12	5.14	28.35
180-190	12.71	46.94	39.52	30.71	8.82	0.83	3.16	111.87
190-200	6.76	32.86	54.80	42.68	12.11	5.59	0.80	572.85
200-210	6.28	19.78	53.33	5.02	48.31	20.61	0.56	678.23
210-220	4.95	14.87	52.81	1.15	51.66	27.37	0.18	880.02
220-230	0.91	1.90	75.36	4.74	70.62	21.83	0.08	944.92
230-240	0.17	0.33	73.65	2.61	71.04	25.85	1.77	293.63
240-250	3.14	9.04	59.17	3.40	55.76	28.66	1.11	463.38
250-260	7.28	17.68	31.46	7.47	23.99	43.58	0.79	579.49

Well 610

Sample Number Depth (ft)	Weight % Clay	Weight % Silt	Weight % Sand	Weight % Fine Sand	Weight % Coarse Sand	Weight % Gravel	Mean Grain-Size (Phi)	Mean Grain-Size (microns)
260-270	11.45	24.16	49.09	8.27	40.82	15.31	0.73	604.90
270-280	18.59	37.26	40.64	20.19	20.45	3.51	0.36	781.01
280-290	10.41	45.69	43.61	28.63	14.99	0.29	0.61	653.57
290-300	1.97	1.92	42.09	2.08	40.01	54.02	0.52	696.41
300-310	3.40	4.22	63.81	0.75	63.05	28.57	5.05	30.18
310-320	14.27	46.84	31.35	18.14	13.21	7.55	1.10	467.91
320-330	20.54	39.19	39.10	10.45	28.65	1.17	3.85	69.32
330-340	37.51	46.43	15.43	9.77	5.66	0.63	1.46	363.88
340-350	37.50	44.32	18.18	12.22	5.96	0.00	0.23	850.23
350-360	21.38	30.68	47.94	20.80	27.14	0.00	5.01	30.94
360-370	9.55	36.85	53.60	51.68	1.92	0.00	4.77	36.67
370-380	30.40	39.74	29.86	28.96	0.90	0.00	4.26	52.19
380-390	27.66	47.44	24.56	22.53	2.03	0.34	4.19	54.65
390-400	17.04	32.53	41.50	14.69	26.80	8.93	3.34	98.60
400-410	44.53	22.70	32.51	0.32	32.19	0.26	3.09	117.20
410-420	51.92	20.99	25.75	14.29	11.46	1.34	3.79	72.39
420-430	38.84	44.67	16.49	9.64	6.85	0.00	4.00	62.48
430-440	36.37	40.56	23.07	15.83	7.25	0.00	2.09	235.34
440-450	8.68	55.06	36.26	30.70	5.56	0.00	4.13	57.20
450-460	26.49	46.03	27.48	23.98	3.50	0.00	3.26	104.46
460-470	15.80	37.21	41.96	6.76	35.20	5.03	3.00	125.17
470-480	31.77	42.42	25.81	11.18	14.63	0.00	4.02	61.85
480-490	21.32	35.37	41.17	25.49	15.68	2.14	2.03	245.01
490-500	0.44	0.84	73.54	2.64	70.90	25.18	2.83	140.65
500-510	17.52	32.95	49.53	40.09	9.44	0.00	3.92	66.06
510-520	2.11	3.88	82.86	2.46	80.39	11.15	5.20	27.28

Well 610

Sample Number Depth (ft)	Weight % Clay	Weight % Silt	Weight % Sand	Weight % Fine Sand	Weight % Coarse Sand	Weight % Gravel	Mean Grain-Size (Phi)	Mean Grain-Size (microns)
520-530	5.46	11.92	72.17	2.36	69.82	10.45	6.57	10.54
530-540	11.48	22.31	62.70	3.66	59.05	3.50	6.09	14.63
540-550	17.41	39.26	39.58	13.64	25.94	3.75	5.68	19.56
550-560	24.00	41.75	34.25	34.00	0.25	0.00	5.54	21.44
560-570	16.96	63.16	19.88	19.37	0.51	0.00	2.50	176.84
570-580	18.95	46.55	33.45	9.31	24.15	1.05	4.94	32.65
580-590	15.10	46.03	38.36	31.73	6.63	0.51	6.45	11.42
590-600	28.54	60.27	11.19	11.19	0.00	0.00	6.82	8.88
600-610	32.76	40.34	25.76	8.78	16.98	1.13	3.52	87.04
610-620	11.81	50.22	36.00	29.00	7.00	1.96	3.96	64.38
620-630	12.21	74.03	13.76	13.03	0.73	0.00	5.66	19.77
630-640	27.77	55.68	14.66	6.36	8.30	1.89	6.18	13.76
640-650	32.47	58.50	5.68	4.16	1.52	3.34	4.13	57.20
650-660	24.74	32.11	42.55	24.07	18.48	0.60	4.13	57.23
660-670	14.24	13.34	63.33	1.31	62.01	9.09	2.85	139.04
670-680	23.17	39.21	33.86	7.48	26.38	3.77	3.47	90.27
680-690	28.22	50.02	21.76	7.88	13.88	0.00	3.94	65.24
690-700	26.31	61.75	11.94	11.37	0.57	0.00	4.39	47.81
700-710	19.34	24.75	55.91	50.89	5.02	0.00	4.34	49.25
710-720	15.47	26.94	54.67	39.95	14.72	2.92	4.36	48.81
720-730	21.57	22.66	52.33	1.33	51.00	3.44	4.88	33.98
730-740	31.01	38.76	28.56	2.47	26.09	1.67	8.02	3.86
740-750	24.54	29.90	33.53	5.44	28.09	12.04	3.85	69.33
750-760	40.45	33.64	25.91	16.85	9.06	0.00	4.37	48.44
760-770	40.68	30.98	28.34	16.86	11.48	0.00	4.32	50.22
770-780	37.66	44.54	17.80	7.70	10.10	0.00	8.01	3.87

Well 610

Sample Number Depth (ft)	Weight % Clay	Weight % Silt	Weight % Sand	Weight % Fine Sand	Weight % Coarse Sand	Weight % Gravel	Mean Grain-Size (Phi)	Mean Grain-Size (microns)
780-790	21.02	51.43	27.55	26.55	1.00	0.00	6.46	11.34
790-800	31.89	44.05	24.07	23.40	0.66	0.00	5.11	28.97
800-810	30.31	54.29	15.40	15.40	0.00	0.00	4.43	46.30
810-820	30.33	55.37	14.31	14.31	0.00	0.00	5.05	30.26
820-830	21.02	51.37	27.62	27.62	0.00	0.00	4.76	36.97
830-840	27.13	49.51	23.36	23.00	0.35	0.00	4.16	55.77
840-850	36.97	40.07	22.96	22.37	0.59	0.00	6.79	9.04
850-860	29.76	47.71	22.53	22.53	0.00	0.00	4.86	34.44
860-870	39.44	40.93	19.62	11.82	7.80	0.00	4.89	33.82
970-880	23.74	41.72	34.54	22.53	12.01	0.00	6.79	9.05
880-890	11.47	50.30	38.23	32.49	5.74	0.00	3.97	63.67
890-900	17.72	60.29	21.99	19.54	2.45	0.00	4.46	45.35
900-910	42.61	42.24	15.15	15.15	0.00	0.00	4.40	47.34
910-920	48.07	45.07	6.86	6.52	0.34	0.00	4.57	42.21
920-930	34.61	39.75	25.64	25.29	0.35	0.00	5.11	29.01

Well 615

Sample Number Depth (ft)	Weight % Clay	Weight % Silt	Weight % Sand	Weight % Fine Sand	Weight % Coarse Sand	Weight % Gravel	Mean Grain-Size (Phi)	Mean Grain-Size (microns)
0-10	12.30	56.73	30.97	26.79	4.18	0.00	1.04	486.57
10-20	0.07	0.22	83.44	2.93	80.51	15.16	0.58	667.60
20-30	0.08	0.31	88.86	3.43	85.43	9.09	0.06	961.16
30-40	0.05	0.33	90.95	3.47	87.48	7.49	2.35	195.97
40-50	0.00	0.23	87.71	3.04	84.68	10.99	1.86	274.91
50-60	0.04	0.25	78.24	2.09	76.15	20.10	2.90	134.13
60-70	16.95	32.50	21.82	17.83	3.99	28.73	4.34	49.43
70-80	25.68	40.88	32.31	24.80	7.52	1.13	2.68	156.01
80-90	19.13	43.87	37.00	35.14	1.87	0.00	1.04	485.59
90-100	15.90	33.65	50.46	42.19	8.26	0.00	0.30	814.17
100-110	29.08	31.39	31.25	8.46	22.79	8.28	3.93	65.47
110-120	34.59	28.70	32.15	7.40	24.75	4.35	3.53	86.35
120-130	76.85	20.72	2.43	0.00	2.43	0.00	0.74	598.64
130-140	55.52	35.97	8.51	1.75	6.76	0.00	0.08	943.75
140-150	21.51	49.54	28.27	23.19	5.07	0.00	3.32	100.14
150-160	21.77	32.55	45.06	8.22	36.84	0.62	4.15	56.15
160-170	0.89	1.05	34.86	4.89	29.96	63.20	0.86	552.64
170-180	0.04	0.06	69.73	0.40	69.32	30.00	5.14	28.35
180-190	0.52	0.36	78.32	0.77	77.55	20.67	3.16	111.87
190-200	1.77	1.15	80.78	0.81	79.97	16.30	0.80	572.85
200-210	3.34	1.09	68.67	0.00	68.67	26.90	0.56	678.23
210-220	24.20	28.87	46.16	10.67	35.50	0.00	0.18	880.02
220-230	11.66	14.72	73.28	2.63	70.65	0.34	0.08	944.92
230-240	34.38	11.70	41.63	1.18	40.45	12.30	1.77	293.63
240-250	39.73	29.33	30.93	30.61	0.33	0.00	1.11	463.38
250-260	16.05	36.86	47.09	44.89	2.20	0.00	0.79	579.49

Well 615

Sample Number Depth (ft)	Weight % Clay	Weight % Silt	Weight % Sand	Weight % Fine Sand	Weight % Coarse Sand	Weight % Gravel	Mean Grain-Size (Phi)	Mean Grain-Size (microns)
260-270	28.86	36.78	34.37	33.30	1.07	0.00	0.73	604.90
270-280	21.92	44.61	33.47	27.09	6.37	0.00	0.36	781.01
280-290	15.65	41.91	42.44	36.03	6.41	0.00	0.61	653.57
290-300	16.47	40.09	43.44	41.21	2.23	0.00	0.52	696.41
300-310	57.89	34.75	7.36	6.49	0.87	0.00	5.05	30.18
310-320	25.64	58.48	15.88	15.88	0.00	0.00	1.10	467.91
320-330	15.00	46.72	37.54	35.30	2.23	0.74	3.85	69.32
330-340	27.36	31.57	27.87	3.34	24.54	13.19	1.46	363.88
340-350	38.88	24.86	30.08	20.14	9.94	6.17	0.23	850.23
350-360	58.58	30.54	8.78	3.36	5.41	2.11	5.01	30.94
360-370	15.81	52.02	24.02	18.08	5.95	8.09	4.77	36.67
370-380	17.67	61.99	16.10	13.07	3.03	4.24	4.26	52.19
380-390	15.64	68.79	13.77	12.87	0.90	1.80	4.19	54.65
390-400	19.31	46.66	29.11	26.01	3.10	4.39	3.34	98.60
400-410	28.62	29.33	41.18	39.43	1.75	0.76	3.09	117.20
410-420	38.09	38.30	23.37	23.17	0.20	0.00	3.79	72.39
420-430	56.57	39.72	3.71	3.71	0.00	0.00	4.00	62.48
430-440	44.13	45.30	8.77	5.88	2.89	1.81	2.09	235.34
440-450	43.69	47.95	8.36	8.02	0.34	0.00	4.13	57.20
450-460	25.09	38.99	30.41	11.28	19.13	5.51	3.26	104.46
460-470	53.97	34.94	11.10	6.78	4.32	0.00	3.00	125.17
470-480	21.59	24.95	53.46	52.79	0.67	0.00	4.02	61.85
480-490	42.30	50.46	7.24	6.24	1.00	0.00	2.03	245.01
490-500	11.96	32.83	52.65	46.03	6.62	2.56	2.83	140.65
500-510	51.07	34.81	4.74	0.21	4.53	9.39	3.92	66.06
510-520	8.25	57.30	34.45	31.69	2.76	0.00	5.20	27.28

Well 615

Sample Number Depth (ft)	Weight % Clay	Weight % Silt	Weight % Sand	Weight % Fine Sand	Weight % Coarse Sand	Weight % Gravel	Mean Grain-Size (Phi)	Mean Grain-Size (microns)
520-530	9.91	38.83	50.94	50.30	0.65	0.32	6.57	10.54
530-540	64.52	32.05	3.43	0.97	2.45	0.00	6.09	14.63
540-550	23.54	56.56	19.90	18.56	1.34	0.00	5.68	19.56
550-560	23.58	65.80	9.93	8.88	1.04	0.69	5.54	21.44
560-570	24.41	43.32	31.93	30.60	1.33	0.33	2.50	176.84
570-580	49.88	35.78	14.34	0.19	14.16	0.00	4.94	32.65
580-590	43.07	27.18	29.10	15.65	13.45	0.37	6.45	11.42
590-600	45.22	26.14	27.42	14.12	13.31	0.92	6.82	8.88
600-610	64.76	29.94	5.30	0.06	5.24	0.00	3.52	87.04
610-620	28.02	45.77	24.17	15.48	8.69	2.04	3.96	64.38
620-630	20.50	56.19	19.01	13.95	5.06	4.30	5.66	19.77
630-640	59.02	36.53	4.45	4.05	0.40	0.00	6.18	13.76
640-650	46.15	43.54	10.31	9.02	1.29	0.00	4.13	57.20
650-660	46.51	41.75	11.13	10.18	0.95	0.00	4.13	57.23
660-670	13.55	39.36	45.79	40.53	5.25	1.22	2.85	139.04
670-680	32.81	34.23	27.10	13.28	13.82	5.18	3.47	90.27
680-690	38.37	31.55	29.78	26.56	3.22	0.00	3.94	65.24
690-700	37.53	27.78	34.19	11.52	22.67	0.00	4.39	47.81
700-710	20.99	40.32	38.59	22.08	16.51	0.00	4.34	49.25
710-720	10.93	21.95	60.53	54.02	6.51	6.59	4.36	48.81
720-730	13.51	43.72	42.77	39.66	3.11	0.00	4.88	33.98
730-740	14.46	37.55	47.99	43.75	4.24	0.00	8.02	3.86
740-750	12.17	29.45	58.38	57.96	0.42	0.00	3.85	69.33
750-760	43.19	44.13	12.68	10.20	2.48	0.00	4.37	48.44
760-770	24.13	16.89	35.99	3.42	32.57	22.69	4.32	50.22
770-780	39.82	40.75	19.43	2.50	16.92	0.00	8.01	3.87

Well 615

Sample Number Depth (ft)	Weight % Clay	Weight % Silt	Weight % Sand	Weight % Fine Sand	Weight % Coarse Sand	Weight % Gravel	Mean Grain-Size (Phi)	Mean Grain-Size (microns)
780-790	23.11	53.53	23.36	15.47	7.89	0.00	6.46	11.34
790-800	16.36	45.13	38.51	38.23	0.28	0.00	5.11	28.97
800-810	45.87	43.26	10.34	10.02	0.31	0.00	4.43	46.30
810-820	16.70	34.59	46.95	45.37	1.58	1.75	5.05	30.26
820-830	41.87	37.36	14.21	3.93	10.28	6.40	4.76	36.97
830-840	20.95	24.81	51.18	40.60	10.58	2.24	4.16	55.77
840-850	41.23	41.90	13.74	8.16	5.58	3.13	6.79	9.04
850-860	45.61	44.21	10.18	9.99	0.20	0.00	4.86	34.44
860-870	48.10	44.30	7.59	6.98	0.62	0.00	4.89	33.82
970-880	47.51	31.10	21.29	16.00	5.29	0.00	6.79	9.05
880-890	32.88	38.68	28.44	27.52	0.92	0.00	3.97	63.67
890-900	34.49	37.57	27.94	26.10	1.84	0.00	4.46	45.35
900-910	54.96	37.33	7.50	7.11	0.39	0.00	4.40	47.34
910-920	31.84	41.55	26.61	26.57	0.04	0.00	4.57	42.21
920-930	43.51	35.27	21.12	20.78	0.34	0.00	5.11	29.01

Well 509A

Sample Number Depth (ft)	Weight % Clay	Weight % Silt	Weight % Sand	Weight % Fine Sand	Weight % Coarse Sand	Weight % Gravel	Mean Grain-Size (Phi)	Mean Grain-Size (microns)
0-50	0.31	0.70	39.04	19.33	19.71	57.94	-0.59	1502.40
50-60	66.77	18.32	14.60	0.00	14.60	0.31	7.86	4.31
60-70	58.19	20.18	12.03	2.07	9.96	9.59	6.93	8.18
70-80	39.11	33.48	25.93	4.04	21.89	1.48	5.94	16.24
80-90	47.71	28.82	11.61	7.75	3.86	11.86	6.40	11.84
90-100	34.36	20.78	29.00	15.54	13.46	15.85	4.88	33.88
100-110	47.29	27.84	14.58	3.55	11.03	10.29	6.27	12.94
110-120	44.93	28.36	17.83	2.80	15.03	8.55	6.10	14.62
120-130	62.48	19.76	14.39	1.93	12.46	3.37	7.42	5.85
130-140	1.80	2.18	83.44	80.06	3.37	12.59	2.15	224.64
140-150	8.92	8.20	82.80	73.19	9.62	0.00	3.28	103.27
150-160	4.83	4.80	75.73	65.25	10.48	14.43	2.16	223.07
160-170	38.77	44.88	12.12	3.66	8.46	4.23	6.57	10.49
170-180	55.22	34.24	10.54	0.41	10.14	0.00	7.66	4.94
180-190	24.14	44.81	29.52	16.88	12.64	1.53	5.44	22.96
190-200	42.98	31.78	14.70	4.49	10.20	10.54	6.18	13.77
200-210	0.00	0.00	99.42	86.62	12.80	0.36	2.12	230.15
210-220	50.43	35.36	14.22	0.11	14.10	0.00	7.09	7.36
220-230	56.06	33.36	10.58	0.47	10.10	0.00	7.62	5.08
230-240	52.57	31.67	15.27	5.87	9.40	0.00	7.31	6.32
240-250	51.88	28.72	19.40	5.46	13.93	0.00	7.03	7.67
250-260	52.21	32.91	14.88	0.65	14.23	0.00	7.21	6.73
260-270	38.30	38.17	23.53	8.64	14.89	0.00	6.29	12.74
270-280	39.80	39.83	20.37	11.83	8.54	0.00	6.59	10.36
280-290	55.91	35.46	8.63	2.43	6.20	0.00	7.73	4.69
290-300	55.19	37.58	7.23	6.31	0.91	0.00	7.84	4.36

Well 509A

Sample Number Depth (ft)	Weight % Clay	Weight % Silt	Weight % Sand	Weight % Fine Sand	Weight % Coarse Sand	Weight % Gravel	Mean Grain-Size (Phi)	Mean Grain-Size (microns)
300-310	61.01	29.39	9.60	6.74	2.86	0.00	8.00	3.91
310-320	46.31	33.68	20.01	14.61	5.41	0.00	7.02	7.69
320-330	61.49	27.31	8.83	5.04	3.79	2.37	7.83	4.40
330-340	53.87	34.68	11.22	7.47	3.75	0.00	7.60	5.16
340-350	50.53	39.97	9.50	6.65	2.85	0.00	7.63	5.05
350-360	47.29	32.46	20.24	9.49	10.75	0.00	6.86	8.63
360-370	36.72	29.21	18.34	9.73	8.61	15.73	5.29	25.48
370-380	49.54	34.28	15.62	3.40	12.23	0.00	7.12	7.19
380-390	50.65	27.37	13.23	0.10	13.13	8.75	6.54	10.77
390-400	53.01	35.86	8.46	1.81	6.65	2.67	7.44	5.75
400-410	33.30	43.90	10.63	2.37	8.26	12.17	5.77	18.36
410-420	33.02	25.68	13.68	2.14	11.54	27.62	4.34	49.49
420-430	48.07	41.62	10.31	1.95	8.36	0.00	7.35	6.14
430-440	52.32	41.07	6.61	1.03	5.58	0.00	7.71	4.77
440-450	43.91	39.39	16.70	2.26	14.44	0.00	6.81	8.90
450-460	38.54	44.79	16.67	7.35	9.32	0.00	6.64	10.04
460-470	52.89	37.40	9.72	1.44	8.28	0.00	7.53	5.42
470-480	40.95	45.92	13.12	5.49	7.64	0.00	6.90	8.35
480-490	45.82	24.69	25.28	3.44	21.84	4.21	6.01	15.56
490-500	55.40	35.60	6.88	1.40	5.49	2.11	7.59	5.18
500-510	52.10	40.05	7.47	1.77	5.70	0.38	7.62	5.10
510-520	42.10	46.28	11.62	6.81	4.81	0.00	7.01	7.74
520-530	57.60	37.17	5.24	3.43	1.81	0.00	7.95	4.05
530-540	50.95	44.02	5.03	4.27	0.76	0.00	7.68	4.86
540-550	47.85	40.97	9.26	7.35	1.92	1.92	7.22	6.72
550-560	48.17	43.42	8.41	7.62	0.79	0.00	7.46	5.67

Well 509A

Sample Number Depth (ft)	Weight % Clay	Weight % Silt	Weight % Sand	Weight % Fine Sand	Weight % Coarse Sand	Weight % Gravel	Mean Grain-Size (Phi)	Mean Grain-Size (microns)
560-570	46.12	48.01	5.86	4.81	1.05	0.00	7.40	5.92
570-580	46.36	43.74	9.91	9.19	0.72	0.00	7.31	6.31
580-590	47.66	49.09	3.25	2.86	0.39	0.00	7.59	5.20
590-600	44.37	49.41	5.77	3.09	2.68	0.45	7.41	5.88
600-610	55.22	38.39	6.39	3.10	3.29	0.00	7.79	4.53
610-620	48.56	43.14	7.28	6.51	0.78	1.02	7.55	5.34
620-630	44.47	50.46	5.07	4.73	0.34	0.00	7.40	5.94
630-640	57.58	37.06	5.36	4.74	0.62	0.00	8.02	3.85
640-650	31.05	45.06	22.21	19.70	2.51	0.00	6.19	13.72
650-660	36.62	49.42	13.96	13.89	0.07	0.00	6.84	8.71
660-670	42.21	49.64	8.14	8.14	0.00	0.00	7.26	6.52
670-680	52.14	35.11	3.39	3.39	0.00	9.36	7.08	7.41
680-690	48.12	39.89	11.99	11.99	0.00	0.00	7.40	5.91
690-700	44.32	46.34	9.34	9.34	0.00	0.00	7.29	6.40
700-710	52.50	45.15	2.36	2.36	0.00	0.00	7.92	4.12
710-720	42.99	43.53	13.48	13.48	0.00	0.00	7.15	7.05
720-730	51.14	42.80	6.06	6.06	0.00	0.00	7.71	4.76
730-740	44.09	46.57	9.34	9.34	0.00	0.00	7.30	6.35
740-750	44.34	43.91	11.76	11.42	0.33	0.00	7.21	6.77
750-760	32.66	49.40	17.94	17.94	0.00	0.00	6.53	10.83
760-770	46.57	45.53	7.90	7.90	0.00	0.00	7.40	5.91
770-780	38.57	50.78	10.65	10.65	0.00	0.00	6.93	8.19
790-800	34.49	50.76	14.75	14.75	0.00	0.00	6.64	10.03
800-810	47.09	47.00	5.91	5.91	0.00	0.00	7.57	5.27
810-820	41.39	52.92	5.70	5.70	0.00	0.00	7.25	6.59
820-830	46.91	49.23	3.86	3.86	0.00	0.00	7.54	5.38

Well 509A

Sample Number Depth (ft)	Weight % Clay	Weight % Silt	Weight % Sand	Weight % Fine Sand	Weight % Coarse Sand	Weight % Gravel	Mean Grain-Size (Phi)	Mean Grain-Size (microns)
830-840	43.18	48.40	8.43	8.40	0.03	0.00	7.26	6.52
840-850	45.58	51.63	2.80	2.80	0.00	0.00	7.59	5.19
850-860	36.75	50.37	12.88	12.88	0.00	0.00	6.87	8.54
860-870	43.26	51.18	5.55	5.55	0.00	0.00	7.43	5.81
870-880	55.58	42.34	2.08	2.08	0.00	0.00	8.03	3.82
880-890	31.66	57.66	10.68	10.68	0.00	0.00	6.68	9.77
890-900	52.41	44.61	2.98	2.98	0.00	0.00	7.85	4.32
850-860	45.61	44.21	10.18	9.99	0.20	0.00	7.31	6.29
860-870	48.10	44.30	7.59	6.98	0.62	0.00	7.60	5.15
970-880	47.51	31.10	21.29	16.00	5.29	0.00	7.07	7.44
880-890	32.88	38.68	28.44	27.52	0.92	0.00	6.26	13.04
890-900	34.49	37.57	27.94	26.10	1.84	0.00	6.31	12.59
900-910	54.96	37.33	7.50	7.11	0.39	0.00	7.84	4.37
910-920	31.84	41.55	26.61	26.57	0.04	0.00	6.28	12.90
920-930	43.51	35.27	21.12	20.78	0.34	0.00	7.07	7.42

Vita

Sandy S. Marrufo was born in El Paso, Texas, on August 15, 1982, the daughter of David Marrufo and Etta E. Armijo. After graduating from Americas High School, El Paso, Texas, in June 2000, she enrolled at the University of Texas at El Paso where she began majoring in theatre arts. After September 2001, Sandy changed her major to education and began working full-time while attending fewer classes. In January 2007 she changed her major to geology and graduated in July 2009 with her Bachelor of Science degree and is awarded the Best Undergraduate Researcher from the geological science department. In August 2009 she began working on her Master of Science degree in Geology at the University of Texas at El Paso.

During her undergraduate career as geology major, Sandy began her research in the Hueco Bolson and presented her research at several meetings. In October 2008, she was awarded second place for the Undergraduate Sigma Gamma Epsilon Poster Session at the Geological Society of America Annual Meeting. In April 2009 she was awarded second place at the Advancing Hispanics/Chicanos and Native Americans in Science Research Exposition at University of Texas at El Paso Undergraduate Poster Session. March 2011 she was awarded first place in oral presentations at the University of Texas at El Paso geological science department's 25th annual colloquium.

During her time as a graduate student at the University of Texas at El Paso, she worked for Dr. Aaron Velasco coordinating the outreach program for geological sciences. In the summer of 2010 from May to August Sandy had an internship with Marathon Oil Company in Houston, Texas. Sandy was offered a full-time position as a geologist with Marathon Oil Company. She graduated from the University of Texas at El Paso with her Master of Science degree in 2011.

Permanent address: 9110 Elgin Dr.
El Paso, TX 79907

This thesis was typed by Sandy Stephanie Marrufo.